Transition of Natural Killer Cells Expansion Platform from Static Flasks to Stirred Tank Bioreactor

Diplomarbeit

zur Erlangung des akademischen Grades

Diplom-Ingenieur

im Rahmen des Studiums

Technische Chemie

eingereicht von

Zavtur Artiom, BSc
01363177

am Institut für Verfahrenstechnik, Umwelttechnik und technische Biowissenschaften

der Fakultät für Technische Chemie der Technischen Universität Wien

Betreuung: **Univ.-Prof. Dipl.-Ing. Dr.nat.techn. Oliver Spadiut**

Mitwirkung: **Bence Kozma, PhD**

Valentin von Werz, MSc

Wien, 31.03.2025

Zavtur Artiom

Die approbierte gedruckte Originalversion dieser Diplomarbeit ist an der TU Wien Bibliothek verfügbar
The approved original version of this thesis is available in print at TU Wien Bibliothek.

Erklärung zur Verfassung der Arbeit

Ich erkläre weiters an Eides statt, dass ich meine Diplomarbeit nach den anerkannten Grundsätzen für wissenschaftliche Abhandlungen selbstständig ausgeführt habe und alle verwendeten Hilfsmittel und Quellen vollständig angegeben habe.

Wien, 31.03.2025

Zavtur Artiom

Die approbierte gedruckte Originalversion dieser Diplomarbeit ist an der TU Wien Bibliothek verfügbar
The approved original version of this thesis is available in print at TU Wien Bibliothek.

Aknowledgements

I would like to express my sincere gratitude to Univ. Prof. Spadiut for welcoming me in his research group for Integrated Bioprocess Development at the TU Vienna.

I am also deeply thankful to Dr. Bence Kozma and Valentin von Werz for their patience, leadership and constructive feedback, and for providing me with the opportunity to contribute to this research. Their advice and mentorship have greatly enhanced my learning experience.

A special thank you goes to Philipp, Karim and Matthias Petsch. Your collaboration, insightful discussions and massive technical support made my time in the lab both enriching and enjoyable.

On a personal note, I would like to express my deep appreciation to my wife Mila. She encouraged me to keep going and supported me emotionally throughout the whole time.

Die approbierte gedruckte Originalversion dieser Diplomarbeit ist an der TU Wien Bibliothek verfügbar
The approved original version of this thesis is available in print at TU Wien Bibliothek.

Kurzfassung

Die Kultivierung von NK-Zellen unter statischen Bedingungen wurde bereits vor vielen Jahren etabliert und untersucht. Seitdem wurden verschiedene Protokolle entwickelt und weit verbreitet eingesetzt, um Zellpopulationen für therapeutische und wissenschaftliche Zwecke zu erzeugen. Häufig verwendete Methoden, die auf statischer Suspensionskultur basieren, haben eine begrenzte Skalierbarkeit, was die kommerzielle Nutzung solcher Zelltherapien erschwert. Der Fokus dieser Arbeit lag auf der Untersuchung der dynamischen Kultivierung von NK-92-Zellen in einem Rührkessel-Bioreaktor und in Schüttelkolben im Vergleich zur statischen Kultivierung in T-Flaschen.

Um die Produktion von NK-92-Zellen zu bewerten und zuverlässige Daten zu generieren, wurde ein vollständiges Laborsystem gründlich getestet und implementiert. Der Scale-up vom Schüttelkolben basierte auf der Leistungsaufnahme pro Volumeneinheit und erwies sich als geeignet. Anschließend wurde ein experimentelles Bioreaktor-Setup entworfen und integriert. Dies umfasste das Inokulationsverfahren, Rühren und Belüftung, die Überwachung der Permittivität, die Messung der gelösten Sauerstoffkonzentration (DO), die Analyse der O_2/CO_2-Konzentrationen im Abgas sowie den pH-Wert. Zudem wurde ein detaillierter off-line Probenahmeplan erstellt. Dieser beinhaltete die Bestimmung der lebenden Zellkonzentration (VCC), Zellviabilität und Zytotoxizität mittels Durchflusszytometrie sowie enzymbasierte Konzentrationsmessungen von extrazellulärer D-Glucose, L-Laktat, L-Glutamin, L-Glutamat, Ammonium und Pyruvat.

Es gelang uns, die statische NK-92-Zellkultivierung auf dynamische Bedingungen in Schüttelkolben und anschließend in einen Rührkessel-Bioreaktor zu übertragen. Nach neun Tagen Batch-Kultivierung wurde in allen drei Bedingungen eine hohe lebende Zellkonzentration erreicht. Die Zellvermehrung Rate betrug dabei 9,96 ± 0,33 in T-Flaschen, 8,97 ± 0,60 in Schüttelkolben und 6,64 ± 0,09 im Bioreaktor. Während der Wachstumsphase wurden keine signifikanten Unterschiede in den spezifischen Aufnahmeraten bzw. Produktionsraten der analysierten Stoffwechselprodukte festgestellt. Trotz der etwas geringeren Zellvermehrung in Schüttelkolben und der deutlich niedrigeren Expansion im Bioreaktor zeigten die Zellen aus allen drei Kultivierungsbedingungen eine vergleichbar hohe Zytotoxizität gegen K562-GFP-Reporterzellen bei einem E:T-Verhältnis von 1. Dies unterstreicht eine der wichtigsten Qualitätsmerkmale dieser Zellen. Abschließend wurden in dieser Arbeit die Dynamiken der spezifischen Aufnahme- und Produktionsraten von D-Glucose, L-Laktat und Pyruvat als Schlüsselmetaboliten der oxidativen Glykolyse sowie die Raten von L-Glutamin, L-Glutamat und Ammonium als Verbindung zwischen Aminosäurestoffwechsel und TCA-Zyklus hervorgehoben.

Schlagwörter: Bioprozess, NK-92-Zellen, Scale-up, Rührkessel-Bioreaktor, Zytotoxizität, Metabolisches Tracking.

Die approbierte gedruckte Originalversion dieser Diplomarbeit ist an der TU Wien Bibliothek verfügbar
The approved original version of this thesis is available in print at TU Wien Bibliothek.
TU Bibliothek Your knowledge hub WIEN

Abstract

NK cells cultivation in static conditions has been established and studied many years ago. Since then, many different protocols have appeared and have been widely used to generate cell populations intended for therapeutic and scientific use. Common methods that utilize static suspension culture have limited scalability, making commercialization of such cell therapies challenging. The focus of this work lay in the investigation of the dynamic cultivation of NK-92 in stirred tank bioreactor and shake flasks compared to static cultivation in T-flasks.

To be able to evaluate the production of NK-92 cells and generate stable data, a complete laboratory set-up was thoroughly tested and implemented. The scale-up from shake flask based on power input to volume unit was found to be suitable. Consequently, an experimental bioreactor set-up was then designed and integrated. This included inoculum procedure, stirring and aeration, monitoring of permittivity, dissolved oxygen (DO) concentration, O_2/CO_2 concentrations in off-gas, pH, as well as a detailed off-line sampling plan. A tailored sampling plan comprised of an assessment of viable cell concentration (VCC), viability and cytotoxicity using flow cytometry and enzyme-based concentration measurements of extracellular D-glucose, L-lactate, L-glutamine, L-glutamate, ammonium, and pyruvate was presented.

We were able to transform the static NK-92 cells cultivation to dynamic conditions in shake flasks to stirred tank bioreactor. Nine days of batch cultivation resulted in high viable cell concentration in all three conditions. Briefly, the fold expansion of 9.96 ± 0.33, 8.97 ± 0.60, and 6.64 ± 0.09 was achieved in T-flasks, shake flasks, and bioreactor respectively. No significant differences in specific uptake/production rates during the growth phase in all three conditions were detected. Despite slightly lower fold expansion in shake flasks and significantly lower fold expansion in bioreactor, the cells from all three conditions demonstrated equally high cytotoxicity against K562-GFP reporter cells at an E:T ratio of 1, highlighting one of the major critical quality attributes of these cells. Lastly, in this work we underlined the dynamics of specific uptake/production rates of D-glucose, L-lactate and pyruvate as the key molecules in oxidative glycolysis as well as specific uptake/production rates of L-glutamine, L-glutamate and ammonium ions as a bridge between amino acid metabolism and TCA-cycle.

Keywords: Bioprocess, NK-92 cells, Scale-up, Stirred tank bioreactor, Cytotoxicity, Metabolic tracking.

Die approbierte gedruckte Originalversion dieser Diplomarbeit ist an der TU Wien Bibliothek verfügbar
The approved original version of this thesis is available in print at TU Wien Bibliothek.

Table of Contents

1 INTRODUCTION 1

1.1 Discovery and recognition of NK cells 1

1.2 Main sources and functions of primary NK cells 2

1.2.1 Origin and isolation sources 2

1.2.2 NK cell maturation and receptor orchestration 3

1.2.3 Crosstalk with other cells and regulation of immune response 4

1.2.4 Killing mechanisms of NK cells 5

1.3 Application of NK cells 7

1.3.1 Adoptive cell therapy with primary NK cells 7

1.3.2 Adoptive cell therapy with NK-92 cell line 8

1.4 Expansion methods of NK cells 9

1.4.1 Expansion of primary NK cells 10

1.4.2 Static expansion platforms 12

1.4.3 Dynamic expansion platforms 14

1.4.4 Expansion of NK-92 cells 16

2 METHODS 18

2.1 Preculture maintenance and bioreactor preparation 18

2.2 NK-92 inoculation in T-flasks, shake flasks and bioreactor 24

2.3 Harvesting and off-line analytics 24

2.3.1 Cell counting and viability assessment 26

2.3.2 Cytotoxicity assay 27

2.3.3 Nutrients and metabolites tracking on Cedex BioHT 30

2.3.4 Off-line pH measurements in shake flasks and T-flasks 30

2.4 Online measurements for bioreactor process monitoring 31

2.4.1 Viable cell density 31

2.4.2 Oxygen and carbon dioxide concentrations in off-gas 32

2.4.3 Dissolved oxygen 32

2.4.4 pH 32

2.5 CALCULATIONS 33

2.5.1 Growth characterization 33

2.5.2 Reaction rates and yields 34

2.5.3 Shake flask-to-stirred tank bioreactor scale-up approach 35

2.5.4 Volumetric oxygen uptake rate, carbon dioxide emission rate and respiration quotient 38

2.5.5 Connection between oxygen uptake rate and volumetric mass transfer coefficient k_La 39

Die approbierte gedruckte Originalversion dieser Diplomarbeit ist an der TU Wien Bibliothek verfügbar
The approved original version of this thesis is available in print at TU Wien Bibliothek.
TU Bibliothek Your knowledge hub WIEN

3 RESULTS AND DISCUSSION 41

3.1 Cell growth and viability of NK-92 cells 41

3.2 Cytotoxicity of NK-92 cells 45

3.3 NK-92 cells and the small insight in their metabolism 47

3.4 Insight into bioreactor online monitoring 53

3.5 Correlation analysis 58

4 CONCLUSION AND OUTLOOK 62

5 SUPPLEMENTARY INFORMATION AND FIGURES 64

5.1 Batch process preparations 64

5.2 kLa determination 65

5.3 Consumables and Reagents 67

5.4 Auxiliary tables for correlation analysis 69

6 REFERENCES 71

Die approbierte gedruckte Originalversion dieser Diplomarbeit ist an der TU Wien Bibliothek verfügbar
The approved original version of this thesis is available in print at TU Wien Bibliothek.

1 INTRODUCTION

Cell subsets of the immune system—leukocytes and lymphocytes—possess a very wide spectrum of functions and are tightly regulated. The immune system can be roughly divided into the innate and adaptive immune systems, addressing the order in which different pathogens are facing the host's protective barriers. While the innate immune system reacts to the common structures that the most invaders share, so-called pathogen-associated molecular patterns (PAMPs), the adaptive immune system reacts to specific structures of these pathogens[1]. To leverage this, cells of the immune system evolved numerous mechanisms—most of them are based on the identification of pathogens with an arsenal of receptors, and others on signaling molecules. Moreover, cells from both innate and adoptive immune systems are capable of distinguishing between endogenous cells and pathogens, so-called "self" and "missing self." However, the repertoire of these tools is limited, which led to many invaders evolving their own strategies for overcoming the immune system and finally spreading the disease.

In this work, the focus will be on one of the cells of the innate immune system that stays a bit apart from the other of its cohort: natural killer cells. It will include the review of origin, functions, communication skills, and expansion methods of NK cells from primary sources, e.g., healthy blood donors, as well as from the permanent NK-92 cell line. As the main part, a detailed description and experimental comparison of three expansion methods of these cells and a small insight into their metabolism will be presented to the reader.

1.1 Discovery and recognition of NK cells

NK cells were first found in spleen from normal nude mice in 1970s and later described by Kiessling et al. and Herberman et al. in 1975 as spontaneous selective cytotoxic cells against Moloney leukemia cells[2, 3]. This "natural" or "spontaneous" killing not only of tumor cells, but also virally or bacterially infected cells without prior immunization or activation, was later identified as their fundamental property and gave them their name - Natural Killer cells[4, 5]. Alongside phagocytes, innate lymphoid cells (ILCs), dendritic cells (DCs) and other leucocytes, NK cells were traditionally considered to be the part of native immune system. Nowadays, NK cells are regarded as a complex subset of lymphocytes that function along the boundaries of innate and adaptive immunity[6].

Die approbierte gedruckte Originalversion dieser Diplomarbeit ist an der TU Wien Bibliothek verfügbar
The approved original version of this thesis is available in print at TU Wien Bibliothek.

1.2 Main sources and functions of primary NK cells

1.2.1 Origin and isolation sources

NK cells have been classified as lymphocytes. Mainly because of their morphology, e.g., size, granules, and their expression of many lymphoid markers, but also because of their origin from the common lymphoid progenitor cell in the bone marrow. These facts, however, do not place them solely in the same column with B or T cells because they lack antigen-specific cell surface receptors, such as BCR and TCR [6]. However, recent evidence in humans and mice suggests that they can also develop and mature in secondary lymphoid tissues (SLTs), including tonsils, spleen, and lymph nodes[7].

When it comes to isolation from blood, the main sources of NK cells are peripheral blood (PB-NK), bone marrow (BM-NK), and umbilical cord blood (CB-NK). Each source provides different populations of NK cells, which can have distinct functional and developmental characteristics based on their environment[8]. If not interested in immature populations of NK cells populations (BM) or no access to umbilical cord is provided, the most common way is to collect the blood from donor and separate the NK cells from peripheral blood mononuclear cells (PBMCs) via density gradient centrifugation followed by magnetic or flow cytometric sorting (Figure 1). The proportion of NK cells in peripheral blood is relatively low, comprising about 5-15% of total lymphocytes with turnover around 2 weeks, consistent with data in the mouse[9].

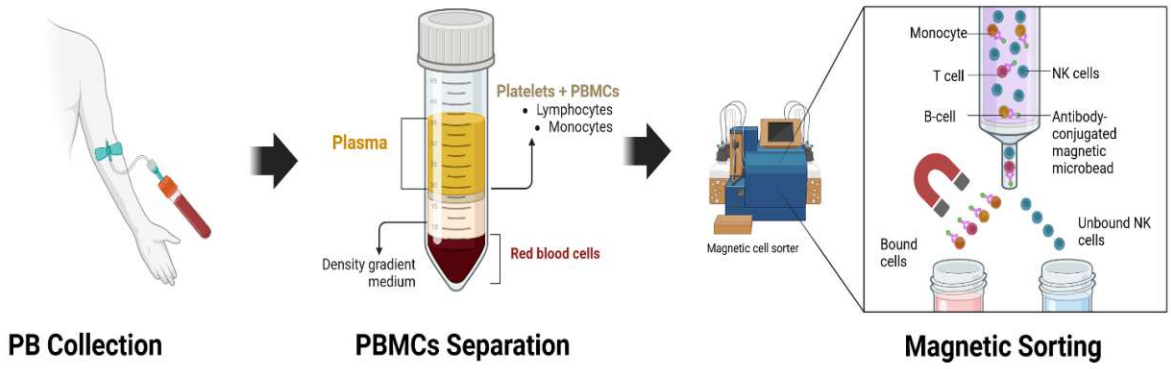

Figure 1*: **Schematic NK cells isolation process.** 1) Collection of peripheral blood from donor 2) Separation of PBMCS fraction from plasma and red blood cells using density gradient centrifugation 3) PBMCs fraction comprising not only NK cells but also B and T cells can be further fractionated using Magnetic-Activated Cell Sorting (MACS) technology to finally isolate the NK cells.*

Die approbierte gedruckte Originalversion dieser Diplomarbeit ist an der TU Wien Bibliothek verfügbar
The approved original version of this thesis is available in print at TU Wien Bibliothek.

1.2.2 NK cell maturation and receptor orchestration

NK cell population is heterogeneous and is determined by expression of plethora of cell surface receptors, which can be encoded by two or more genes, occurring in various forms depending on species. Moreover, the number of receptors with different functions, such as stimulation or inhibition may vary depending on the environment – healthy cell in steady state, infected cell or malignant cells[10]. Due to high interest in immunotherapeutic potential of NK cells, most of well-known described receptor-function dependencies were investigated in conditions when NK cells encountered stressed cells.

It has been recently appreciated, that substantial fraction of NK cells isolated from human peripheral blood are not killer cells due to their immaturity and lack of special receptors[11]. In this context, before being activated, NK cells require several maturation steps, so called "education", through the recognitions of self-molecules like MHC class I, that are constitutively expressed in steady-state conditions by almost every self-cell[12]. Moreover, for full activation, NK cells require "priming" by cytokines, such as IL-15 (presented by DCs), IL-2, IL-18 or IL-12[13, 14]. After maturation and priming further signaling is required to shape the responsiveness and activity of NK cells. Most of these functions are dictated by a variety of cell surface activating and inhibitory receptors. Thus, the interaction with neighboring cells is the process which influences the dynamic equilibrium, regulating activation and downregulation of NK cells functions[15].

Receptors, which activate NK cells detect the presence or absence of specific molecules – antigens. These antigens can be expressed on stressed cells like tumor cells, hyperactivated DCs or macrophages, pathogenic bacteria cells, e.g. Toll-like receptor ligands, or virus particles, e.g. cytomegalovirus-encoded peptides, and are recognized by specific NK cell receptors, among others - NKG2D and NCR-family (NKp46, NKp30, NKp44)[16, 17]. The absence of constitutively expressed molecules on the surface of target cells can be also recognized by NK cells and lead to their activation. One of these molecules, which is expressed on almost every cell in the system, is the abovementioned MHC class I-complex. When MHC class I-complex is missing, such NK cell receptors like killer cell immunoglobulin like receptors (KIR) become activated, as demonstrated in several *in vitro* and *in vivo* models and described as "missing self"[18, 19]. Moreover, the antibody-coated target cells can be recognized by low-affinity receptor CD16, leading to antibody-dependent NK-cell cytotoxicity (ADCC)[20]. Altogether, receptor-mediated responsiveness comprises the first NK cell effector function – direct target cell lysis.

Die approbierte gedruckte Originalversion dieser Diplomarbeit ist an der TU Wien Bibliothek verfügbar
The approved original version of this thesis is available in print at TU Wien Bibliothek.

Consequently, the inhibitory receptors can detect the presence of specific molecules and lead to inhibition of NK cells. For example, same receptors which can activate NK cells - KIR-family or lectin-like CD94-NKG2A heterodimers in human, can specifically recognize the MHC class I complex which leads to tolerance and no activation[21]. It is possible that some of the mechanisms that lead to tolerance are the same as those that operate when NK cells become activated due according to "missing self" scenario[22].

1.2.3 Crosstalk with other cells and regulation of immune response

Each receptor type can recognize only one specific type of ligand, but there are different effects which one specific type of ligand can cause in different cells. Other cells, like DCs, macrophages and T cells can be activated through different cytokines, e.g. IL-10 or TNF- α, chemokines such as IFN-γ and growth factors secreted from NK cells upon activation[6]. Production of aforementioned cytokines and chemokines is considered to be the second NK cell effector function.

Whereas the biological function of the growth factors secreted by NK cells remains to be clarified, secretion of IFN-γ is key to colocalization with dendritic cells in areas of inflammation[23]. Furthermore, production of IFN-γ by NK cells helps to shape T cell responses in lymph nodes, possibly by a direct interaction between naïve T cells and NK cells migrating to secondary lymphoid compartments from inflamed peripheral tissues [24]. Also, an indirect T cell response can be mediated by NK cells. Most probably by decreasing the antigenic load through the killing activity and/or by increasing antigen cross-presentation of target cell debris from DCs to CD4+ helper T cells[25]. Macrophage recruiting to eliminate stressed cells can be also counted as regulatory functions of NK cells. As the first line involved in fighting tumors, NK cells reach the tumor site early and work in reciprocal partnership with macrophages M1. It has been found that T cells and NK cells are the dominant IFNγ producers, when encountering tumors [26]. This member of the type II IFN-family is a typical macrophage "activator". Together with lipopolysaccharides (LPS) and many others TLR-ligands it is supposed to enhance the antitumor activity of these phagocytes by promoting the secretion of proinflammatory cytokines, e.g.IL-12[27] and induction of reactive oxygen species (ROS)/reactive nitrogen species (RNS)-producing enzymes, e.g. NO-Synthase(iNOS)[27]. Reciprocally, macrophages can stimulate primary NK cells to proliferate, secrete IFNγ and augment NK cytotoxicity against susceptible target cells[28].

Die approbierte gedruckte Originalversion dieser Diplomarbeit ist an der TU Wien Bibliothek verfügbar
The approved original version of this thesis is available in print at TU Wien Bibliothek.

1.2.4 Killing mechanisms of NK cells

When the activating signals outweigh the inhibitory signals, NK cells are capable to lyse target cells[4]. The first well-described mechanism of apoptosis induction in tumor cells is the capability of NK cells to release cytolytic granules containing perforin and granzyme B. Further, it was shown that NK cells can interact with tumor cells through Fas ligand (FASL) and TNF related apoptosis-inducing ligand (TRAIL), recognized by so called death receptors on the surface of tumor cells[29].

Granzymes belong to the family of serine proteases, mostly with trypsin-like activity. The members including granzyme A, B , H, K and M have all similar functions, with A and B studied most[30]. One prominent substrate of granzyme B is caspase-3. Cleavage of caspase-3 results in its activation and subsequently cleavage of different structural and regulatory proteins in the nucleus, in the cytosol and at the cytoskeleton. Additionally, granzyme B triggers the mitochondrial apoptotic pathway through direct cleavage of Bid-protein [31]. To enter the target cell granzymes and perforins have first leave the NK cells granules in the multi-step process called degranulation. Briefly, lytic granules are transported to the immunologic synapse between the NK cell and the target, where they fuse with the plasma membrane, releasing their contents, including perforin and granzymes. Perforin forms pores in the target cell membrane, allowing granzymes, particularly granzyme B, to enter and induce apoptosis[32,33].

Fas ligand (FasL) is a 40-kDa transmembrane protein from the TNF superfamily, expressed on activated T cells and NK cells[34, 35]. After synthesis, FasL is transported to secretory lysosomes, aided by a proline-rich domain in its cytoplasmic tail, which undergoes phosphorylation and ubiquitination for proper sorting. Unlike granules containing perforin and granzymes, FasL is stored in distinct secretory granules but the mechanism remains similar to classical cytotoxic granules[29].

Upon degranulation, FasL is externalized and may be constrained at the immunologic synapse, where it engages the CD95 receptor on target cells, initiating an apoptotic signaling cascade through the formation of the death-inducing signaling complex (DISC) and activation of caspases 8 and 10[36, 37]. With mechanism less understanded than FasL, TRAIL-mediated cytotoxicity has been shown to be important in control of viral infection and cancer[38, 39]. TRAIL is a type II transmembrane and belongs also as FasL to TNF superfamily. Although TRAIL is not present on the surface of freshly isolated NK cells, it can be expressed upon activation with IL-2,IL-15 or IL-12[14, 40]. Figure 2 summarizes the proposed mechanisms and provides better overview.

Die approbierte gedruckte Originalversion dieser Diplomarbeit ist an der TU Wien Bibliothek verfügbar
The approved original version of this thesis is available in print at TU Wien Bibliothek.

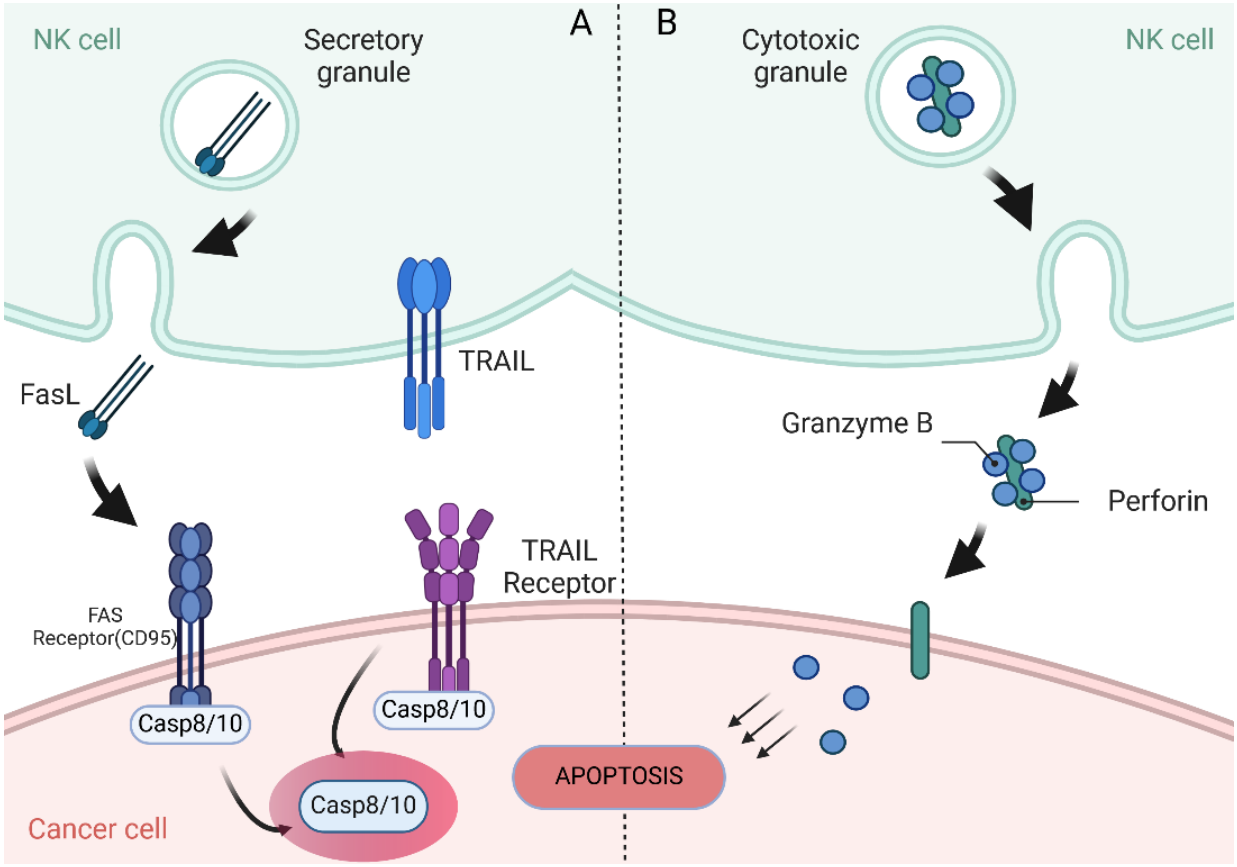

Figure 2: Mechanisms of NK cell-mediated cytotoxicity. *A) Receptor mediated induction of apoptosis involves engagement of externalized FasL after degranulation or membrane-bound TRAIL and their respective receptors. Cleavage and consecutive activation of Caspase 8 or 10 leads to the assembly of the DISC complex and as a result – apoptosis of target cell. B) Packed in cytotoxic granules, perforin and granzyme B can be released in extracellular space. Perforin than facilitates the entry of granzyme B in target cell, inducing the apoptosis*[41].

Die approbierte gedruckte Originalversion dieser Diplomarbeit ist an der TU Wien Bibliothek verfügbar
The approved original version of this thesis is available in print at TU Wien Bibliothek.

1.3 Application of NK cells

Since mid-1970s, advances in understanding of NK cell signaling balance and regulation of immune system have led to an appealing candidates for immunotherapy. In contrast to traditional cancer therapies, such as surgery, chemotherapy and radiotherapy, immunotherapy doesn't target cancer cells directly. Instead, it stimulates the immune system to recognize and combat cancer cells more effectively [42]. At present, NK cell-based immunotherapy has aroused wide attention in tumor treatments, including NK cell adoptive therapy, CAR NK cell therapy, immune checkpoint inhibitors and engineered cytokines[43],[44]. Following, the adoptive cell therapy (ACT) with primary NK cells and the off-the-shelf cell therapy potential of NK-92 cell line will be discussed.

1.3.1 Adoptive cell therapy with primary NK cells

Adoptive cell therapy is a highly personalized cancer therapy that involves administration of immune cells with direct anticancer activity to the cancer-bearing patient. This approach involves the administration of either autologous, using host-derived cells or allogeneic immune cells that are harvested from healthy donor, expanded ex vivo, potentially genetically modified and injected back to any other matched recipient[45]. NK cells are from higher interest for both allogeneic and autologous immunotherapies and very often considered as safer than cytotoxic T cells, mainly because of their MHC independence and missing TCR receptors, which can trigger the rejection of therapeutic cells by host, described as Graft vs. Host Disease [46]. Table 1 summarizes the advantages and limitations of both strategies[47].

Autologous	Allogeneic
Human Leucocyte Antigen (HLA) compatible	KIR-HLA mismatch with donor may trigger alloreactivity of NK cells
Low risk of getting GvH disease	Potential risk of getting graft versus host disease
Designed to be used in the same patient	Can be used with any recipient ("off-the-shelf" product)
Compatible environment facilitates the NK cell expansion and persistence	More probability of reaching cell exhaustion
No need to use immunosuppressive therapy before starting immunotherapy	To avoid immunological rejection, chemotherapy is needed before the therapy
The cell source is the patient, who usually possesses cells with reduced effector function("exhausted")	Wide range of NK cells sources

Table 1: *Comparison between autologous and allogeneic NK cell therapies with focus on donor-acceptor compatibility.*

Die approbierte gedruckte Originalversion dieser Diplomarbeit ist an der TU Wien Bibliothek verfügbar
The approved original version of this thesis is available in print at TU Wien Bibliothek.

Allogeneic NK cells, taken from healthy donors can be improved by numerous approaches. These can be roughly divided into four categories: 1) the ones increasing effector responses by activating receptor antibody agonist, 2) decreasing the immunosuppression, e.g. checkpoint blockade, 3) improving in vivo functional persistence or 4) enhancing the targeting by using genetically engineered Chimeric Antigen Receptor (CAR)[47]. For the last category, the usage of cell lines like NK-92 cells is from high interest. CAR is composed from Ig-derived variable regions Fab and TCR-derived Fc regions which can be expressed on the surface of NK cells allowing to specifically target the cancer cells[47]. Since 2018, 24 clinical trials with CAR-NK cells which are active or are on the stage of recruitment were registered indicating high interest in this approach[48]. Similarly, to the sources of NK cells, described in subchapter 1.2.1, sources of CAR-NK cells also include PB, CB and bone marrow, e.g. induced Pluripotent Stem Cells – iPSC. Additionally to those listed, CAR-NKs can be produced from permanent cell lines, the most prominent one is NK-92[49]. Next, the NK-92 cell line will be introduced in a more detailed manner.

1.3.2 Adoptive cell therapy with NK-92 cell line

NK-92 is a highly cytotoxic cell line that possesses properties that make it an excellent candidate for adoptive cellular immunotherapy[50]. NK-92 cells were generated by Hans Klingemann in 1992 from mononuclear blood cells from a patient who had been diagnosed with an aggressive NK cell lymphoma [51]. NK-92 cells express multiple activating receptors, such as NKG2D and NKp30 but lack the CD16 Fc receptor and, with exception of CD94/NKG2A and LIR1, almost all inhibitory receptors (KIR)[52, 53]. Additionally, NK-92 cells release relatively high amount of granzymes, even higher than the NK cells from blood and perform serial killing of target cells (NK-92 redirected to the tumor-associated HER2 antigen)[54, 55]. Most importantly, repeated infusions with NK-92 cells, even at high cell numbers, did not induce any side effects greater than grade 3-4[56, 57]. Taking all this into consideration, NK-92 cells have become a critical NK cell line for preclinical research and are the only cell line approved by US Food and Drug Administration (FDA) for clinical studies[56-60]. For the successful development of the NK-92 cells and their genetically modified CAR-NK92 for patient treatment, three major issues can be outlined from different publications:

a) The risk for lymphoma developing in recipients due to NK-92 cells originating from a patient with lymphoma
b) The issue of potential patients own immune system rejection due to the allogeneic nature of NK-92 cells
c) Difficulties in expansion process scalability

At least a partial solution for the first issue is irradiation. Navarette-Galvan et al. showed that after exposure to 2.5, 5 and 10 Gy (recommended by FDA), NK-92 cells survival and cytotoxic activity after one day of incubation is greatly impacted towards negative side. Contrary, also after 24-h post irradiation

Die approbierte gedruckte Originalversion dieser Diplomarbeit ist an der TU Wien Bibliothek verfügbar
The approved original version of this thesis is available in print at TU Wien Bibliothek.
TU Bibliothek Your knowledge hub WIEN

but with modified NK-92 cells – high affinity NK cells (haNK), Jochems et al. detected an increase in cytotoxicity toward multiple carcinoma cell lines compared to haNK cell killing immediately post irradiation [55, 61]. One possible explanation of this difference in post irradiation activity could be endogenous expression and linkage of IL-2 on the endoplasmic reticulum by haNK cells. Thus, the IL-2 signaling is on-going and no need in receptor engagement is needed. Second possible explanation exhibits another "feature" of haNK cells – expression of CD16 receptor and therefore additional killing capacity via ADCC.

To address the immunogenicity issue, several studies of private company with NK-92 variants exclusive license, demonstrated that allogeneic donor T cells do not exhibit increased proliferation or IFN-γ production when exposed to NK-92 cells [62]. This result was partially validated in phase I studies in Toronto [59] and Frankfurt [60] with six out of twelve patients developed HLA antibodies against NK-92 in Toronto and with similar results achieved in Frankfurt.

The third issue arises from the need to expand NK cells to reach clinically relevant numbers, usually 1-5 * 10^7 Cells/kg and affects both NK-92 and primary NK cells expansion processes[63-65]. Whereas consistent generation of 10^8 – 10^9 cells using existing NK-92 expansion protocols to support small scale phase I or II clinical studies didn't seem to be a problem, the availability of large quantities of functionally effective NK cells isolated from peripheral blood mononuclear cells (PBMCs) represents one of the major challenges for NK cell-based immunotherapy due to low abundancy and heterogeneity. However, to mitigate the risk of cell shortage during future phase II and III clinical trials even higher numbers of NK cells will be needed. To find the solution to this issue, it could be beneficial to start from more consistent and continuously growing NK-92 cell line and then transfer the technology to primary cells. From this point, the focus of further discussion will be shifted towards review of currently available expansion methods.

1.4 Expansion methods of NK cells

As discussed previously, ACT can be divided into autologous and allogeneic. Decision about which of these immunotherapies to use is often taken as a basis for ex-vivo cell expansion protocols. Since the late 90s every research groups tried to establish their own expansion protocol which results in numerous publications, some of them are summarized in tables below. Pursuing one single goal – fast generation of clinically relevant amount of highly efficient and safe cell product, scientist confronted multiple issues at the same time. While generation of high number of cells sufficient for small clinical trials with up to 15 patients with single dose administration of 10^7 Cells/kg seems not to be an issue, the expansion duration, presence of activating feeder cells or other functionally different cell subpopulations, number of vessels and manual steps to obtain the final product and lack of tight manufacturing control, demonstrated big challenges.

Die approbierte gedruckte Originalversion dieser Diplomarbeit ist an der TU Wien Bibliothek verfügbar
The approved original version of this thesis is available in print at TU Wien Bibliothek.

1.4.1 Expansion of primary NK cells

Author/ Year	Cell Source	Expansion platform	Cultivation mode	Priming/ activation	Media/ Serum	Duration [days]	Fold-expansion
Pierson/ 1996[66]	PBMCs w/o sorting	stirred bioreactor 24-well plates spinner flasks	repetitive batch (RB) with 50% cell removal	IL-2	DMEM/ Hams F12 10% human serum (HS)	33	352-fold in reactor 51-fold in 24-well plates 120-fold in spinner flasks
Carlens/2001[67]	PBMCs w/o sorting	T25-flasks	pulsed batch (PB)	IL-2	SCGM + 5% HS	21	110-fold w/ serum
					SCGM serum free		6-fold w/o serum
Luhm/ 2002[68]	PBMCs (CD3/CD4/CD19/CD33 depleted)	PTFE Bags	PB	feeder cells (FC)+IL-2+IL-15	X-Vivo 20	18	100-fold from pooled 6 L apheresis product
Sutlu/ 2010[69]	PBMCs w/o sorting	T75-flasks Wave bags	PB	IL-2	SCGM 5% HS	21	770-fold in flasks 77-fold in Wave (direct start) 550-fold in bags

Table 2: ***Chronologically listed expansion methods of NK cells from primary sources in both autologous and allogeneic settings - Part 1.*** *No intensified processes, only pulsed or repetitive batch. Only one work from Pierson dealing with glass stirred reactor cultivation of primary NK cells, which resulted in fold expansion even higher than in other vessels but is underrepresented compared to other expansion platforms. Usage of feeder cells by Luhm et al. allowed to reach high fold expansion despite using the serum free media X-Vivo 20. In contrast, the cultivation carried out in T25 flasks by Carlens et al. didn't yield high number of cells.*

Die approbierte gedruckte Originalversion dieser Diplomarbeit ist an der TU Wien Bibliothek verfügbar
The approved original version of this thesis is available in print at TU Wien Bibliothek.

Spanholtz/2011[70]	Umbilical blood hematopoietic stem cells (UB-hSC)	CliniMACS-Prodigy	PB	IL-2+IL-15	GBGM 10% HS	42	1300-fold CliniMACS-Prodigy
		Wave					2100-fold Wave
Lapteva/2012[71]	PBMCs w/o sorting	G-Rex(static)	batch	FC+IL-15+IL-2	SCGM 10% heat inactivated FBS	10	442-fold G-rex
	Allogeneic &autologous	PTFE bags	PB				227-fold bags
Shah/2013[72]	UB (no CD56+ selection)	G-Rex100	PB	FC+IL-21+IL-2	45%RPMI 45% Clicks media 10%HS	14	1848-fold fresh UB
							2389-fold frozen UB
Granzin/2015[73]	PBMCs (CD3-depl, CD56+ enrich)	CliniMACS-Prodigy	PB	w/ FC + IL-2	TexMACS 5% HS	14	850-fold in CliniMACS-Prodigy w/ FC
				w/o FC + IL-2			No data
		T75		w/ FC + IL-2			1344-fold in T75 w/ FC
				w/o FC + IL-2			14-fold in T75 w/o FC
Klöß/2017[74]	PBMCs (sorted CD3-CD56+)	CliniMACS-Prodigy (only sorting) T25-T250(expansion)	RB	w/o FC +IL-2	NKMACS 5% HS	14	30-fold w/o FC + IL-2
				w/ FC + IL-2			50-fold w/ FC+IL-2
				w/ FC+IL-21+IL-2			90-fold w/ FC + IL21+IL-2
Oberschmidt/2019[75]	PBMCs(sorted CD3-CD56+)	CliniMACS-Prodigy(sorting &expanding)	RB (static/gentle shaking)	IL-21+IL-2+IL-15	NKMACS 5% HS	14	12.5-fold

Table 3: ***Chronologically listed expansion methods of NK cells from primary sources in both autologous and allogeneic settings - Part 2.*** *Human serum was used in almost all cultivations indicating a much safer alternative to animal-sourced serum. A wide variety of complete media formulations were used in the studies indicating the lack of uniform expansion protocols. Usage of Interleukin "Cocktail" of IL-2 and IL-15 seems to be inevitable for cultivation of primary NK cells. Adding of feeder cells to stimulate the NK cells can significantly increase the fold expansion, as demonstrated by Granzin et al. and Klöss et al. Additionally, appearance of new devices like CliniMACS-Prodigy and G-rex created a small shift towards more reproducible and easy-to-handle expansion platforms. In some cases, cultivation in static T-flasks still remained as main expansion platform or was used as control.*

Die approbierte gedruckte Originalversion dieser Diplomarbeit ist an der TU Wien Bibliothek verfügbar
The approved original version of this thesis is available in print at TU Wien Bibliothek.
TU Bibliothek Your knowledge hub WIEN

1.4.2 Static expansion platforms of primary NK cells

The first-ever vessel used to cultivate human cells was a Pyrex glass bottle developed in the early 20th century. However, the most famous example came in 1951 when Dr. George Otto Gey used a glass flask to culture the first immortal human cell line, known as HeLa cells. Over time, this technology evolved significantly, leading to specialized multi-well plates, T- flasks, gas-permeable membrane bottles and bags, and eventually vertical cell factories (Figure 3). However, the culture principle remains the same – cells are resting at the bottom covered with media containing all important nutrients. Despite high cell numbers that can be generated and relatively low cost, static expansion has some drawbacks. Due to low volumetric capacity of the vessels, generation of high cell numbers requires multiple vessels operated in batch-split mode, e.g. multi-well plates and T-flasks, increasing the risk of contamination[66,67]. To address this issue the usage of gas-permeable bags and G-Rex bottles was found to be a reasonable alternative. Luhm et al., Sutlu et al. and Lapteva et al. were successful in expanding NK cells from PBMCs with or without prior sorting in both autologous and allogeneic settings[68, 69, 71]. Moreover, Lapteva et al. demonstrated the expansion of highly pure NK cells from PBMCs without sorting (> 90% $CD56^{+}CD3^{-}$) in numbers sufficient for clinical application. For this, Grex100 as an expansion platform was used, cultivating cells in one batch without cell manipulation or feeding during 8-10 days. Despite very promising expansion results and possibility to remove of $CD3^{+}$ T cells subpopulation after harvesting, the usage of non-GMP conform Fetal Bovine Serum (FBS) and K562-mb15-41BBL feeder cells can lead to up-regulated surface HLA class I antigen expression and stimulation of alloreactive $CD8^{+}$ T cells, as demonstrated in additional ex-vivo test within the NK cultures. Both of these outcomes are not favorable for cancer patients and need to be carefully evaluated when working without prior cell sorting and with addition of stimulants like feeder cells[71].

Die approbierte gedruckte Originalversion dieser Diplomarbeit ist an der TU Wien Bibliothek verfügbar
The approved original version of this thesis is available in print at TU Wien Bibliothek.

In general, the usage of feeder cells to stimulate the growth of NK cells seems to have more prominent effect as just supplementation with cytokines like IL-21, IL-15 and IL-2. Both Granzin et al. and Klöß et al. concluded this by directly comparing the fold-expansion of cells supplemented only with cytokines with the cells stimulated by feeder cells. Results showed almost 100 times and 3 times higher fold-expansion in case of feeder cells during 14 days T-Flask cultivation[73, 74]

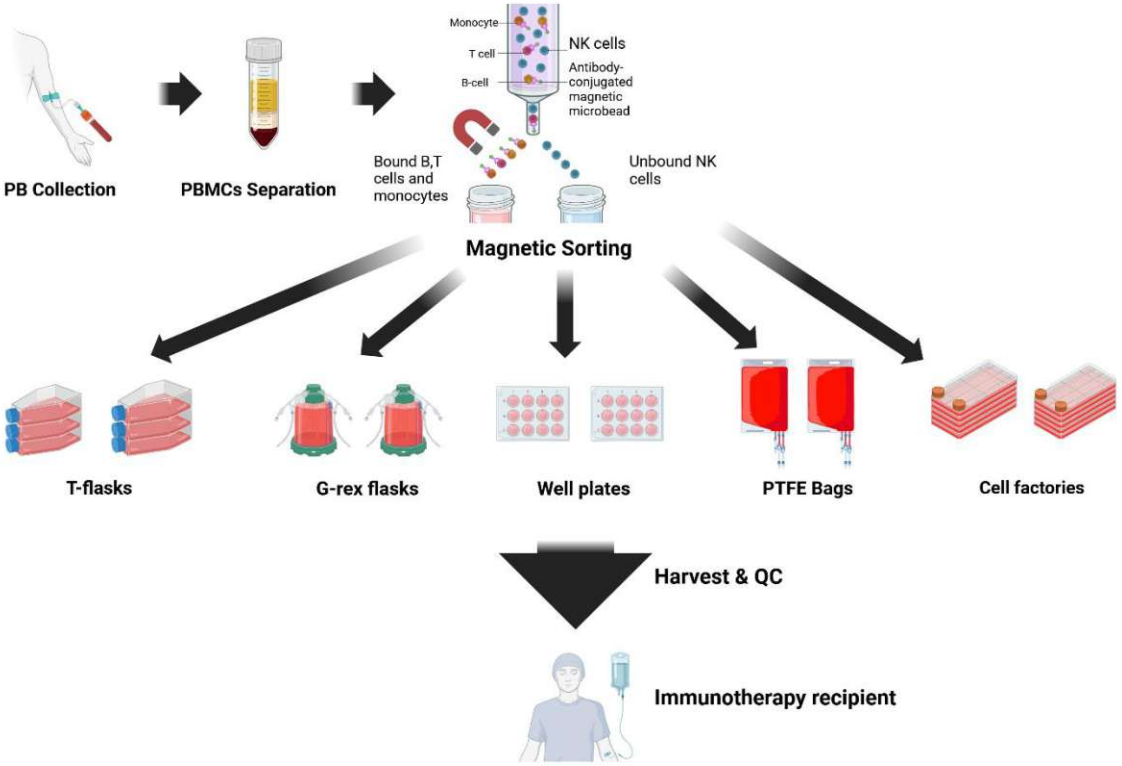

Figure 3: ***Overview of static cultivation of primary NK-cells****. In some cases, magnetic sorting can be skipped or included at QC stage after expansion and harvesting. Before administering to patients, cells are harvested and checked for the viability and presence of specific surface marker/markers needed for chosen immunotherapy.*

Die approbierte gedruckte Originalversion dieser Diplomarbeit ist an der TU Wien Bibliothek verfügbar
The approved original version of this thesis is available in print at TU Wien Bibliothek.

1.4.3 Dynamic expansion platforms of primary NK cells

Chronological character of both Table 2 and Table 3 makes it easier to notice the shift to dynamic expansion platforms, were the media and cell suspension is in partial or permanent movement. Several issues can be related to both static and dynamic culturing platforms. Main challenges like unfavorable effects of adding feeder cells and low fold-expansion without adding them combined with low amount of $CD56^{+}CD3^{-}$ NK cells in initial apheresis product, still must be resolved. Another two challenges – reducing the number of culturing vessels and more advanced process control could be at least partially resolved by introducing closed systems like bioreactors.

Less ACT specialized culturing platforms like the Wave®(Cytiva) or stirred tank bioreactor (STR) can be adopted for NK cells culturing and are simply accessible. These systems have proven to be useful for controlled generation of high amount of NK cells even without involving feeder cells[66, 69, 70]. Sutlu et al. made a step forward and demonstrated the direct cell expansion initiation from non-sorted PBMCs in 2 L Wave-reactor without pre-expansion[69]. Furthermore, Spannholtz et al. showed the similar $CD56^{+}CD3^{-}$ NK cells yield obtained with Wave-reactor compared to the cell yield in Vuelife PTFE bags, starting from hematopoietic stem cells(hSC) and culturing for 42 days. Moreover, the amount of proliferated $CD56^{+}CD3^{-}$ in bioreactor was significantly higher than in bags[70]. Important process parameters like aeriation, temperature and pH were monitored and controlled. Rocking motion of wave-bioreactor and stirring motion of STR enabled media and gas mixing without cell damage.

Since its full release in 2013, Clinimacs Prodigy®(Miltenyi) has set the bar for ACT specialized automated system. The Prodigy system integrates cell washing, separation, gene transfer, enrichment and expansion into a fully automated GMP compliant workflow. Accordingly, since then the protocols for NK cells expansion were adapted to this platform resulting in successful 14-day expansion process and direct transfer to clinical application[73-75]. However, especially for cancer treatment with large number of lymphocytes needed, the Prodigy system is still limited in scalability. Thus, multiple devices will be needed for successful therapy[76]. Taking into consideration the price of one single device, single used kits, antibodies and other consumables needed to expand the cells in GMP environment, which rounds up to a very high sum, the Prodigy platform might be only affordable for the laboratories at the hospital site. In contrast, STR is more affordable and easier to parametrize which is ideal for process intensification and scale-up from engineering point of view. Its fit-for-purpose was demonstrated in allogenic therapies with CAR-T cells, where process scale-up is more important than in patient-specific autologous applications[77].

Die approbierte gedruckte Originalversion dieser Diplomarbeit ist an der TU Wien Bibliothek verfügbar
The approved original version of this thesis is available in print at TU Wien Bibliothek.

Main concern when using STR is shear stress, which can be induced by impeller[78]. Combined with the existence of other expansion platforms and relatively small clinical trials, stirred bioreactors were significantly underestimated which resulted in a very low number of investigations and research articles dealing with NK cells. Nevertheless, in 2001 Hilbert et al. were able to successfully expand primary T cells from PBMCs in 20 Liter Applikon stirred bioreactor. Additionally, no differences were found between a stirred and a static cultivation[79]. Later, in 2019 and 2020, Costariol et al. clearly demonstrated that T cells can sustain the shear stress when cultivated in Ambr bench-top single-use bioreactors for 7 days[80, 81]. With T cells having same lymphoid progenitor as NK cells and generally regarded as „big brother" in terms of immunotherapy applications and research potential, NK cells cultivation in stirred bioreactor has to be intensively investigated.

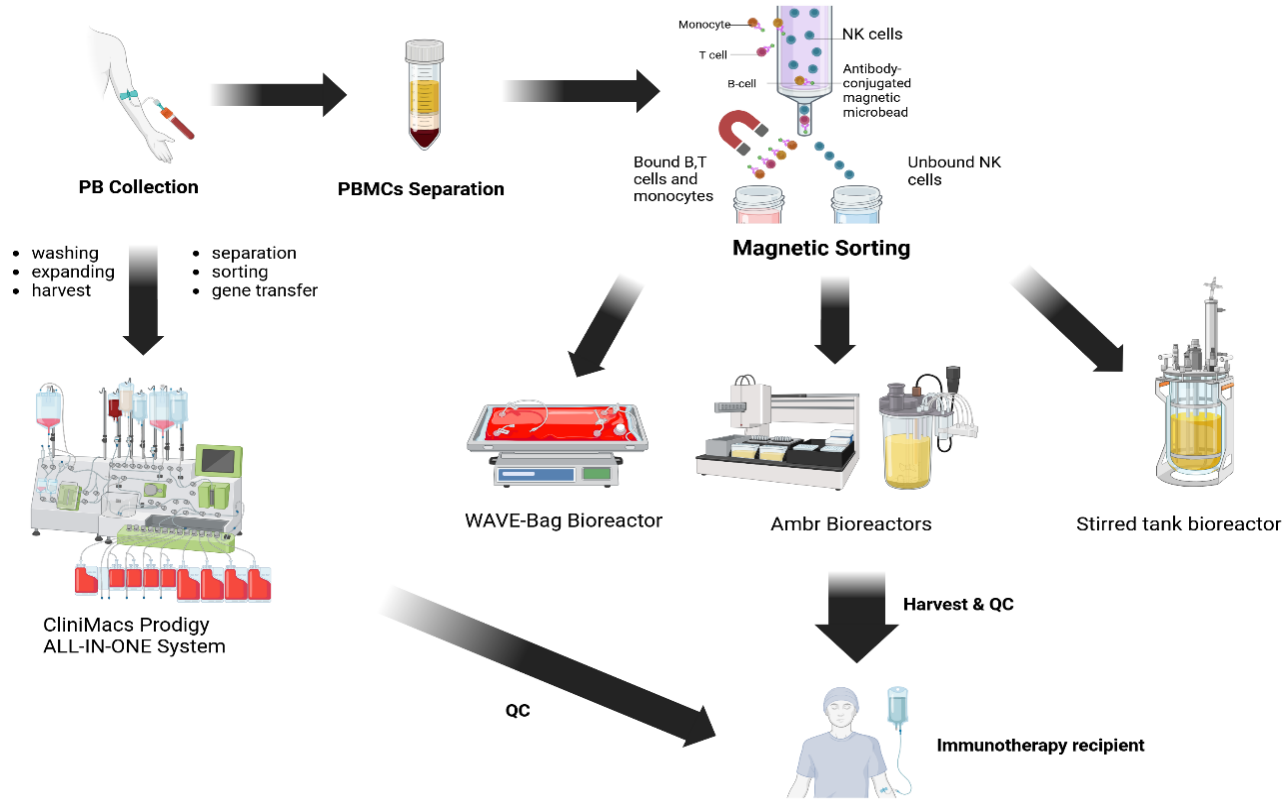

Figure 4: ***Overview of dynamic NK cells expansion platforms.*** *CliniMACS device allows the user to harvest the cells in the bags prepared for administration, avoiding additional manual filling or temporary storage. Well mixed and highly versatile dynamic expansion systems enable the achievement of high volumes of precious product – cells. Pumping systems and cell retention devices open up the different fermentation modes, such as fed-batch, continuous and perfusion to achieve optimal feed of nutrients and wash out of by-products like lactate and ammonium which in high amounts affects the cell viability.*

Die approbierte gedruckte Originalversion dieser Diplomarbeit ist an der TU Wien Bibliothek verfügbar
The approved original version of this thesis is available in print at TU Wien Bibliothek.

1.4.4 Expansion of NK-92 cells

Use of a master cell bank, e.g. NK-92 cell line is an attractive option in manufacturing of cellular therapy products because the cell source can be thoroughly standardized and characterized [82]. Moreover, NK-92 cell line avoids the need for donor selection and enables the production of large cell doses making them attractive source of the "off-the-shelf" immunotherapies from a frozen cell bank [83].

Author/ Year	Expansion platform	Cultivation mode	Priming/ activation	Media/Serum	Duration [days]	Fold-expansion	Used in clinical trial Yes/No
Tam/2003[84]	bags	PB	IL-2	X-Vivo 10 2.5% HS	15-17	218-250-fold	N/A
Arai/2008[56]	bags	PB	IL-2	X-Vivo 10 2.5% HS	15-17	218-250-fold	yes/P1
Tonn/2013[60]	bags	B	IL-2	X-Vivo 10 5% hi HS	9	35-fold	yes/P1
Boyiadzis/ 2017[57]	T25(10 days) Grex10 Grex100	PB	IL-2	X-Vivo 10 5% hi HS	24	64-fold (from Grex10)	yes/P1/2
Williams/2017[59]	bags	PB	IL-2	X-Vivo 10 2.5% HS	21	128-fold	yes/P1/2
Lee/2024[85]	T-flask Wave 2 L Wave 10 L	RB Perfusion	IL-2	Cytiva_Xuri Tcell 5% hi HS X-Vivo 10 5% hi HS	21-22 all conditions (Days in preculture in T-flask added!)	100-fold in all conditions (different exp.time)	N/A

Table 4: ***Summary of NK-92 cell line expansion protocols with focus on direct usage in clinical trial.*** *X-Vivo 10 supplemented with 2.5-5% human serum and IL-2 was universally used across all studies in different expansion platforms which resulted in high fold expansion after 2-3 weeks of culturing. Similar to studies with primary NK cells, the usage of dynamic systems is very limited or undesirable. Widely used pulsed batch or repetitive batch fermentation modes were extended to perfusion mode only once in study of Lee et al, disclosing very conservative expansion approach in culturing of NK-92 cells.*

Die approbierte gedruckte Originalversion dieser Diplomarbeit ist an der TU Wien Bibliothek verfügbar
The approved original version of this thesis is available in print at TU Wien Bibliothek.

As can be seen in *Table 4*, bags, T-flasks and G-Rex bottles are still widely used for NK-92 cells expansion, similarly to primary NK cells. Also, protocols up to three weeks in duration with X-Vivo 10 as complete medium and 2.5-5% human serum seems to be the standard, which was set at the beginning of 21st century and was even used for couple of clinical trials. Assuming that clinical trials using cellular therapies will expand, controlled systems, such as the bioreactor will become increasingly important in maximal cell production as well as documenting the quality assurance of cellular products[66]. Recently, Lee et al. conducted experiments to evaluate the NK-92 expansion efficiency performance in two media – Xuri (Cytiva) and X-Vivo10(Lonza). Choosing 2 L and 10 L Wave bioreactor as expansion platform, they were able to generate 1 x 10^{10} Cells and 2.5 x 10^{10} Cells in 2L and 10L-Wave respectively, demonstrating similar performance of aforementioned two media. T-flask cultures were run in parallel and ended up at same fold-expansion and expansion duration. However, the study was mainly focused on comparing the media, assessment of cell stability and target cell killing immediately after thawing. Therefore, cytotoxicity results during and at the end of expansion are missing[85].

With this in mind and multiple other expert opinions expressed in decent number of reviews[76, 86-89], highlighting the importance of further investigation of bioreactor expansion platforms, decision to explore stirred bioreactor as a promising platform for NK-92 cells would be beneficial. Subsequently, important considerations like impeller compatibility and agitation speed approximation together with the methods for the cell culture, cell count, and cytotoxicity assessment will be presented.

Die approbierte gedruckte Originalversion dieser Diplomarbeit ist an der TU Wien Bibliothek verfügbar
The approved original version of this thesis is available in print at TU Wien Bibliothek.
TU Bibliothek Your knowledge hub WIEN

2 METHODS

2.1 Preculture maintenance and bioreactor preparation

NK-92 were precultured in vented T25-T175 T-flasks (Nunc) in incubator (Binder, model CB-S 170) at 37°C and 5% CO_2 further referred as static expansion platform. In parallel, NK-92 were precultured in the same incubator in 250 mL vented polycarbonate shakeflasks (Corning) on a shaker platform with 2.5 cm orbital diameter at 85 rpm, as depicted in supplementary figure *S 2*. Cultivation in shake flasks together with stirred tank bioreactor will be further referred as dynamic expansion platforms. Alongside NK-92 cells, the K562-GFP reporter cell line were precultured in T75 flasks in the same incubator at same conditions as static NK-92. The complete culture media for the expansion of NK-92 and K562-GFP cell lines in cell culture flasks have been previously optimized in the laboratory. Components of NK-92 α-MEM media and K562-GFP RPMI 1640 media and their concentrations are listed in Table 5 and Table 6[90, 91]. Components marked as bold text were supplied extra on top of what was already present in commercially available media or added separately in order to meet the internal requirements for NK-92 and K562-GFP expansion. Human serum (PanBiotech, Cat,Nr. P30-0702) was added separately during cell passage. IL-2 (Miltenyi Biotec, Cat.Nr.130-097-74) was supplemented directly to the cells every second day at a concentration of 500 IU/mL.

For both cell lines, seeding density was always maintained at 0.2 $\cdot 10^6$ viable cells/mL. Complete or only half of the medium for NK-92 cells was replenished every second day by centrifugation at room temperature (rt), 300 xG/3 min and gentle resuspension of cells. Human serum was centrifuged at 15000 xG/15 min/ 4°C to remove excessive lipid, triglycerides and cloth to avoid needle blocking and high background signal in flow cytometer. K562-GFP cells were splitted 1:4 every second day and maintained in T75-flask. Both cell lines were sampled and counted every other day using flow cytometer to monitor the viable cell concentration and viability.

Starting from 1.75 $\cdot 10^6$ viable NK-92 cells in T25-flask, cells were expanded to 15 $\cdot 10^6$ viable cells in T175-flask, splitted 1:10 and reseeded in 250 mL shake flask to start the cell adaptation to shaking conditions. Remained cells in T175-flask were expanded to reach absolute cell number of at least 24 $\cdot 10^6$ viable cells and were used as a starter culture for static expansion platform. After one week of adaptation, viable cells from shake flasks were splitted into another six shake flask and expanded to reach the absolute number of at least 156 $\cdot 10^6$ Cells . These cells were intended to be used as a starter culture for dynamic expansion platforms – shake flasks and bioreactor.

Die approbierte gedruckte Originalversion dieser Diplomarbeit ist an der TU Wien Bibliothek verfügbar
The approved original version of this thesis is available in print at TU Wien Bibliothek.

Supplement	Initial concentration [mg/L]	Adjusted final concentration [mg/L]
Amino acids		
L-Arginine	127.0	200.2
L-Asparagine-H_2O	50.0	57.3
Glycine	50.0	
L-Alanine	25.0	
L-Aspartic acid	30.0	
L-Cysteine hydrochloride-H_2O	100.0	
L-Cystine 2HCl	24.0	
L-Glutamic Acid	75.0	
L-Glutamine	292.0	366.0
L-Histidine	42.0	
L-Isoleucine	52.4	
L-Leucine	52.4	
L-Lysine	72.0	
L-Methionine	15.0	
L-Phenylalanine	32.0	
L-Proline	40.0	
L-Serine	25.0	39.0
L-Threonine	48.0	
L-Tryptophan	10.0	
L-Tyrosine disodium salt	52.0	
L-Valine	46.0	
Vitamins		
Ascorbic Acid	50.0	
Biotin	0.1	
Choline chloride	1.0	
D-Calcium pantothenate	1.0	
Folic Acid	1.0	
Niacinamide	1.0	
Pyridoxal hydrochloride	1.0	
Riboflavin	0.1	
Thiamine hydrochloride	1.0	
Vitamin B12	1.36	
Myo-inositol	2.0	34.7
Inorganic salts		
Calcium Chloride (CaCl2) (anhyd.)	200.0	
Magnesium Sulfate (MgSO4) (anhyd.)	97.67	
Potassium Chloride (KCl)	400.0	
Sodium Chloride (NaCl)	6800.0	
Sodium Phosphate monobasic (NaH2PO4-H2O)	140.0	
Calcium Chloride (CaCl2) (anhyd.)	200.0	
Other components		
D-Glucose	1000.0	4568.8
Lipoic Acid	0.2	
Phenol Red	10.0	
Sodium Pyruvate	110.0	
β-mercaptoethanol		1.1
Sodium hydrogen carbonate		2000
Insulin		10
Transferrin		5.5
Sodium selenite		0.007
IL-2		500 IU/mL
Human serum		10% (v/v)

Table 5*: Adjusted complete media used for culturing of NK-92. Components marked as bold text were added separately or on top of what was already present in commercially available a-MEM media.*

Die approbierte gedruckte Originalversion dieser Diplomarbeit ist an der TU Wien Bibliothek verfügbar
The approved original version of this thesis is available in print at TU Wien Bibliothek.

Supplement	Initial concentration [mg/L]	Adjusted final concentration [mg/L]
Amino acids		
Glycine	10.0	
L-Arginine	200.0	
L-Asparagine	50.0	
L-Aspartic acid	20.0	
L-Cystine 2HCl	65.0	
L-Glutamic Acid	20.0	
L-Glutamine	300.0	584.6
L-Histidine	15.0	
L-Hydroxyproline	20.0	
L-Isoleucine	50.0	
L-Leucine	50.0	
L-Lysine hydrochloride	40.0	
L-Methionine	15.0	
L-Phenylalanine	15.0	
L-Proline	20.0	
L-Serine	30.0	
L-Threonine	20.0	
L-Tryptophan	5.0	
L-Tyrosine disodium salt dihydrate	29.0	
L-Valine	20.0	
Vitamins		
Biotin	0.2	
Choline chloride	3.0	
D-Calcium pantothenate	0.25	
Folic Acid	1.0	
Niacinamide	1.0	
Para-Aminobenzoic Acid	1.0	
Pyridoxine hydrochloride	1.0	
Riboflavin	0.2	
Thiamine hydrochloride	1.0	
Vitamin B12	0.005	
i-Inositol	35.0	
Inorganic Salts		
Calcium nitrate ($Ca(NO_3)_2 4H_2O$)	236.0	
Magnesium Sulfate ($MgSO_4$) (anhyd.)	120.0	
Potassium Chloride (KCl)	75.0	
Sodium Chloride (NaCl)	58.0	
Sodium Phosphate dibasic (Na_2HPO_4) anhydrous	142.0	
Other Components		
Glutathione (reduced)	1.0	
Phenol Red	5.0	
D-Glucose	2000.0	4500.0
$NaHCO_3$		2000.0
Hi-FBS		10% (v/v)

Table 6*: Adjusted complete media used for culturing of K562-GFP cells. Components marked as bold text were added separately or on top of what was already present in commercially available RPMI 1640 media.*

Die approbierte gedruckte Originalversion dieser Diplomarbeit ist an der TU Wien Bibliothek verfügbar
The approved original version of this thesis is available in print at TU Wien Bibliothek.

Sartorius Univessel 2 L glass stirred tank bioreactor (Sartorius, Germany) was assembled as shown in Figure 5. Additional information about stirrer configuration, positioning of sample tube and permittivity sensor is provided in Figure 6. Moreover, Figure 7 provides a better overview over all installed connections and probes. Preparation procedure started from installation and calibration of pH probe (two-point) prior autoclavation. Once this was done, all tubes, air filters, liquid filters and probes were installed and the bioreactor was autoclaved (Systec, Germany) for 30 min at 120°C, 1 bar overpressure and cooled down overnight.

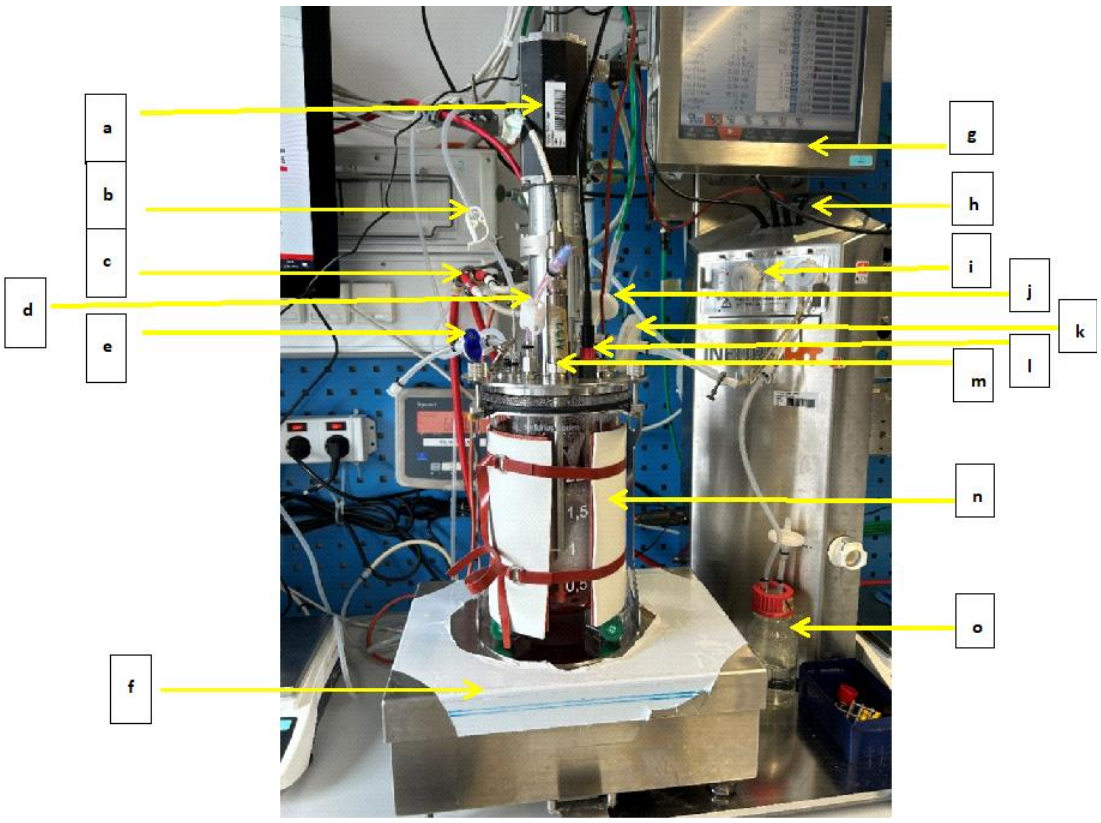

Figure 5: *Bioreactor final assembly after autoclavation and before the inoculum with NK-92 cells.*

a	Stirrer motor (Inforns,DC/140W, Switzerland)
b	Batch media feed
c	Off-gas cooler in/out tubings (Infors)
d	Sampling port (Sartorius,Germany)
e	IL-2 addition port with 0.2 µm filter (B.Braun, Germany)
f	Reactor scale (Kern,Germany)
g	Tower control screen (Infors)
h	MODBUS connections plate
i	Tower peristaltic pump (not used)
j	Air filter for aeriation via sparger (Milipore, USA)
k	Air filter for headspace aeriation (not used)
l	pH probe (Hamilton, Switzerland)
m	Permittivity probe (Hamilton Incyte)
n	Heating blanket 120/230 V (Volton, Germany)
o	0.5 M $NaHCO_3$ for pH adjustment (not used)

Table 7: *List of reactor satellites, tubings and external devices as shown in Figure 5. Due to explorative nature of planned experiment, several connections were coupled with the idea to be more flexible during cultivation but at the end not used. Sodiumhydrogencarbonate solution was prepared and connected to reactor via peristaltic pump in case of very quick pH-decrease and the need to adjust it. Air filter for headspace aeriation was prepared for the case of sparger blocking due to serum protein precepitation during exponential cell growth phase. Important to note that DO probe was installed behind the stirrer motor, away from sparger and is therefore not visible in the figure above.*

Die approbierte gedruckte Originalversion dieser Diplomarbeit ist an der TU Wien Bibliothek verfügbar
The approved original version of this thesis is available in print at TU Wien Bibliothek.
TU Bibliothek Your knowledge hub WIEN

Next day, the bioreactor was placed on scales (Kern, Germany), coupled to the cooling water and connected to process air aeriation tubes via 0.2 µm air filter (Sartorius, Germany). After that, the thermostat (Lauda, Germany) was switched on to cool down the circulating water in off-gas cooler to 10°C and the heating jacket was wrapped around the glass body of the bioreactor. Next, 480 mL of sterile a-MEM complete media and 60 mL of sterile human serum (AB,off-the-clot) were pumped into the reactor via media feeding port using peristaltic pump (Watson-Marlow, 120U, Austria) at 60 mL/min flow rate. Heating control unit on tower (Infors, Switzerland) was then turned on with 37°C set-point. As a next step, stirrer motor (Infors, DC/140W) was started at 95 rotations per minute (rpm). Lastly, the process air and carbon dioxide were supplied to the reactor through the 0.2 µm gas filter and entered the liquid phase through the microsparger at flow rates of 5.7 mL/min and 0.3 mL/min accordingly. All set points are additionally summarized in

Table **8**. To finalize the preparation phase, Lucullus API (data acquisition for reactor scales and off-gas analyzer) and Hamilton ArcAir Software (data acquisition DO and permittivity) were checked for signal consistency and bioreactor was left to equilibrate overnight.

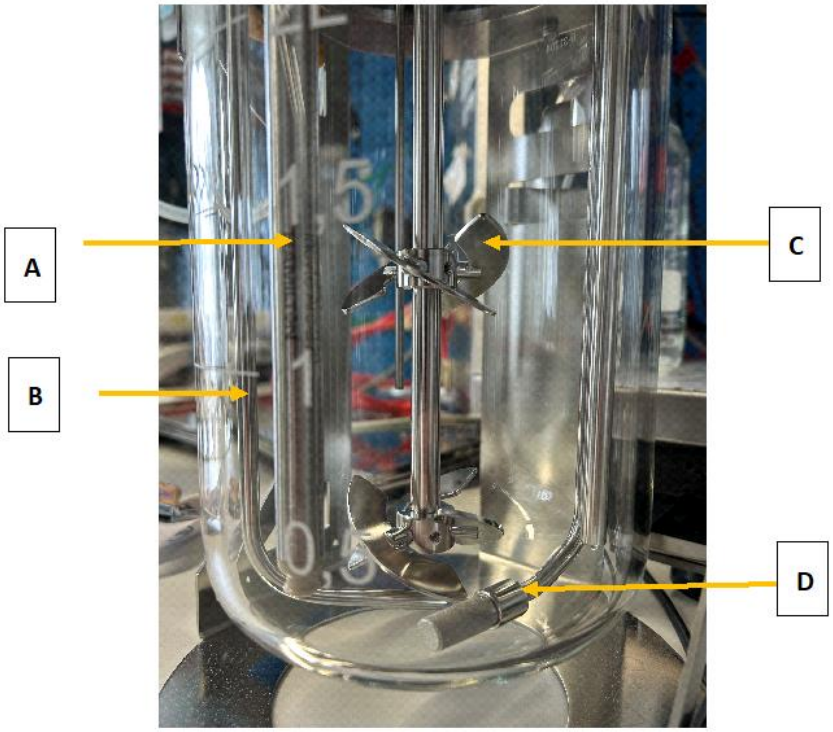

Figure 6: *This figure serves the purpose for better visualization of reactor inner parts which cannot be seen at Figure 5.* ***A:*** *permittivity sensor* ***B:*** *sampling tube* ***C:*** *impeller* ***D:*** *microsparger. Sampling tube was placed right underneath the impeller to assure the representative sample collection. Two 30°, three-blade segment impellers were mounted on stirrer shaft but only one was operated in liquid phase.*

Die approbierte gedruckte Originalversion dieser Diplomarbeit ist an der TU Wien Bibliothek verfügbar
The approved original version of this thesis is available in print at TU Wien Bibliothek.

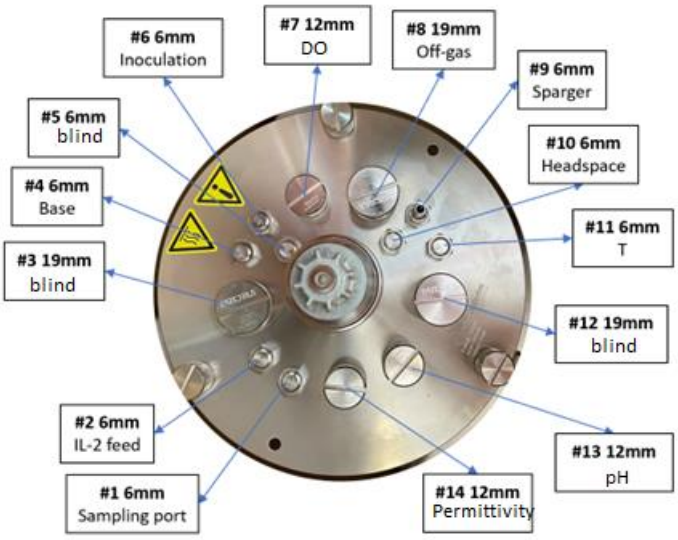

Figure 7: *Thread sizing, positioning of sensors and tube connections. Stirrer coupling point is in the middle. Positions nr.3 and nr.12 with 19 mm thread size and position nr.5 with 6 mm thread size were not used and therefore closed with blind plugs. Inoculation port was used twice, for medium fill and inoculum. Base ($NaHCO_3$) and headspace aeriation tubings were coupled to reactor but not used.*

Bioreactor characteristic/ process parameter	**Type/Dimension/set-point**
General	
Bioreactor scale (working volume) [L]	0.6
H/D ratio (tank height to tank ID)	1.8
D/T ratio (impeller ID to tank ID)	0.41
$\boldsymbol{k_L a}$ [h-1]	0.05
T [°C]	37
Stirrer	
Stirrer speed [rpm]	95
Impeller number/type	1/three 30° pitched-blades
Impeller ID [mm]	54
Power number	0.7
$(\mathbf{P/V})_{ø}$ [W/m3]	2.12
Aeration	
Sparger type	Micro sparger
Air flow rate [mL/min]	5.7
CO2 flow rate [mL/min]	0.3

Table 8: *Summary of bioreactor characteristics and set points. Calculation of k_La and P/V ratio is shown below in the subchapter 2.5.*

Die approbierte gedruckte Originalversion dieser Diplomarbeit ist an der TU Wien Bibliothek verfügbar
The approved original version of this thesis is available in print at TU Wien Bibliothek.

2.2 NK-92 inoculation in T-flasks, shake flasks and bioreactor

On Day 0 (Inoculation), precultured NK-92 cells from static and dynamic precultures were harvested and counted, as described later in the subchapter 2.5. Cells from shake flasks which were adapted to shaking conditions were pooled, spun down at 300 xG/3 min/rt and resuspended in 60 mL fresh complete α-MEM media. Cell suspension was then pumped into an already equilibrated reactor using same peristaltic pump as described before (flowrate 60 mL/min) and shown in supplementary figure *S 1*. Final concentration of NK-92 cells in bioreactor at D0 was $0.2 \cdot 10^6$ cells/mL.

Due to the handling error during removal of old media after centrifugation of dynamic precultures, the final cell number of NK-92 cells adapted to shaking conditions were only enough to start the bioreactor cultivation ($120 \cdot 10^6$ cells), but not the cultivation in shake flasks. Therefore, another $36 \cdot 10^6$ viable cells were taken from static T175-flask preculture and reseeded in three shake flasks with 60 mL in each, at final concentration of $0.2 \cdot 10^6$ cells/mL without adaptation.

NK-92 static precultures were harvested from preculture T175-flasks, spund down at 300 rpm/3 min/rt and resuspended in 108 mL fresh α-MEM complete media and 12 mL human serum (AB, off-the-clot). Cell suspension was then aliquoted into twenty T25-flasks 6 mL in each at final concentration of $0.2 \cdot 10^6$ cells/mL. Both T-flask and shake flask cultures were placed in an incubator at 37°C, 5 Vol.% CO_2 as shown in supplementary figure *S 2* . Additionally, shake flasks were placed on orbital shaker with 2.5 cm orbital diameter (Edmund Bühler, Germany) at 85 rpm.

2.3 Harvesting and off-line analytics

Several process variables like concentration of nutrients like glucose and glutamine and metabolites like pyruvate, lactate, ammonium ions and glutamate, as well as pH (T-flasks and shake flasks) were measured off-line. Viable cell concentration and cytotoxicity of NK-92 cells against K562-GFP reporter cell line were also measured off-line using flow cytometer.

The cells from bioreactor were harvested through check valve sampling port using the sterile 10 mL syringe (B.Braun, Austria). To collect the representative culture sample from bioreactor, the first 5 mL of dead volume from sample tube were discarded and only the second 5 mL were harvested and further analyzed. Cells from shake flasks were taken out from incubator, weighted, sampled (average of 2 mL) under the laminar flow in sterile cabinet and then placed back to incubator. To avoid the disruption of cell aggregates and cell growth distortion, the whole volume (6 mL) of correspondent T-flasks was collected and the flasks discarded. Addition of 5 mL IL-2 to bioreactor was done through another port, equipped with 0.2 µm liquid filter (B.Braun, Austria). Cells in shake flasks and T-flasks were supplied with 60 µL and 6 µL of IL-2 stock solution accordingly by careful addition directly into the vessels in

Die approbierte gedruckte Originalversion dieser Diplomarbeit ist an der TU Wien Bibliothek verfügbar
The approved original version of this thesis is available in print at TU Wien Bibliothek.
TU Bibliothek Your knowledge hub WIEN

sterile cabinet under the laminar flow. IL-2 adding regimen and final concentration was held the same as during preculture - every second day at final concentration of 500 IU/mL in all vessels. No further feeding was done to any culture, as supposed by batch process principles. An overall off-line analytics plan is shown and described in Figure 8.

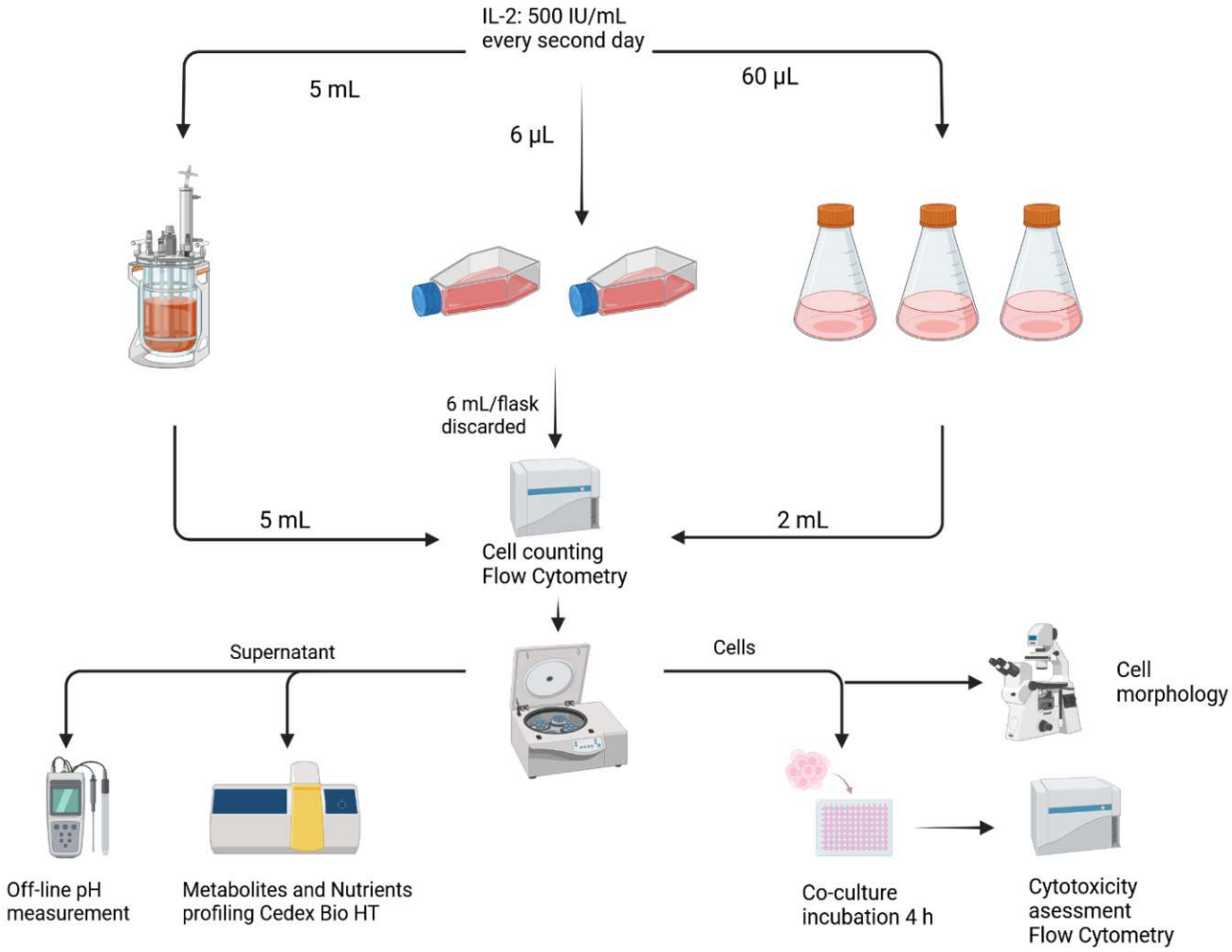

Figure 8: ***Experimental plan and analytical procedures***. *After harvesting the cells, the sample volume was divided between cell counting, cytotoxicity assay and the rest of the analytics. For this, maximum of 1 mL of cell suspension from each expansion platform was collected and used for cell counting on flow cytometer. Upon receiving the cell counts, the next portion of sample volume was used for co-culture incubation with K562-GFP cells. Detailed proceedings for sample preparation are described later. The rest was spun down at 300 xG, 3 minutes, rt. Supernatant was used for metabolites and nutrients tracking and external pH measurements. Cell pellet was resuspended in a-MEM medium without human serum and used for assessment of cell morphology under the light microscope.*

Die approbierte gedruckte Originalversion dieser Diplomarbeit ist an der TU Wien Bibliothek verfügbar
The approved original version of this thesis is available in print at TU Wien Bibliothek.

2.3.1 Cell counting and viability assessment

Samples during preculture and main experiment were counted on Cytoflex S (Beckmann-Coulter) flow-cytometer. Mix of beads with the size from 2 µm to 10 µm was measured prior cell counting in order to set the parental gate P1 in the right position on SSC/FSC plot, as demonstrated in Figure 9, section A. In practice, 150 µL cell suspension was pipetted with 50 µL counting beads and 50 µL 10 µg/mL 7-AAD stock solution in 96-well plate and placed into Cytoflex-S plate reader. By staining the cells with 7-Aminoactinomycin D (7-AAD) fluorescent dye which emission maxima can be detected at 690 nm, it was possible to differentiate between live and dead cells due to the ability of this DNA-intercalating dye to penetrate through cell membrane of apoptotic cells and thus causing a shift in side-scatter signal. To quantify this signal, the counting beads with defined size and light scatter properties were added to the cell sample as an internal standard and plotted against R712 channel as shown in Figure 9, section B. The following equation was used to calculate the viable cell count:

$$Absolute\ count\ \left(\frac{Cells}{\mu L}\right) = \frac{Cell\ count\ x\ counting\ beads\ volume}{Counting\ beads\ count\ x\ cell\ volume} x\ Counting\ beads\ concentration\ \left(\frac{beads}{\mu L}\right) \qquad \textbf{(Equation 1)}$$

To express viability as a percentage of viable cells from total amount of cells following gating strategy was applied:

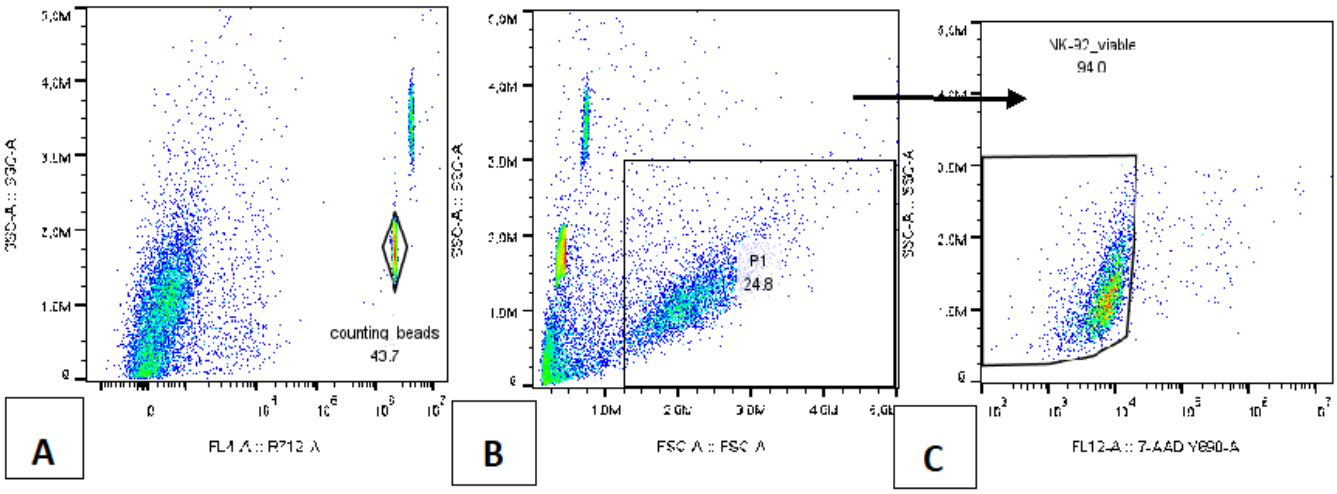

Figure 9: ***Gating strategy to assess viable cell concentration and cell viability in one sample replicate from Reactor measured on D0.*** ***B****: Selecting the 7000 counts for counting beads from overall population in R712-A channel.* ***C****: Setting the borders for overall population of NK-cells at SSC-A and FSC-A axis – Parental gate P1.* ***D****: Selecting the characteristic SSC-A count for viable cells by plotting it against 7-AAD fluorescence channel – Y690-A. "NK-92_viable" gate with 94% viable NK-92 cells in it represents the ratio of viable NK-92 cells to all counts acquired in P1-gate and captured in Y690-A channel.*

Die approbierte gedruckte Originalversion dieser Diplomarbeit ist an der TU Wien Bibliothek verfügbar
The approved original version of this thesis is available in print at TU Wien Bibliothek.

2.3.2 Cytotoxicity assay

To assess the killing activity of NK-92 effector cells towards co-cultured K562-GFP target cell line an additional fluorescent dye to the 7-AAD was used – Annexin V. Living NK-92 and K562-GFP cells maintain a distinct membrane asymmetry, with different phospholipids segregated into specific leaflets of the cell membrane[92]. For example, aminophospholipids like phosphatidylserine (PS) which is restricted to the inner leaflet. However, when a cell undergoes apoptosis, the membrane asymmetry is disrupted, leading to the exposure of PS on the outer leaflet of the cell membrane[92]. In this altered state, PS becomes accessible for recognition and binding by specific antibodies or proteins, such as Annexin-V. Annexin-V can not only bind to phosphatidylserine externalized on apoptotic cells, but also binds to the internal PS of permeable necrotic cells [93]. Therefore, in combination with 7-AAD, not only a reliable measurement of apoptosis was possible, but also the categorization into early apoptotic, late apoptotic and necrotic state of target cell. Moreover, purchased K562-GFP cell line enabled better discrimination between effector and target cells due to intracellular expression of Green Fluorescent Protein (GFP) and the strong signal with emission maxima at 509 nm.

In practice, after counting the cells, the sample volume needed to obtain 0.5 $\cdot 10^6$ NK-92 cells from each expansion platform was calculated and collected in 15 mL sample tube from each expansion vessel correspondently. Same number of K562-GFP cells was collected in another 15 mL sample tube. Both cell lines, independently from each other were centrifuged at 300 xG/3min/rt and resuspended in fresh α-MEM media to obtain 0.1 $\cdot 10^6$ cells/mL. After that, 100 µL of NK-92 and 100 µL of K562-GFP were pipetted in V-bottom 96 well-plate to form co-culture, as shown in *Figure 10*. Additionally, 200 µL of K562-GFP cells and 200 µL NK-92 cells were pipetted separately in different wells as negative controls. The 96-well plate was spun down 1 minute at 100 xG for cells to settle down and incubated for 4 hours at 37°C / 5 Vol.% CO_2. After incubation, the media was discarded and remaining cells were washed twice with 200 µL FACS-Buffer (1x PBS, 1% BSA, 0.1% NaN_3). After washing and centrifugation 300 xG/3 min/rt, cells were resuspended in 100 µL 0.3 µg/mL Annexin V stock solution and incubated for 15 minutes in darkness. After incubation, cells were spun down 300 xG/3 min/rt and washed once only with 150 µL Annexin binding buffer, to wash out the unbounded Annexin V. As a last step, cells were resuspended in 200 µL FCM-buffer and 50 µL 10 µg/mL 7-AAD stock solution and loaded into plate reader in flow cytometer.

Die approbierte gedruckte Originalversion dieser Diplomarbeit ist an der TU Wien Bibliothek verfügbar
The approved original version of this thesis is available in print at TU Wien Bibliothek.

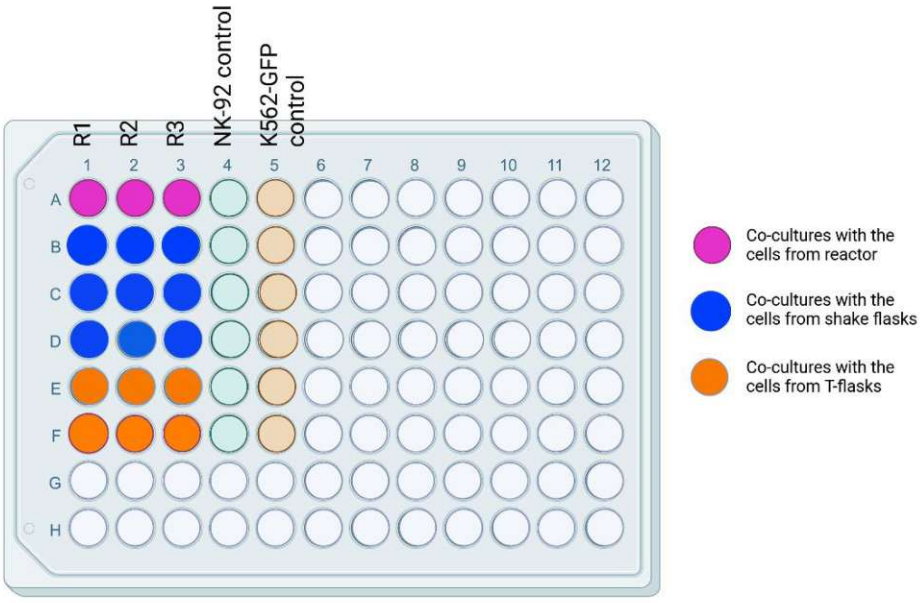

Figure 10: Loading scheme for cytotoxicity assay in V-bottom 96-well plate. *Additionally to co-cultures, assay also includes the measurement of negative controls with only NK-92 cells from corresponding expansion platform and only K562-GFP, expanded in parallel in T-flasks.*

To be able to compare all measurements in our experimental setting with three different fluorescent chromophores (7-AAD, GFP, Annexin V) and two different cell lines, the voltage needed to accelerate the electron through detector had to be adjusted. Consequently, compensation matrix was empirically measured according to Cytoflex workflow sheet and applied to our detector settings during the cytotoxicity assay.

Using the gating strategy described below in *Figure 11* (Plot A B, D, F), the percentage of viable and apoptotic/necrotic K562-GFP and NK-92 cells was outlined. After subtracting the percentage of spontaneous cell lysis observed in K562-GFP negative control, the specific lysis of K562-GFP cells as a result of NK-92 cytotoxic activity can be formulated analogue to the equation described by Qili et al.[94]

$$Cytotoxicity\% = \frac{(100 - K562_{dead_{cc}})\% - (100 - K562_{dead_{ctrl}})\%}{K562_{dead_{ctrl}}\%} \quad \textbf{(Equation 2)}$$

$K562_{dead_cc}$ ... sum of early apoptotic, late apoptotic and necrotic K562-GFP cells in co-culture %

$K562_{dead_ctrl}$ ... sum of early apoptotic, late apoptotic and necrotic K562-GFP cells in negative control %

Similar to equation above the number of apoptotic/necrotic NK-92 cells can be formulated and provides additional insight at reversive effect on NK-92 after co-culturing with K562-GFP target cells:

$$Apoptotic\ NK92\ after\ target\ killing\ \% = \frac{(100 - NK92_{live_{cc}})\% - (100 - NK92_{live_{ctrl}})\%}{NK2_{live_{ctrl}}\%} \quad \textbf{(Equation 3)}$$

Die approbierte gedruckte Originalversion dieser Diplomarbeit ist an der TU Wien Bibliothek verfügbar
The approved original version of this thesis is available in print at TU Wien Bibliothek.
TU Bibliothek Your knowledge hub WIEN

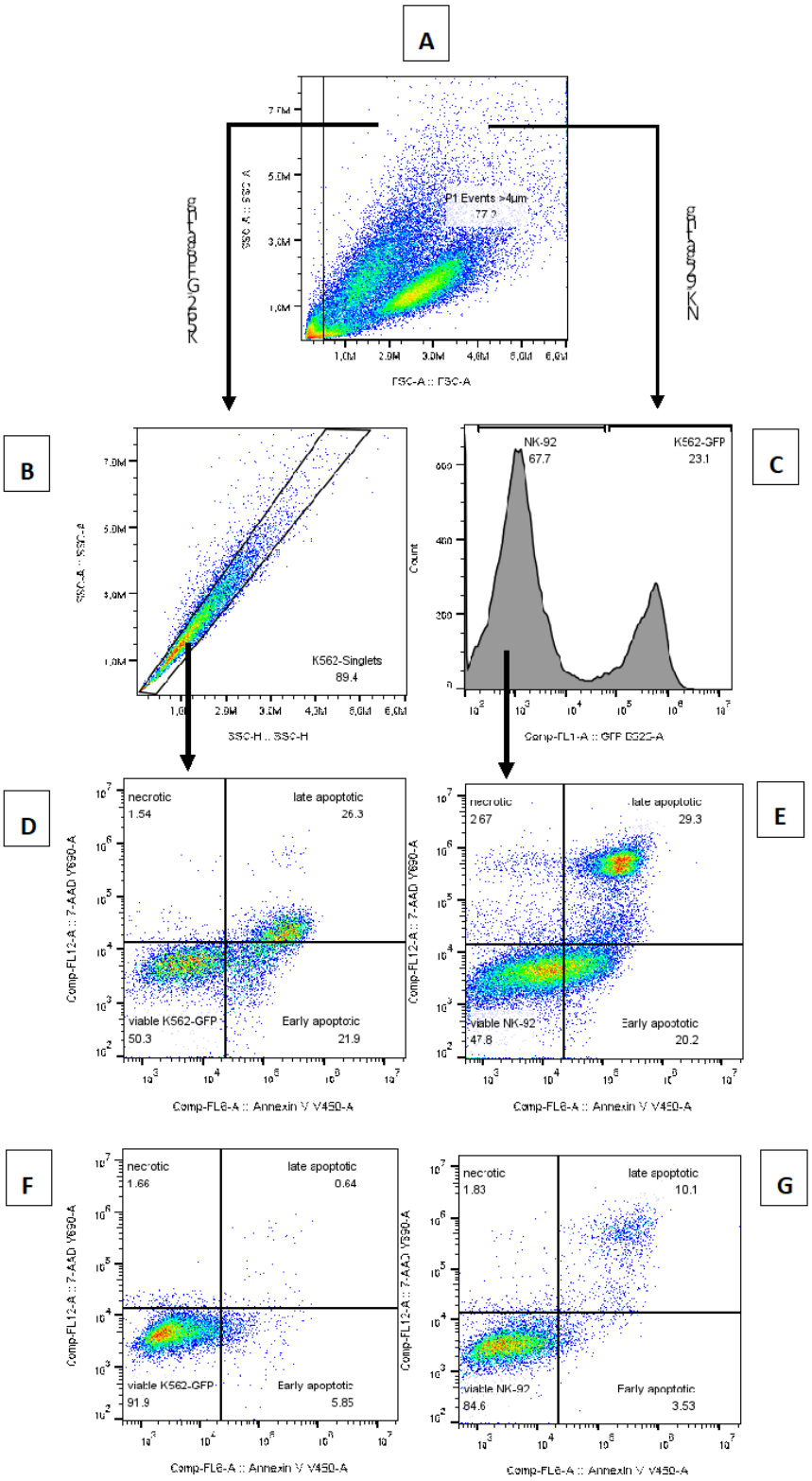

Figure 11*: Gating strategy for cytotoxicity assessment.* ***A:*** *Parental gate P1 with co-cultures after 4 h incubation at D4 in reactor.* ***B:*** *Primary selection of K562-singlets.* ***C:*** *Separating NK-92 from K562-GFP in GFP B525-A channel* ***D:*** *Subdividing of live and dead populations of K562-GFP cells in four categories using 7AAD Y690 and Annexin V V450 channels.* ***E:*** *Subdividing of live and dead populations of NK-92 cells in four categories using 7AAD Y690 and Annexin V V450 channels.* ***F:*** *K562-GFP negative control to compare with co-culture in graph D* ***G:*** *NK-92 negative control to compare with co-culture in graph E.*

Die approbierte gedruckte Originalversion dieser Diplomarbeit ist an der TU Wien Bibliothek verfügbar
The approved original version of this thesis is available in print at TU Wien Bibliothek.
TU Bibliothek Your knowledge hub WIEN

2.3.3 Nutrients and metabolites tracking on Cedex BioHT

Concentration analysis of such nutrients and metabolites like glucose, glutamine, glutamate, ammonium and pyruvate in culture supernatants was performed on Cedex BioHT analyzer (Roche). Prior analysis, two standards for each desired analyte were measured in duplicates to obtain calibration curves. To assure the method accuracy for each analyte, quality control with three assigned values for each analyte was measured in triplicates, as stated in device operation manual. None of the measured values during quality control exceeded 5% measurement error. Metabolites and nutrients concentrations were assessed via enzymatic assays and were detected photometrically. Detailed description of each enzymatic reaction is listed in Cedex BioHT manual available online. Calibration, quality control and sample measurements were done fully automated by the instrument. The only sample preparation needed was the cell separation, which was achieved through centrifugation at 300 xG/5min/rt. 200 µL of the NK-92 culture supernatant was transferred into a 1.5 ml tube and inserted into Cedex rack. Previous small experiments (data not shown) showed slightly decreasing concentration of L-glutamine and slightly increasing concentration of ammonium ions in the complete α-MEM media without cells at incubation temperature of 37°C. Therefore, values of L-glutamine and ammonia concentrations measured in cell culture samples were corrected with the corresponding values to obtain correct net depletion/production resulted solely from cell culture activity.

2.3.4 Off-line pH measurements in shake flasks and T-flasks

To measure the pH in the supernatants of the the shake flasks and T-flasks cell cultures, the laboratory pH-meter (WTW, Profiline pH3110) was used. First, two-point calibration at room temperature with the reference pH solutions 4 and 7 was performed to assure the precision of the pH electrode. After successful calibration (slope > 95%, off-set ±20 mV), the 1.5 mL sample tubes with supernatants remained after cell centrifugation were placed in incubator at 37°C and 5% CO2 atmosphere to mimic the culture conditions. After 1 hour of equilibration, the supernatants were immediately measured outside of the incubator. Obtained pH values were manually corrected with -0.02 pH units to include the temperature effect on pH when measured at 37°C instead of 25°C.

Die approbierte gedruckte Originalversion dieser Diplomarbeit ist an der TU Wien Bibliothek verfügbar
The approved original version of this thesis is available in print at TU Wien Bibliothek.

2.4 Online measurements for bioreactor process monitoring

To make one step forward towards understanding the bioprocessing of NK-92 cells, following process variables were monitored online – viable cell density, off-gas concentrations of oxygen and carbon dioxide, dissolved oxygen concentration and pH. Temperature as process parameter was set to 37°C and controlled by tower electrical output using the feedback signal from temperature sensor inside the reactor.

2.4.1 Viable cell density

To monitor cell concentration in real time inside the bioreactor, Hamilton Incyte VCD-Sensor was used. Measurement principle is based on cell capacity measurement in the presence of electrical field. Viable, but not dead cells can store the charge distribution within the cellular membrane. This charge is measured by Incyte sensor and reported as permittivity in pF/cm. Figure 12 illustrates the measurement principle.

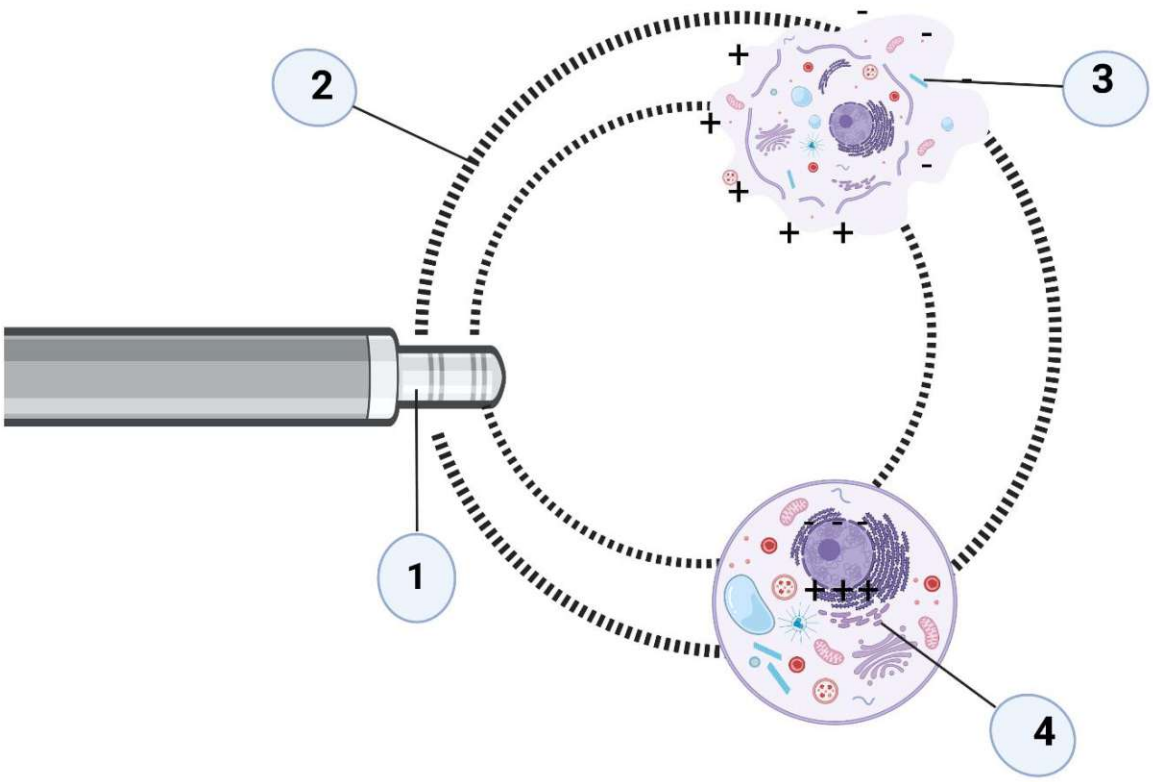

Figure 12*: **Overview of permittivity measurement principle** 1) Pt electrodes incorporated in permittivity probe 2) Electric field. 3) dead cells with damaged membrane 4) Polarized viable cells*

Die approbierte gedruckte Originalversion dieser Diplomarbeit ist an der TU Wien Bibliothek verfügbar
The approved original version of this thesis is available in print at TU Wien Bibliothek.

To quantify the permittivity signal, sensor relies on frequency scan. Viable mammalian cells possess a specific frequency, usually 1 MHz. Measurement of permittivity at this frequency can be directly correlated to viable cell density, especially during the exponential growth phase. In our case, the internal multi linear regression model with frequency scans obtained during CHO-cell bioprocessing was uploaded in ArcAir software prior inoculation with NK cells.

2.4.2 Oxygen and carbon dioxide concentrations in off-gas

To measure the off-gas concentrations, the BlueInOne Cell (BlueSens) gas analyzer was used. This gas analyzer doesn't require calibration and was flushed with process air to correct the off-set prior connection to the bioreactor. The oxygen measurement was based on paramagnetic properties of oxygen molecules. The measurement of carbon dioxide was based on interaction with infra-red radiation.

In this proof-of-concept bioreactor batch run, the process air was mixed with volume parts of carbon dioxide (5% CO_2 and 95% process air) and supplied at a constant flow rate via microsparger right underneath the stirrer as shown in Figure 6. Data acquisition was performed in Lucullus API system.

2.4.3 Dissolved oxygen

The concentration of dissolved oxygen (DO) was measured with Hamilton VisiFerm probe and was based on oxygen dependent luminescence quenching. On the day of inoculation (D0) and after overnight equilibration, the dissolved oxygen sensor was calibrated with process air at the flow rate used during the experiment. One-point (100% oxygen saturation) calibration and data acquisition was performed in ArcAir software according to the manufacturer.

2.4.4 pH

pH inside of the bioreactor was measured using Hamilton EasyFerm Plus K8 225. Two-point calibration with pH 4 and pH 7 reference solutions was performed before autoclavation of bioreactor. pH probe was connected via analog connection to the tower. Due to connection problems to data acquisition software Lucullus, pH value was monitored on tower and noted down manually three times per day. Desired pH value (7.2-7.5) was adjusted in culture media and wasn't controlled during the batch run.

Die approbierte gedruckte Originalversion dieser Diplomarbeit ist an der TU Wien Bibliothek verfügbar
The approved original version of this thesis is available in print at TU Wien Bibliothek.

2.5 CALCULATIONS

2.5.1 Growth characterization

To begin with, some general assumptions for all further calculations must be mentioned. In our case, if we consider the majority of NK-92 cell population to be $CD56^{+}CD3^{-}$, the growth model can be simplified to non-segregated (minor cell populations are not involved). As in mammalian cells, metabolism is very complicated and comprises thousands of different reactions, exact stoichiometry of which is the subject of intense holistic research. This simplifies the growth model even further to non-structured, where the cells can't be differentiated according to their metabolic profile and considered to be the same. These general assumptions were the basis for calculation of all rates and yields across this work. Equations used in this work were the part of book chapters written by Professor Paula Doran at al.[95] and Professor Horst Chmiel et al.[96].

Specific growth rate μ is well established definition of how fast the cells have grown under certain conditions and can be generalized as shown in Equation 3:

$$\mu = \ln\left(\frac{VCC_2 - VCC_1}{24}\right) [1/h] \qquad \textbf{(Equation 4)}$$

VCC ... viable cell concentration [Cells/L]

Per definition of batch-process, during the exponential growth phase, the cells are growing with maximum growth rate. To define this maximum - μ_{max} was calculated as the average of three consecutive exponential growth days:

$$\mu_{max} = \frac{\mu_{t_{exp1}} + \mu_{t_{exp2}} + \mu_{t_{exp3}}}{3} [1/h] \qquad \textbf{(Equation 5)}$$

The time needed for cells to double in their numbers comprises another useful characteristic for cell growth:

$$t_d = \frac{\ln(2)}{\mu_{max}} [h] \qquad \textbf{(Equation 6)}$$

Die approbierte gedruckte Originalversion dieser Diplomarbeit ist an der TU Wien Bibliothek verfügbar
The approved original version of this thesis is available in print at TU Wien Bibliothek.

2.5.2 Reaction rates and yields

The backbone for reaction rates calculation is based on general mass balance:

$$Cin_i * Vin_i + Cout_i * Vout_i + r_i * V_r = ci \frac{\partial V_r}{\partial t} + V_r \frac{\partial c_i}{\partial t} \quad \textbf{(Equation 7)}$$

$Cin_i * Vin_i$ ... *mass flow of substance i into the reactor [µmol]*

$Cout_i * Vout_i$ ... *mass flow of substance i out from the vessel [µmol]*

r_i... *reaction rate of substance i in vessel working volume [µmol/L/h]*

V_r ... *vessel working volume [L]*

Given the assumption for batch process, no volume flow either in nor out of the vessel occurred. In practice, the sample volume was held as small as possible to avoid the washing out of the cells. Liquid stripping with very low gas flowrate in reactor was considered very small and the weight loss due to water evaporation was negligible in all vessels. With that in mind, Equation 6 can be simplified to Equation 7 and is valid for all vessels.

$$r_i = \frac{\partial ci}{\partial t} \left[\frac{\mu mol}{L * h}\right] \quad \textbf{(Equation 8)}$$

Thus, the volumetric reaction rate of component *i* is only dependent on metabolite/nutrient concentration. To link the concentration of metabolites and nutrients at time point *t* to the cell activity at the same time, volumetric reaction rate can be divided through cell concentration to obtain the cell specific uptake/production rate. To obtain reasonable values factor 10^9 was added to the right side of Equation 8.

$$q_{x/i} = \frac{r_i}{c_x} * 10^9 \left[\frac{nmol}{10^6 cells * h}\right] \quad \textbf{(Equation 9)}$$

Cx ... *Viable cell concentration at Day X [Cells/L]*

To address the effectiveness of cell generation per unit of glucose, the total biomass yield can be formulated as:

$$Y_{X/Glc} = \frac{\mu_{total}}{q_{Glc\,total}} \left[\frac{cells}{nmol}\right] \quad \textbf{(Equation 10)}$$

Die approbierte gedruckte Originalversion dieser Diplomarbeit ist an der TU Wien Bibliothek verfügbar
The approved original version of this thesis is available in print at TU Wien Bibliothek.
TU Bibliothek Your knowledge hub WIEN

μ_{total} *... difference between the last day when the cell growth was registered and the first day of cell growth [1/h]*

$q_{Glc\ total}$ *... biomass specific glucose uptake rate for total glucose consumption, registered from the first day until last day of cellular growth*

Additionally, to showcase the glucose-lactate pair in the metabolism of NK-92 cells, lactate yield from glucose is expressed as follows:

$$Y_{Lac/Glc} = \frac{q_{\ Lac\ total}}{q_{\ Glc\ total}} \left[\frac{nmol}{nmol}\right] \quad \textbf{(Equation 11)}$$

2.5.3 Shake flask-to-stirred tank bioreactor scale-up approach

Multiple engineering parameters exist to scale-up the mammalian cell culture process from bench-top reactor to big-scale reactor. To name some – impeller tip-speed[97], volumetric O_2 mass transfer coefficient (k_La)[98] and power input per volume unit (P/V)[99]. Yet, regarding the upscale from shake flask to bioreactor, the big difference in power introducing elements – impeller and flask wall, makes scale-up procedure much more complicated and was found to be less applicable. Nevertheless, in the case of mammalian cells, where the impeller power have to be set carefully without damaging the cells, this difference might be less pronounced when considering the ratio of power input to volume unit.

P/V calculation in shake flasks

Power consumption to volume unit is regarded as one of the crucial values for characterizing and upscaling microbial cultures from shake flasks to stirred bioreactor and was first published by Sumino et al. in 1972. Later in 2000-2001 Büchs et al. published three scientific papers, where two new approaches of power measurement were introduced. First was the measurement of a mechanical torque with indicator placed in the external drive of the shaking platform agitator, describing the average specific power input per unit volume $P/V_{Ø}$. Second was the measurement of drop size as indicator of agitator intensity and formulation of maximum specific power consumption to average specific power consumption ratio - $(P/V)_{max}/(P/V)_{Ø}$, which included differentiation between "in-phase" shaking (predominantly turbulent flow) and "out-of-phase" shaking (low rpm or elevated viscosity of culture)[100-102]. In this work, the $P/V_{Ø}$ in shakeflasks will be calculated based on the torque measurement experiments and the model elucidated by Büchs et al. In their first work Büchs et al. derived $P/V_{Ø}$ from torque (M) and angular velocity (w) measurements in shake flasks and related them to modified power number Ne':

$$(P/V)_{Ø} = M * w = Ne' * \frac{\rho * n^3 * d^4}{V_L^{2/3}} \quad \textbf{(Equation 12)}$$

Die approbierte gedruckte Originalversion dieser Diplomarbeit ist an der TU Wien Bibliothek verfügbar
The approved original version of this thesis is available in print at TU Wien Bibliothek.
TU Bibliothek Your knowledge hub WIEN

With Ne´ being dimensionless power number adapted to shakeflasks and defined as:

$$Ne' = C_1 * Re^{-0.2} \quad \textbf{(Equation 13)}$$

resulting in:

$$(\mathrm{P/V})_{Ø} = C_1 * Re^{-0.2} * \frac{\rho * n^3 * {\mathrm{d}_{ID}}^4}{V_L^{2/3}} \quad \textbf{(Equation 14)}$$

With C_1 = 1.94 being a fitting parameter which occurs when $(\mathrm{P/V})_{Ø}$ measured at different shaking frequencies and filling volumes is compared to calculated $(\mathrm{P/V})_{Ø}$ by the means of least-squares nonlinear fitting described in the already mentioned work of Büchs et al. Under the assumption that turbulent flow prevails in large and small flasks, Reynolds number was formulated as:

$$Re = \frac{\rho * n * {\mathrm{d_{ID}}}^2}{\eta} \quad \textbf{(Equation 15)}$$

With following inputs, aligned with boundary condition of viscosity being low - < 4 mPa*s, which meets our case with aqueous cell suspension, we can now calculate $(\mathrm{P/V})_{Ø}$ for shaking flasks according to first work of Büchs et al:

C_1 … *fitting parameter* $(P/V)_{Ø\,measured}$ *vs* $(P/V)_{Ø\,calculated}$ = *1.94*

d_{ID} … *flask max. inner diameter = 0.0417 m*

n … *shaking frequency = 1.42 rev/s*

η … *dynamic viscosity of water at 37°C = 6.9 x* 10^{-4} *kg/m*s*

ρ … *density of water at 37°C = 993,3 kg/*m^3

V_L … *filling volume = 0.00006* m^3

Reynolds Number	3554.6
Power Number	0.38
$(\mathrm{P/V})_{Ø}$[W/m³]	2.12

Table 9: *Values calculated based on suggested workflow in Büchs´ work I.*

Die approbierte gedruckte Originalversion dieser Diplomarbeit ist an der TU Wien Bibliothek verfügbar
The approved original version of this thesis is available in print at TU Wien Bibliothek.

Same can be calculated based on work II of Büchs et al [101]. In this work, a nondimensional equation for specific power consumption calculation was demonstrated. Compared to first work where only turbulent flow was considered, the terms for laminar and transition fluid flow, which can occur at low shaking speed were considered:

$$Ne' = 70 * Re^{-1} + 25 * Re^{-0.6} + 1.5 * Re^{-0.2} \quad \textbf{(Equation 16)}$$

With $70Re^{-1}$, $25Re^{-0.6}$ and $1.5Re^{-0.2}$ being responsible for laminar, transition and turbulent flow accordingly and Reynolds number unchanged, $(P/V)_{Ø}$ can be now calculated and compared to first work.

Reynolds Number	3554.6
Power Number	0.5
$(P/V)_{Ø}$ [W/m³]	2.77

Table 10: *Values for shakeflasks, calculated based on suggested workflow in Büchs´ work II.*

The difference between calculated P/V is 24 %, which can be explained by larger errors in measurements made at low shaking frequencies (85 rpm) and, therefore, at low Reynolds number (3554.6). As for actual work, we fully relied on correction factor (1.94) elucidated from direct torque measurements of Büchs et al. Therefore, to avoid overestimation of stirring frequency in bioreactor, $(P/V)_{Ø}$ = 2.12 W/m³ resulted from (Equation 14 was used to calculate stirrer frequency in following section.

Calculation of stirrer frequency in bioreactor

With calculated $(P/V)_{Ø}$ value for shakeflasks and power number Ne = 0.7, provided by Sartorius company for Univessel 1L bioreactor and already used by Elena Costariol in her work[103] , the stirrer frequency *n* can be calculated:.

$$n = \left(\frac{(P/V)_{Ø} * V_L}{Ne * \rho * {d_{ID}}^5}\right)^{1/3} = 95\ rpm \quad \textbf{(Equation 17)}$$

d_{ID} … *impeller diameter = 0.054 m*

Ne … *power number = 0.7*

ρ … *density of water at 37°C = 993,3 kg/m³*

V_L … *filling volume = 0.0006 m³*

$(P/V)_{θ}$ ... *average power input to volume ratio = 2.12 W/m³*

Die approbierte gedruckte Originalversion dieser Diplomarbeit ist an der TU Wien Bibliothek verfügbar
The approved original version of this thesis is available in print at TU Wien Bibliothek.
TU Bibliothek Your knowledge hub WIEN

2.5.4 Volumetric oxygen uptake rate, carbon dioxide emission rate and respiration quotient

To describe the oxygen dependency of NK cells, the uptake/production rate of oxygen and carbon dioxide can be of great interest. The ability of cells to uptake the oxygen and release carbon dioxide was formulated as Oxygen Uptake Rate (OUR) and Carbon Dioxide Emission Rate (CER):

$$OUR = \frac{Q_g}{V * V_m} c_{O_2,out} - c_{O_2,in} * 1000 \text{ [mmol/L/h]:} \quad \textbf{(Equation 18)}$$

$$CER = \frac{Q_g}{V * V_m} c_{CO_2,out} - c_{CO_2,in} * 1000 \text{ [mmol/L/h]:} \quad \textbf{(Equation 19)}$$

Q_g … gas inlet flow [L/h] = 0.36 L/h

V … reactor working volume [L] = 0.6 L

V_m … molar volume of air = 22.414 [L/mol]

$c_{i,out}$, $c_{i,in}$ … in/out concentration of CO_2 / O_2 in inlet and off-gas stream = read out from off-gas analyzer

Respiratory quotient (RQ) can be related to metabolic activity of the cell. RQ = 1 indicates the match between carbon dioxide emission rate and oxygen consumption and points towards cell respiration, hence complete glucose oxidation in OXPHOS. RQ < 1 occurs when low molecular weight products are produced. Respiratory quotient (RQ) was calculated as:

$$RQ = \frac{CER}{OUR} \quad \textbf{(Equation 20)}$$

Next, biomass specific oxygen consumption rate q_{O_2} and carbon dioxide generation rate q_{CO_2} were determined by dividing the OUR/CER by the viable cell concentration:

$$q_{O_2} = \frac{OUR}{VCC} * 10^9 \text{ [nmol } 10^6 \text{ Cells}^{-1} \text{ h}^{-1}] \quad \textbf{(Equation 21)}$$

$$q_{CO_2} = \frac{CER}{VCC} * 10^9 \text{ [nmol } 10^6 \text{ Cells}^{-1} \text{ h}^{-1}] \quad \textbf{(Equation 22)}$$

Die approbierte gedruckte Originalversion dieser Diplomarbeit ist an der TU Wien Bibliothek verfügbar
The approved original version of this thesis is available in print at TU Wien Bibliothek.

2.5.5 Connection between oxygen uptake rate and volumetric mass transfer coefficient k_La

As shown in *Figure 13*, to reach cells oxygen needs to be transported from gas bubble to liquid. This transport process is highly dependent on molecular diffusion. The frequency of oxygen mass transfer is called mass transfer rate and is directly proportional to mass transfer coefficient k_L, gas-liquid interfacial area unit per volume fluid a and oxygen concentration gradient from saturated gas concentration C_o^* and gas concentration in liquid C_o. Combined to Equation 23, the oxygen transfer rate (OTR) can be now formulated:

$$OTR = k_L * \mathrm{a} * (C_o^* - C_o) \qquad \textbf{(Equation 23)}$$

C_o^* ... saturated oxygen concentration at 37°C, 1 bar pressure and 8.5 ppt Salinity (18.3 mS/cm) [mol/m3]

C_o … oxygen concentration in the liquid calculated from DO [mol/m3]

k_L ... mass transfer coefficient [m/s]

a ... gas-liquid interfacial area per unit volume fluid [m2/m3]

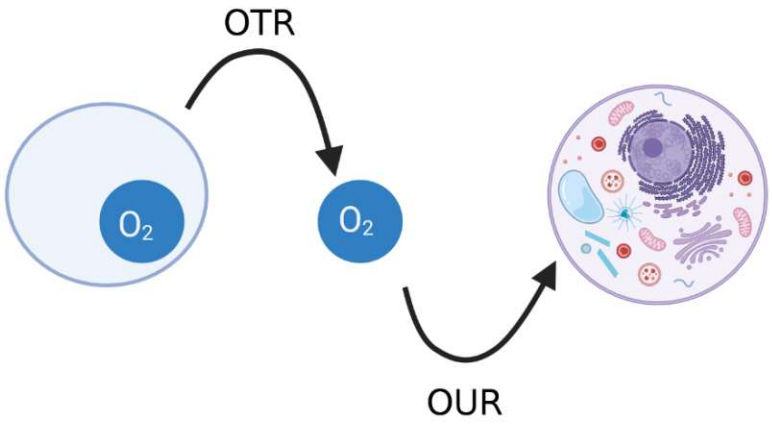

Figure 13*: OTR describes transfer from gas phase to liquid and OUR describes transfer from liquid phase into the cell.*

To determine OTR k_L and a are needed. It is extremely different though, to measure these parameters separately in turbulent flow system like bioreactor, therefore they are combined to k_La and termed volumetric mass-transfer coefficient. k_La cannot be calculated and can be only determined experimentally. In a well-mixed suspension system, the state when oxygen transferred from gas phase to liquid phase and concomitantly to the cells, is called steady state. In steady state OTR = OUR and combined with (Equation can be expressed as follows:

$$\frac{\partial c_{o2,L}}{\partial t} = \mathrm{k_L a} * (C_o^* - C_o) = q_{O_2} * \mathrm{VCC} \qquad \textbf{(Equation 24)}$$

Die approbierte gedruckte Originalversion dieser Diplomarbeit ist an der TU Wien Bibliothek verfügbar
The approved original version of this thesis is available in print at TU Wien Bibliothek.

Ultimately, to characterize the oxygen transfer in bioreactor, oxygen volumetric mass transfer coefficient k_La was experimentally determined. To obtain experimental $k_L a$, specific for the bioreactor configuration, static gassing out method was applied. First, the reactor was flushed with pure nitrogen at the same flow rate as during the experiment. After that, oxygen was scrubbed to approximately 70% and then restored with air, as supposed by static gassing out method without cells.

As a result, $(C_o{}^* - C_o)$ were obtained from DO-signal decrease and $q_{O_2} * VCC$ was calculated as suggested in (Equation . $k_L a$ was determined as a slope after assuming the $k_L a$ is constant with time and $\frac{\partial c_{o2,L}}{\partial t} = 0$. Therefore, after integration of (Equation , the resulting equation for $k_L a$ is:

$$\mathrm{k_L a} = \frac{\ln \frac{(C_o{}^* - C_{o1})}{(C_o{}^* - C_{o2})}}{t_2 - t_1} \qquad \textbf{(Equation 25)}$$

Corresponding DO measurements and obtained $k_L a$ values are presented in supplementary information section - *S 3* and *S 4*. Comparison to $k_L a$ values from literature was presented and discussed in supplementary table TS 1.

Die approbierte gedruckte Originalversion dieser Diplomarbeit ist an der TU Wien Bibliothek verfügbar
The approved original version of this thesis is available in print at TU Wien Bibliothek.

3 RESULTS AND DISCUSSION

The products of ACT are the cells themselves. That could be the adherent cells like, for e.g. human embryonic kidney cells (HEK) or mesenchymal stem cells (MSC), suspension cells like T cells or NK cells, or the cells which can be expanded in both conditions – induced pluripotent stem cells (iPSC). For each of these cell types exists several expansion protocols tailored to obtain as much as possible viable and functional cells that can be used for cell therapies. In this work we aimed to test the fit-for-purpose of stirred bioreactor as easy to scale-up and economical platform to cultivate the NK-92 cell line in comparison to well established cultivation in shake flasks and T-flasks.

3.1 Cell growth and viability of NK-92 cells

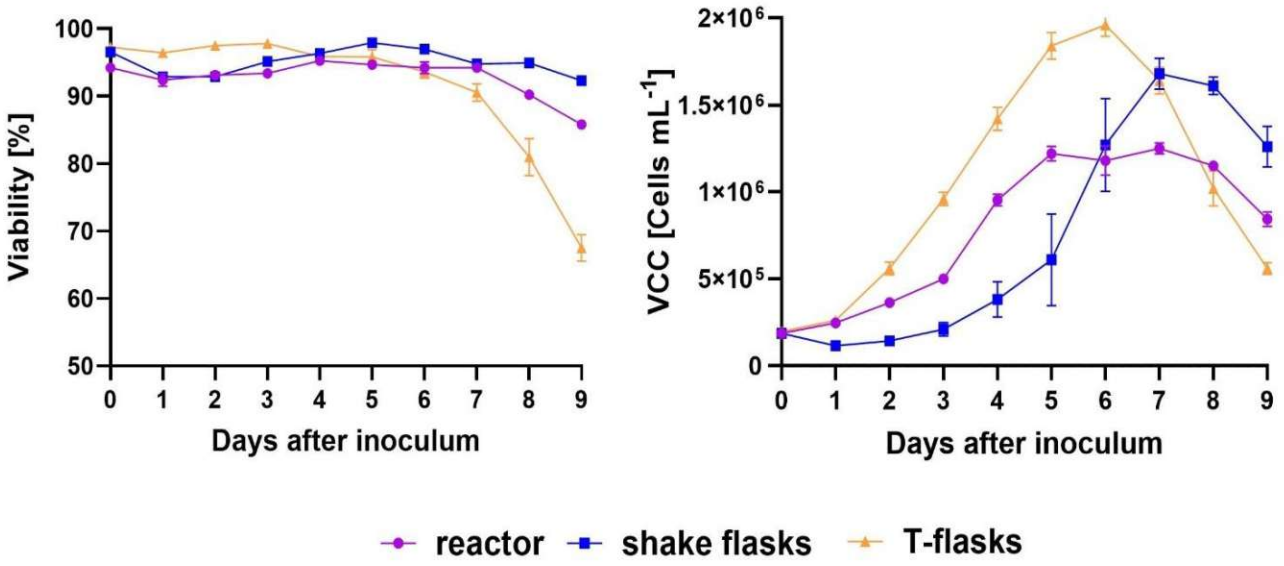

Figure 14: *Growth curves for each expansion platform expressed as concentration of viable cells (VCC) per mL culture with corresponding viability of cell populations. Error bars represent standard deviation of pooled technical replicates were n=3 for one bioreactor, n =6 for two T-flasks and n = 9 for three shake flasks.*

NK-92 cells were subjected to the batch cultivation process in three different expansion platforms over 9 days without media replenishment but with IL-2 supplementation every second day and sampling interval of 24 hours. Growth curves on the right-hand scatter plot demonstrates peak-shaped form with lag-phase at the beginning (shake flasks), first transition phase and exponential growth phase in the middle (all platforms), second transition phase (all platforms) and stationary phase (reactor) and finally death phase (all platforms).

Die approbierte gedruckte Originalversion dieser Diplomarbeit ist an der TU Wien Bibliothek verfügbar
The approved original version of this thesis is available in print at TU Wien Bibliothek.

Despite similar shapes of the curves, several growth off-sets can be spotted. Starting at the same initial VCC ($0.2 \cdot 10^6$ cells/mL), cells from shake flasks (SF) exhibited the longest lag-phase from D0 until D3, followed by much more shorter lag phases in stirred tank bioreactor (STR) and static T-flasks (ST), both between D0 and D1. Despite almost identical growth within first day in STR and in ST, significant differences in the following growth parkour between D1 and D6, in particular extended stationary phase (D5-D7) in STR can be noted. The presence of mentioned growth off-sets resulted in different maximum VCC in all three platforms – $1.9 \pm 0.05 \cdot 10^6$ cells/mL in ST by the D6, $1.7 \pm 0.1 \cdot 10^6$ cells/mL in SF by the D7 and $1.25 \pm 0.05 \cdot 10^6$ cells/mL in STR by the D5. Cells from all expansion platforms demonstrated high viability at the beginning of cultivation at day zero (D0) and until roughly day seven (D7) were viability started to drop due to cell exhaustion., as shown on the graph to the left. The first six to seven days can be described with viability over 90%, even in case of SF cells, which had to overcome the longer lag-phase and STR cells with longer stationary phase between exponential growth phase and death phase (D5-D7).

It is important to mention that cells from SF were precultured in static conditions without adaptation to shaking conditions, as described in section 2, and the cells for STR were precultured in dynamic conditions with adaptation phase already passed. The consequences of this difference in preculturing can be best seen in the minor viability and VCC drop in SF between D0 and D3 and was also observed during the preculture experiments (data not shown). The appearance of stationary phase from D5 until D7 without compromising the cell viability in STR might be the consequence of stirring conditions in STR in comparison to shake flasks and static T-flasks. Better mixing prevented concentration gradients and accumulation of inhibitory products of NK-92 cell metabolism like lactate and ammonia and provided better access to the nutrients. Further discussion should be done after the section with metabolites and nutrients uptake/production rates.

Die approbierte gedruckte Originalversion dieser Diplomarbeit ist an der TU Wien Bibliothek verfügbar
The approved original version of this thesis is available in print at TU Wien Bibliothek.

Usually, specific growth rate is used to describe kinetics based on cell mass and can be determined as volumetric growth rate in relation to current biomass concentration. After the cell counting using flow cytometer and calculation according to (Equation 1, the cell concentration per mL was accessible and was used to calculate specific growth rate, expansion fold and doubling time.

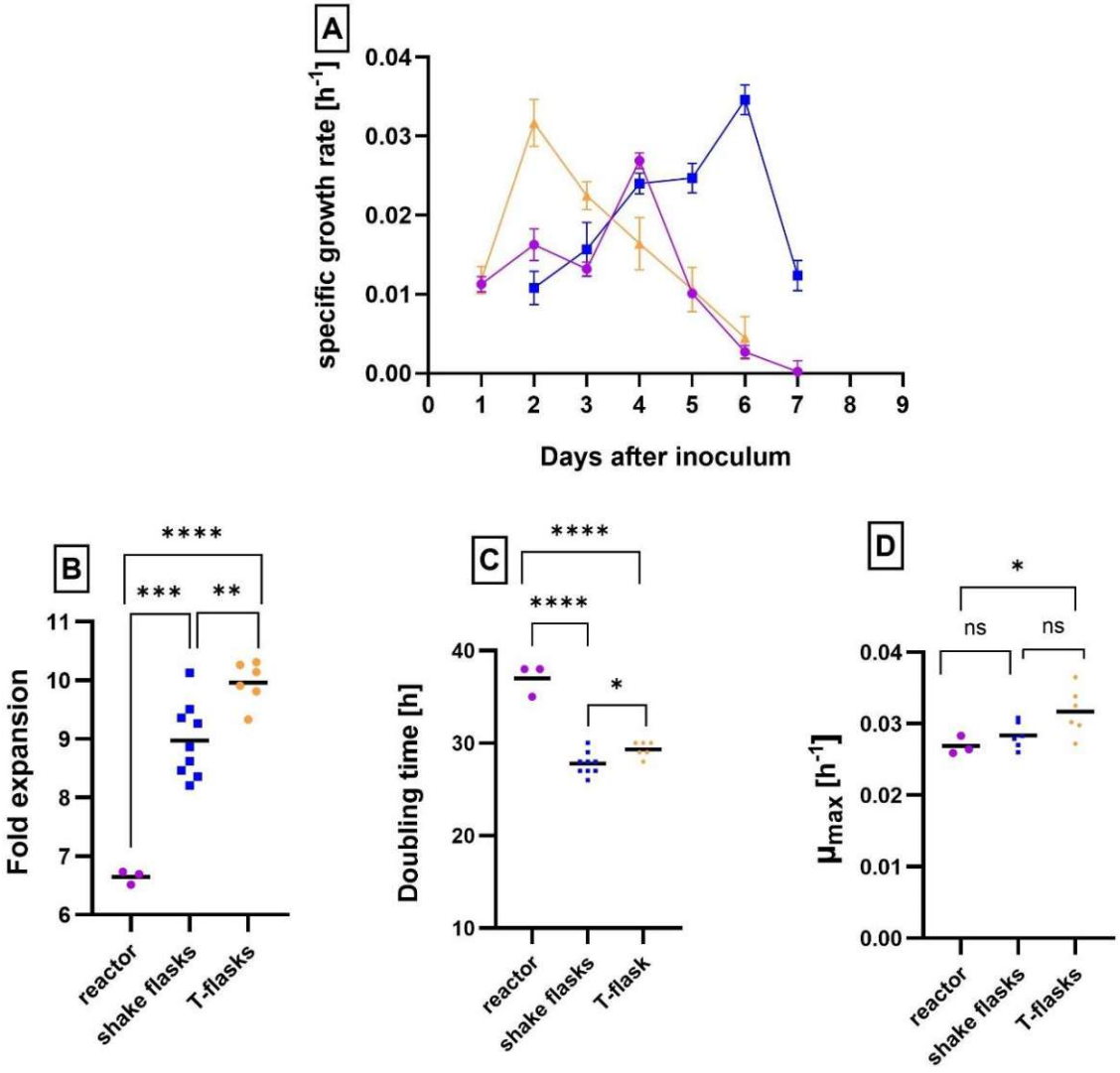

Figure 15: ***A:****Display of NK-92 growth as a specific rate calculated as stepwise integration on 24 hours base according to*(Equation 4*. Cells were assumed to be in the same state of division. Missing values in SF at D1, ST D7 and in all conditions after D7 underline a negative growth rate and were excluded.* ***B:*** *Fold expansion presented as ratio between VCC at the end of growth phase and VCC at D0.* ***C:*** *Doubling time presented as replicates with horizontal bar showing the mean value, calculated according* (Equation 6*.* ***D:*** *Maximum specific growth rate read out from plot A to showcase the similarity between expansion platforms on the day when the cell doubling occurred. After positive testing for normality across all platforms, parametric, non-paired t-test were used to evaluate the differences in means between three expansion platforms. All statistical tests and correlation analysis were performed in GraphPad Prism 10.*

Die approbierte gedruckte Originalversion dieser Diplomarbeit ist an der TU Wien Bibliothek verfügbar
The approved original version of this thesis is available in print at TU Wien Bibliothek.

As demonstrated in Figure 16, (plot A), the faster growing cells from static flasks achieved the total maximum growth rate (0.31 ± 0.03 $h^{-}1$) already at D2 and then gradually decreased until D7 where the cells entered death phase. In less "explosive" SF and STR dynamic conditions the growth rate mirrors the slower growth speed during lag-phase and first transition phase at the beginning and highest speed during the exponential phase with both maxima at D4 with the values close to static platform.

Fold expansion (Figure 16, B) is useful metrics to compare different expansion platforms between each other. In our case, cells from shake flasks (9.0 ± 0.6 fold) and T-flasks (10.0 ± 0.3 fold) outperformed the cells expanded in reactor (6.6 ± 0.1 fold). The means of fold expansion from all expansion platforms were significantly different from each other, as demonstrated with the asterisks on plot B.

Time needed for cells to double is expressed as doubling time t_d and is characteristically for the cells (Plot C). If assuming the growth offset in shake flasks was only due to operator error and not due to expansion conditions, doubling time in shake flasks is significantly higher (than in static T-flasks and reactor if calculating according to (Equation 5 and (Equation 6. If excluding the adaptation phase (D0-D3) from SF platform, SF and ST cell populations needed 28 ± 0.5 hours and 29 ± 1 hours respectively, compared to 37 ± 1.5 hours in reactor. Exclusion of adaptation phase in calculation of doubling time in shake flasks is not ideal and was only proposed in accordance with preliminary results where cells from T-flasks and shake flasks were compared in their growth (data not shown).

Along doubling time, maximum specific growth rate μ_{max} is another characteristic of the cells. As shown in plot D all expansion platforms demonstrated similar μ_{max}. Moreover, if looking at growth curves in Figure 15 and at growth rates in Figure 16 (plot A), the cell concentration increased twofold during one single day in all platforms, namely between D1-D2 in ST, between D5-D6 in SF and between D3-D4 in STR – exactly where the μ_{max} was registered. Statistically expressed, the only significant difference in means of cell populations were found between STR and ST (p-value = 0.0498). With the p-value being very close to significance level 0.05, this result must be critically evaluated.

Assuming there is no difference in NK-92 cell phenotype and no other serious limitations occurred during cultivation, μ_{max} must be the same. Therefore, with the p-value very close to significance level, it can be preliminary concluded that the expansion platform has no significant impact on maximum growth rate of the NK-92 cells. It is though, the cell concentration and the doubling time, which differ significantly between reactor and other two platforms, indicating the existence of limitations when cultivating the NK-92 cells in stirred bioreactor with described process parameters.

Die approbierte gedruckte Originalversion dieser Diplomarbeit ist an der TU Wien Bibliothek verfügbar
The approved original version of this thesis is available in print at TU Wien Bibliothek.

3.2 Cytotoxicity of NK-92 cells

Cytotoxicity is a key characteristic of NK-92 cells and describe the ability to lyse target cells by releasing cytolytic granules or engage death receptors. The assessment of cytotoxicity was performed after co-culturing with K562-GFP target cells, by using the 7-AAD and Annexin V live/dead staining strategy and measurements on flow cytometer.

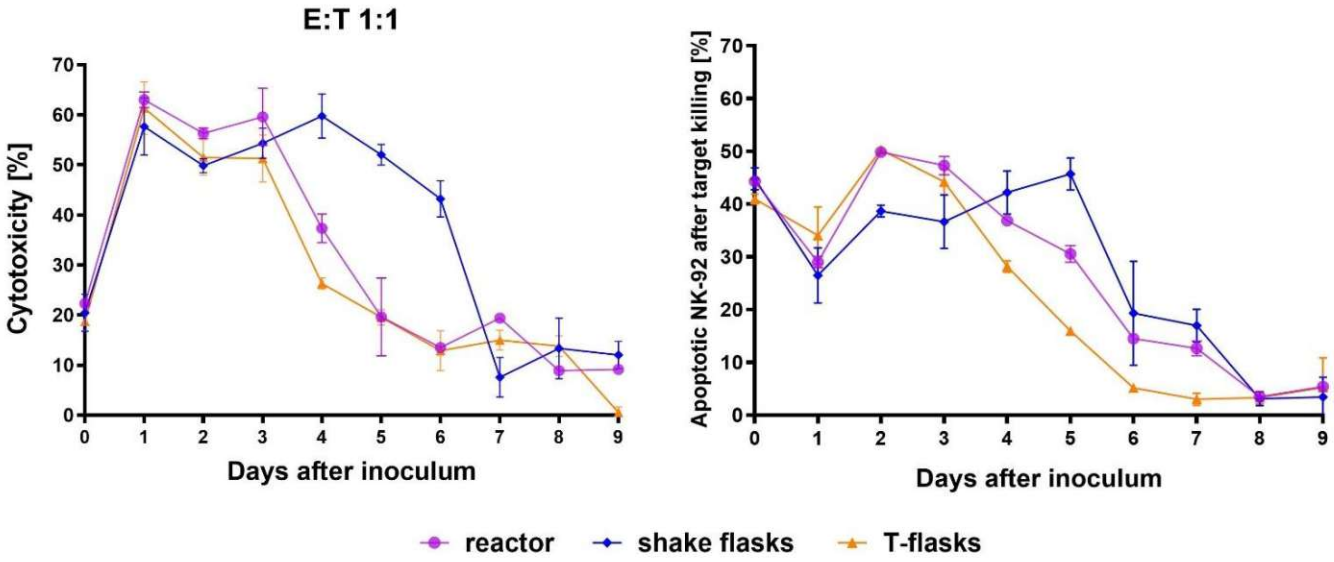

Figure 16: *Percentage of apoptotic and necrotic K562-GFP as a result of 4-hour-incubation at 1:1 effector to target ratio (E:T) with NK-92 cells. On the right-hand side is the percentage of NK-92 cells which were found to be apoptotic/necrotic after co-culturing with K562-GFP cells. Both normalized with the percentage of apoptotic and necrotic cells from the K562-GFP and NK-92 negative controls as stated in (Equation* **2** *and (Equation* **3**.

In the given experiment settings, after 4 hours of incubation with target cells, cells cultivated in static and dynamic platforms demonstrated high cytotoxicity (over 50%) from D1 to D3 as shown on the left side of the figure above. Important to mention, that the co-culture at D0 was seeded at false E:T ratio, namely 1:3 instead of 1:1 and the incubation lasted 2 hours longer - 6 hours instead of 4 hours, which resulted in lower cytotoxicity but still high death rate among NK-92 cells (right-hand graph). Interestingly, after D3 only NK-92 cells from shaking flasks continued to showcase the high cytotoxicity, killing around the half of seeded target cells until D7 where the abrupt loss of cytotoxicity occurred. Meantime, NK-92 cells from other two platforms lost almost the half of killing ability by the D4 and continued the rapid decline until the cytotoxicity reached the baseline at around 10%. If looking again at Figure 14 where the growth curves were plotted, it can be easily seen that slow or no growth of SF cells from D1-D4 didn't affect cytotoxicity of the cells in this period. This finding indicates that NK-92 cytotoxicity is not necessarily coupled to active cell growth and can be influenced by another factors, e.g. presence of specific nutrients and the speed of their depletion.

Die approbierte gedruckte Originalversion dieser Diplomarbeit ist an der TU Wien Bibliothek verfügbar
The approved original version of this thesis is available in print at TU Wien Bibliothek.

Ham et al. hypothesized in their work that NK cells possess special mechanism, which protect them from cytolytic activity of granules released when killing target cells[104]. In this regard, we made use of flow cytometry gating strategy, which allowed us to differentiate between viable and dead NK-92 cells in co-cultures. Results can be seen on the right-hand side plot of **Fehler! Verweisquelle konnte nicht gefunden werden.** Main message of this plot is based on the observation of possible direct correlation between the higher death rates and high killing efficiency, which points to some degree of susceptibility of NK-92 cells during killing activity. To be more precise, this pattern could be seen at D2 and D3 in static flasks and bioreactor, and at D2-D5 in shake flasks.

Die approbierte gedruckte Originalversion dieser Diplomarbeit ist an der TU Wien Bibliothek verfügbar
The approved original version of this thesis is available in print at TU Wien Bibliothek.

3.3 NK-92 cells and the small insight in their metabolism

L-Glutamine and D-Glucose were reported multiple times as main nutrients used in culturing of T cells and NK cells, with L-Lactate, Pyruvate, Ammonium and L-Glutamate as main by-products of glycolysis and amino acid metabolism[105-108].

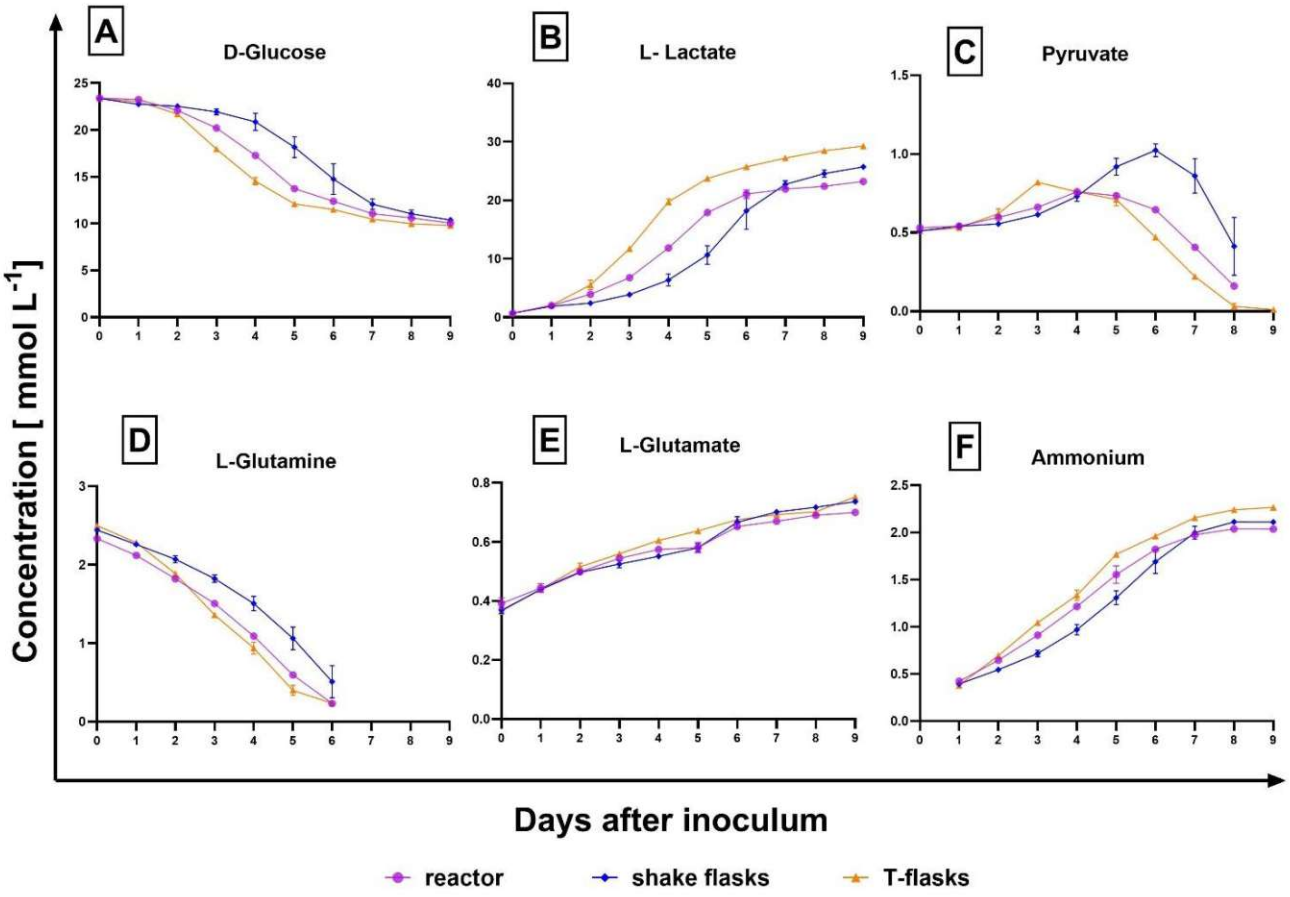

Figure 17: *Extracellular nutrients and metabolites concentrations in supernatants of NK-92 cell cultures. Mean and standard deviation were calculated from three individual measurements for each expansion platform. As mentioned in 2.3.3, to reduce the non-cellular effect on concentrations of L-glutamine and ammonium, data was normalized with the values obtained from condition flasks (only complete medium, no cells). Missing data points, e.g. glutamine D7, D8, D9, pyruvate D9 and ammonium D0 indicate concentrations lower than limit of quantification (LOQ).*

Die approbierte gedruckte Originalversion dieser Diplomarbeit ist an der TU Wien Bibliothek verfügbar
The approved original version of this thesis is available in print at TU Wien Bibliothek.

Glucose concentration started to decrease rapidly in all expansion platforms from D2 and stabilized after D7 with half of supplemented glucose left in the culture media, as shown in plot A in figure above. In the meantime, lactate and ammonium, which in high concentration are considered to be toxic for the cells[109, 110], started to accumulate extracellularly, reaching twenty times higher concentrations, in case of lactate and eight times higher, in case of ammonium, compared to D0 (plot B and F). While the concentration of ammonia seemed to reach the plateau in all conditions, the lactate together with glucose continued to slowly accumulate/decrease in the cell culture. Moreover, the glucose and lactate at plot A and B seemed to be in direct stochiometric relationship. The lowest concentration of glucose was registered around 10 mM and the final concentration of lactate around 20 mM, which aligns with stochiometric ratio of net glycolysis reaction where, i.e. from one mole of glucose two moles of pyruvate (further oxidation to lactate) are formed. Notably, glutamine concentration was already lower than LOQ by the D7 in all expansion platforms (plot D). As depicted in plot C, pyruvate was only analyte with a transition between two states – with concentration first increased until maximum at D3, D4, D6 and then decreased until LOQ was reached in T-flasks, shake flasks and bioreactor respectively. The extracellular concentration of L-glutamate, depicted in plot E was slightly increased from 0.4 mmol/L at D0 up to 0,6 mmol/L at the D9. In general, in contrast to glucose and L-lactate and L-glutamine and ammonium, extracellular concentration dynamics in L-glutamate and pyruvate (Plots C and E) are rather subtle, which is most probable due to intermediate character of this molecules.

Die approbierte gedruckte Originalversion dieser Diplomarbeit ist an der TU Wien Bibliothek verfügbar
The approved original version of this thesis is available in print at TU Wien Bibliothek.

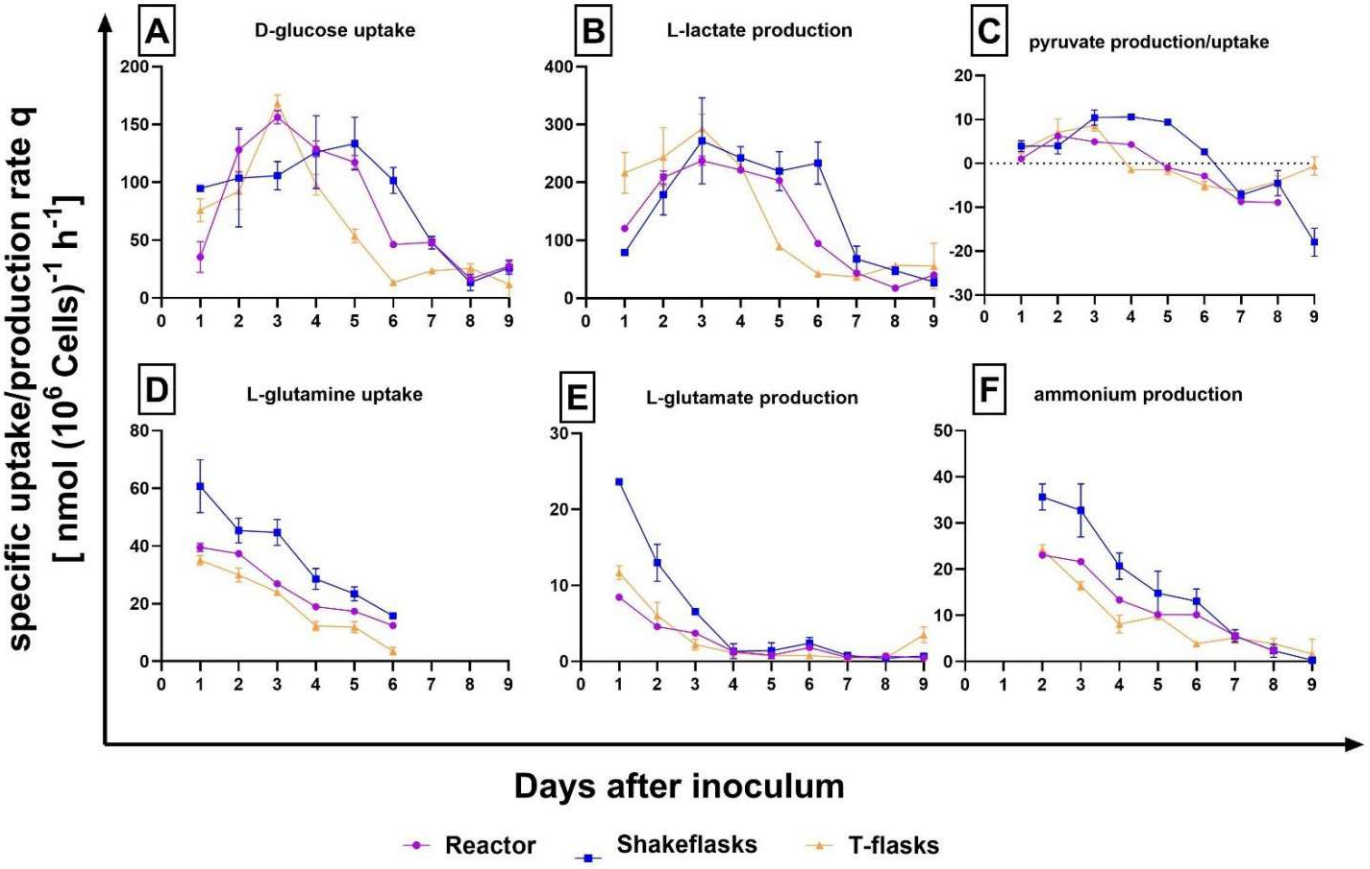

Figure 18: *Specific uptake/production rates per million cells of extracellular metabolites calculated as explained in* (Equation 9. *High standard deviation in SF cells resulted from the growth off-set in all three shakeflasks together with differences in concentrations. Values from D7, D8 and D9 in plot D are missing due to the registered concentration values under LOQ, as shown in Figure 17. Similar reason for missing values in plot F, where the ammonium production is depicted from D2 onwards. Negative values in plot C intended to showcase the uptake phase of pyruvate.*

To answer the questions how fast the concentrations change due to cellular activity, cell specific uptake/production rates can be formulated. Faster growing cells in static platform reached their maximum glucose uptake and congruent lactate and pyruvate production rates on D3, as seen in figure above on plots A, B and C. High lactate production accompanied by glucose uptake was observed until D5 in all conditions. For the platform with the highest cell density at D1-D5 (Figure 14), cells from T-flasks used glutamine and produced ammonium at slightly lower rates than the cells in other expansion platforms. Cells from shake flasks demonstrated an off-set in glucose uptake (Plot A), lactate production (Plot B) and pyruvate production/uptake (Plot C), as the consequence of longer lag-phase in the beginning of experiment, shown in Figure 14. During the lag-phase cells are not using the nutrients for growing but rather to support the DNA repair, synthesis of degraded RNA and other household operations.

Die approbierte gedruckte Originalversion dieser Diplomarbeit ist an der TU Wien Bibliothek verfügbar
The approved original version of this thesis is available in print at TU Wien Bibliothek.

Indeed, if looking again at Figure 14 and Figure 17, no growth was registered between D0 and D1 in shake flasks, but the concentrations of nutrients like glucose and glutamine, as well as lactate and ammonium were decreasing. Notably, no such off-set was registered in L-glutamine, L-glutamate and ammonium. Contrary, the uptake/production rates of mentioned analytes in shake flasks were even slightly higher than in faster growing cells from shake flasks and reactor (D2-D7 in plot D, D2-D3 in plot E and D2-D6 in plot F). Cells from reactor, similar to the cells from shake flasks and T-flasks also heavily relied on glucose, as seen in the glucose uptake rate on the graph A, but produced lactate and pyruvate on slightly slower rate than other two platforms, as shown on graph B and C.

Glucose metabolism group: glucose, lactate and pyruvate

The high dynamics in specific uptake/production rates, carbon backbone, and common metabolic pathways—such as glycolysis and the TCA cycle—suggest a relationship between these three molecules and carbon metabolism as the primary energy source in NK-92 cell culture.

In general, the course of specific rates of glucose, lactate and pyruvate have bell-shaped form similar to the form of growth curves demonstrated in Figure 14. This include lower rates at the beginning where the cells were in lag phase, e.g. T-flasks and reactor in plot A, B and C, rates increased up to the maximum during exponential cell growth, rates slowly decreased (in case of pyruvate even changed from production to uptake) within stationary phase and finally, rates decreased drastically when cells entered the death phase. Following, glucose, lactate and pyruvate specific rates can be dubbed "direct uptake/production rates", as they increased when the cell concentration increased and decreased when the cell concentration decreased, as shown in Figure 17. Next, the relationship between these three molecules will be examined in detail, leading to the formulation of a hypothesis.

Briefly, upon stimulation with cytokine like IL-2, the glucose enters cytoplasm through GLUT1 transporter it can be immediately breakdown to pyruvate during glycolysis [111]. After transporting into mitochondrial inner membrane, pyruvate can be used as a substrate for Pyruvate Dehydrogenase Complex (PDC) catalyzes the decarboxylation reaction with Acetyl-CoA as a product, which can then enter the TCA-Cycle, if the oxygen is present. If oxygen is missing, pyruvate can be processed to lactate by a process termed anaerobic glycolysis and might resonate in some minds when remembering last high intensity training. However, glucose can be also metabolized to lactate and NAD+ in the presence of oxygen, which was first recognized by Warburg in cancer cells and called in his name – the Warburg metabolism[112]. As shown in pyruvate production/uptake rate in figure above, pyruvate was secreted during active cell growth out of the cells and after passing the maximum growth rate at D3 in ST, D5 in STR and D7 in SF (Figure 15), was either transported back into the cell or reacted with other accumulated by-products of cell activity.

Die approbierte gedruckte Originalversion dieser Diplomarbeit ist an der TU Wien Bibliothek verfügbar
The approved original version of this thesis is available in print at TU Wien Bibliothek.

Two main questions arise from this observation:

1) How is it possible that during the time when energy demand of the cell is very high, pyruvate was transported out instead of utilized to acetyl-CoA in mitochondria with consequent entrance in TCA cycle and further fueling to oxidative phosphorylation (OXPHOS), hence ATP synthesis?
2) How can the depletion of pyruvate, which began immediately after D4 in ST, D5 in STR and after D6 in SF, be explained in relation to the significant drop in the specific uptake and production rates of glucose and lactate on the same days?

The answer to these questions is not trivial at all. First, the errors due to analytical measurement must be excluded. Given the fact that Gibbs energy of reverse reaction from lactate to pyruvate catalyzed by Lactate Dehydrogenase (LDH) in presence of NADH is + 25 kJ/mol and is therefore thermodynamically not favored, it is unlikely that lactate, which was also accumulated exogenically, could affect the enzymatic reaction of pyruvate formation. It is also unlikely that NADH, which is very important cellular redox equivalent and is needed in many other reactions inside the cell, was also transported out from cell and negatively affected the detection of pyruvate. Impact of other alpha-ketoacids on the reaction of LDH-catalyzed reaction can be also regarded as unsignificant due to substrate specificity of LDH. After analytics are sorted out, further explanations of pyruvate accumulation can be developed.

As one possible explanation for increase in exogenic pyruvate during active cell growth can be the inhibition of pyruvate dehydrogenase (PDH) and promotion of Warburg effect. The activity of PDH is tightly regulated, primarily through reversible phosphorylation by specific kinases known as pyruvate dehydrogenase kinases (PDKs). Phosphorylation of PDH by PDKs leads to its inactivation, thereby inhibiting the conversion of pyruvate to acetyl-CoA[113]. Alternatively, conversion of glutamine to malate via TCA-cycle in mitochondria and it subsequent transport to cytoplasm could be the source of accumulated pyruvate. Malate, formed in cytoplasm can be decarboxylated by malate dehydrogenase to pyruvate and NADPH, needed for anabolic reactions[114]. Finally, additionally to the pyruvate formed during oxidative glycolysis, pyruvate from glutamine could be used for lactate generation or transported out of the cell, which will explain the increased concentration of pyruvate during the active growth phase. After D3, D5 and D7 in T-flasks, shake flasks and reactor respectively, the cell growth slowed down, the uptake of glucose dropped in all conditions and the concentration of glutamine has decreased more than twofold – from 2.5 to 1 mM in all platforms. All these factors may have led to intracellular pyruvate limitation, forcing its transport back into the cell to regenerate NAD+ for further utilizing to glucose at lower rates and may also provide an answer to the second question. This reverse mechanism could also explain the continuous production of lactate until the end of the experiment, even after glutamine depletion—an additional lactate source—was no longer detected.

Die approbierte gedruckte Originalversion dieser Diplomarbeit ist an der TU Wien Bibliothek verfügbar
The approved original version of this thesis is available in print at TU Wien Bibliothek.

What are the cellular gains by metabolizing glucose to lactate via aerobic glycolysis? To answer this question from the perspective of this work, some general "biochemical logic" can be used. Besides fast generation of two ATP molecules and two NADH redox equivalents that are generated during glycolysis to support fast cell proliferation, the additional gain of glucose utilization to lactate could be the fast regeneration of NAD^+, that can be redirected to glycolysis to help oxidize the next glucose molecule and generate ATP.

L-glutamine, L-glutamate and ammonium as nitrogen sources

Consequently, to the first group, the second group of production/uptake rates including glutamine, glutamate and ammonium can be dubbed "indirect production/uptake rates". This group differs from the first because it has an inverse relationship with VCC. More specifically, the highest efficiency of catalysator (cells) was achieved only at the beginning of cultivation, which means the affinity to the glutamine as a substrate was decreasing with increasing cell concentration during the exponential growth phase. Similarly, the production of glutamate and ammonium decreased with increased cell density because they are the by-products of glutamine and amino acid metabolism in general. Data obtained by Juretic et al. and Watzl et.al suggests that glutamine deficit negatively affects the growth and killing activity of lymphokine-activated killer cells and natural killer cells[115, 116]. This highlights the importance of glutamine in the medium to support the overall cell metabolism even during the time were slow or no growth was observed. Accordingly, the cells with longest lag-phase – SF cells, demonstrated higher glutamine uptake than R and ST and presumably, because of that, were able to keep their cytotoxicity as shown in Figure 16. As mentioned during the discussion below the Figure 17, glutamine concentration was below LOQ after D6 and therefore resulted in missing specific uptake rates. The nearly twofold decrease in extracellular glutamine between D4 and D6 across all expansion platforms, coupled with the greatest decline in cytotoxicity during this period, as shown in Figure 18, suggests a potential dependency.

Die approbierte gedruckte Originalversion dieser Diplomarbeit ist an der TU Wien Bibliothek verfügbar
The approved original version of this thesis is available in print at TU Wien Bibliothek.

3.4 Insight into bioreactor online monitoring

One of the main goals of this thesis was to perform the batch cultivation of NK-92 cells in STR as a proof-of-concept and to compare it to well established expansion methods like shake flasks and T-flasks. Previously in the methods chapter, the agitation speed of bioreactor stirrer was calculated based on power to volume ratio in shakeflasks. Additionally, the data presented in Figure 14 and Figure 18 demonstrated moderate growth and nutrients uptake rates similar to other conditions, indicating the feasibility of scale-up approach. However, when transferring expansion in stirred bioreactor, handful of other process parameters have to be monitored and controlled to assure robust cultivation. Bioreactor set-up and set points for process parameters such as aeriation rate, gas composition, dissolved oxygen concentration were selected mostly based on bioreactor cultivations of T cells, with only one cultivation of NK cells published in 1996 by Pierson et al.[66]. Next, the results of online monitoring of process parameters will be presented and discussed.

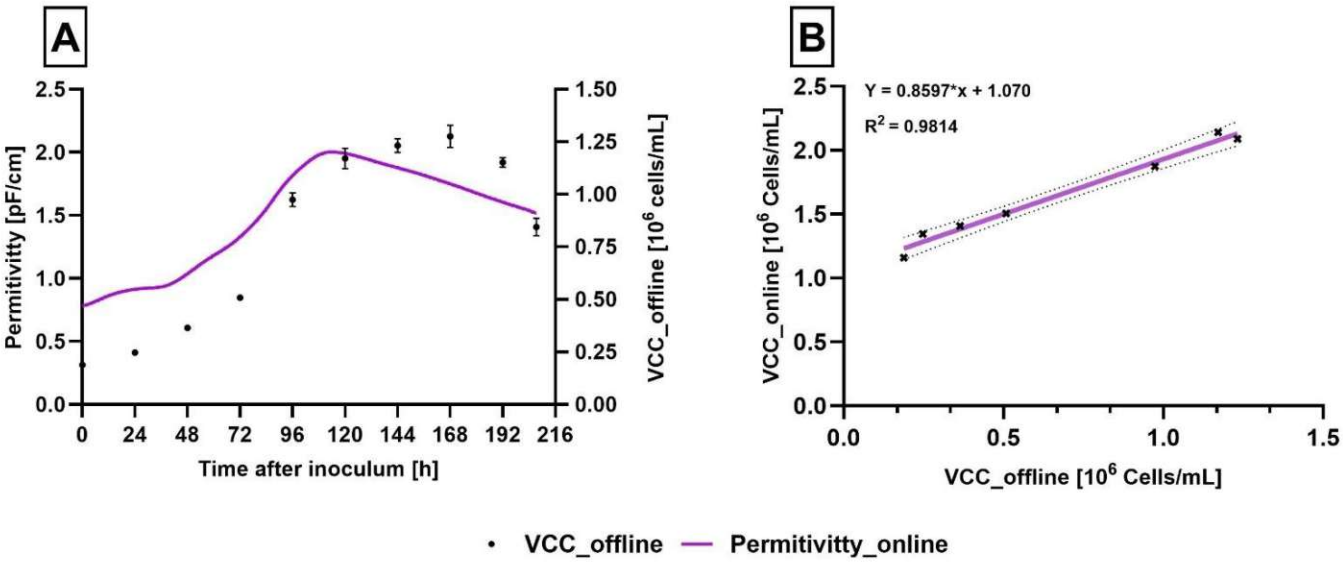

Figure 19: ***A:*** *Permittivity signal measured with the permittivity probe inside of the reactor. VCC measured offline using flow cytometer (FCM) can be seen on the secondary y-axis. Signal was smoothed using Locally Weighted Scatterplot Smoothing (LOWESS), 10 points per smoothing window.* ***B:*** *Permittivity signal from D0 until D9 transformed in VCC and plotted against values from offline VCC measurement. Correlation underlined by the means of simple linear regression with coefficient determination and correspondent linear equation. Dotted lines represent 95% confidence interval. Values from online VCC measurement started from 1 x 10^6 Cells/mL as predicted by MLR-model based on CHO cell cultivations and were found to be typical starting concentration for the bioreactor inoculation with CHO cells.*

Die approbierte gedruckte Originalversion dieser Diplomarbeit ist an der TU Wien Bibliothek verfügbar
The approved original version of this thesis is available in print at TU Wien Bibliothek.

The course of the permittivity signal measured online using the permittivity probe matched well with the course of VCC measured offline using established method on flow cytometer, covering the first transition phase, exponential phase and second transition phase, as shown on plot A. However, the signal delivered less information about stationary phase and death phase, showcasing the linear signal decrease right after 120 hours, in comparison to the data obtained from FCM. During the stationary phase cells start to undergo different size deformation, which can be harder to recognize for the probe, resulting in certain data inconsistency in post exponential phases. Maximum cell density according to online measurement was $2 \cdot 10^6$ cells/mL, compared to $1.3 \cdot 10^6$ cells/mL measure on FCM, as can be seen on plot B. Sensor relied on the predefined multi linear regression model, based on frequency scans obtained from CHO-cells fermentations. It was the first time it was used in culturing NK-92 cells and therefore the model wasn't refined, resulting in exaggerated maximum cell concentration. The potential reason why the model designated for CHO-cells predicted well the NK-92 growth, may lay in the similar average cell size during active phase growth, which is 14-15 µm for CHO-cells [117] and 15-17 µm for NK-92 cells[118]. Data obtained from offline VCC measurements explains 92 % of variation in online VCC measurements, as indicated by R^2 on plot B. More data is needed to validate this method for NK-92 cells. Nevertheless, this small dataset represents the first step in future implementation of this method for rapid assessment of viable cell concentration during NK-92 cell expansion.

Die approbierte gedruckte Originalversion dieser Diplomarbeit ist an der TU Wien Bibliothek verfügbar
The approved original version of this thesis is available in print at TU Wien Bibliothek.

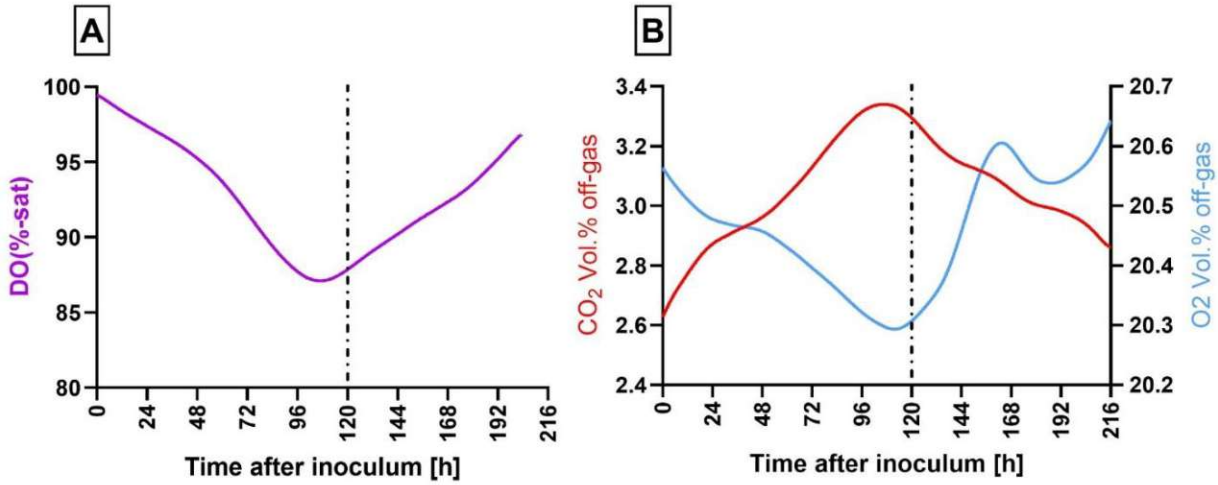

Figure 20: ***A:*** *The course of partial oxygen pressure measured electrochemically with Clark electrode inside of the reactor.* ***B:*** *Concentration profile of CO_2 and O_2 in off-gas stream measured in-line and expressed as volumetric percentage. Dotted lines represent the alignment with maximum cell density registered by permittivity probe and off-line VCC measurements on FCM, as shown in Figure 19 and Figure 15* ***Fehler! Verweisquelle konnte nicht gefunden werden.****. Signals were smoothed using Locally Weighted Scatterplot Smoothing (LOWESS), 10 points per smoothing window.*

Oxygen transfer is always a concern in aerobic biological systems. On one hand, if the supply of oxygen is limited, cell growth can be severely affected. On the other hand, if the concentration is too high the formation of oxygen and nitrogen reactive radicals leads to uncontrolled oxidation and damage to the cells. Therefore, the right balance between dissolved oxygen concentration and cell culture demand has to be found. As described previously, oxygen was supplied with the process air together with 5% vol. CO_2 through 0.2 µm filter using microsparger at 6 mL/min. During the first 48 hours of cultivation DO sensor signal gradually decreased from 98% to approximately 95% and then accelerated to the point of 86% from initial saturation during the next two days. This point corresponds to maximum VCC in reactor shown in Figure 15 (between D4-D5) and recorded maximum cell capacitance measured by the permittivity sensor between the same time – 96-120h. Aligned with the scope of this experiment, DO signal wasn't controlled, only monitored.

Hysteresis in CO_2 and O_2 concentrations from 0h until approximately 48 h were observed directly from the start, similarly to the DO concentration in plot A. After 48 hours both concentrations of measured gases demonstrated similar profile, with O2 concentration dropping from 20.6 vol.% to 20.3 vol.% between 96-120h and CO2 concentration increasing until the same point marked as 3.3 vol.% CO_2. Unexpected signal distortion in O2 concentration occurred between 120-144 hours. After short troubleshooting the potential problem was found in substantial temperature increase inside the laboratory overnight from D5 to D6. Temperature inside of BlueInOne off-gas measuring unit with built in temperature, humidity and gas sensors, raised from 28°C to 31°C degree exactly at that time. The temperature inside the reactor wasn't affected. The reason why CO_2 signal wasn't affected in similar way as O_2 remains unclear.

Die approbierte gedruckte Originalversion dieser Diplomarbeit ist an der TU Wien Bibliothek verfügbar
The approved original version of this thesis is available in print at TU Wien Bibliothek.
TU Bibliothek Your knowledge hub WIEN

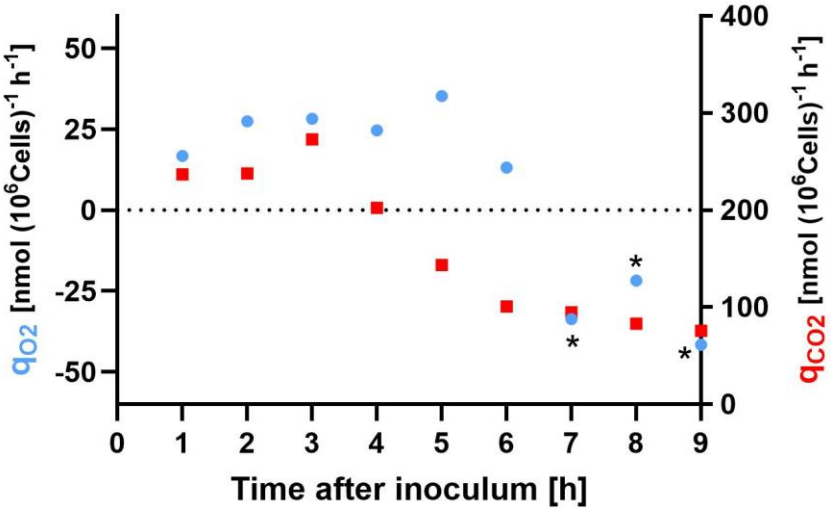

Figure 21: *Specific uptake/generation rates of oxygen and carbon dioxide calculated as specified in* (*Equation 21 and Equation 22. The values of qO_2 after D6 (marked with stars), are the consequences of signal turbulency and are not of the cell origin.*

To relate metabolite concentrations to cell metabolism, specific uptake and production rates can be formulated. Disproportionality in these rates is evident when comparing the values of qCO_2 and qO_2. Carbon dioxide was produced at rates nearly ten times higher than oxygen uptake, with peak production and uptake occurring at D3 and D5, respectively. This clearly indicates that cells consumed oxygen and produced carbon dioxide during the active growth phase.

Building upon the discussion of specific uptake and production rates of glucose, lactate, and pyruvate, shown in **Figure** 18, it was assumed that pyruvate conversion to lactate is stoichiometric and predominates over oxidative phosphorylation (OXPHOS). This assumption is supported by the nearly twofold higher lactate concentration relative to glucose and the possible inhibition of pyruvate dehydrogenase (PDH), which led to lactate accumulation during active cell growth. From the specific rates described above, it can be observed that oxygen was utilized for respiration until D6, while CO_2 production remained continuous, reaching its maximum at D3. This suggests that, despite pyruvate being halted at the PDH level, the TCA cycle may still have been supplied with acetyl-CoA, citrate, α-ketoglutarate, and oxaloacetate through alternative pathways. Consequently, CO_2 production continued, and oxygen entered OXPHOS via respiration chain enzymes, where it was ultimately assimilated to produce ATP.

According to previous studies, one alternative source of acetyl-CoA could be the β-oxidation of fatty acids, which are released from triglycerides present in the human serum used in this experiment[119]. Another potential source of acetyl-Coa is the degradation of ketogenic amino acids, such as lysine, and leucine, which were also supplied to the cells. Additionally, α-ketoglutarate can be directly synthesized from aspartate or glutamine via transamination, further contributing to TCA cycle intermediates[120].

Die approbierte gedruckte Originalversion dieser Diplomarbeit ist an der TU Wien Bibliothek verfügbar
The approved original version of this thesis is available in print at TU Wien Bibliothek.
TU Bibliothek Your knowledge hub WIEN

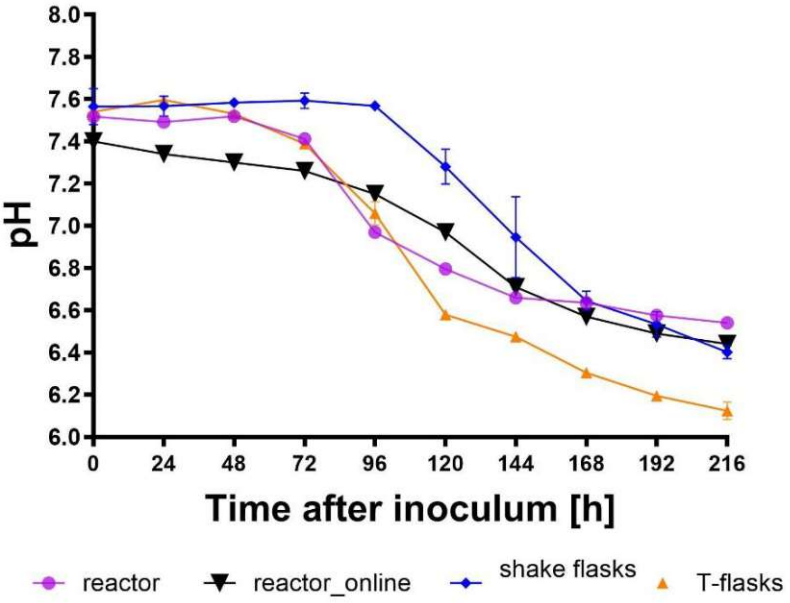

Figure 22: *Results of off-line pH measurements using laboratory pH-meter in all expansion conditions and on-line pH measurement using pH sensor installed inside of the reactor. Due to connection problem between tower and Lucullus, pH values were manually noted down during the working hours and recorded on camera during the night, hence the discontinuity in data points.*

In cultivation of mammalian cells, pH plays crucial role in cell homeostasis and functionality. Thus, adjusting the right pH range when preparing the media and during the fermentation is a must. Figure 23 demonstrates a good overall correlation between pH measurements inside of the reactor and outside of it. Started at pH 7.4-7.5, which was slightly above recommended working range for a-MEM medium (7.0-7.4), pH decrease at the end of experiment was noted at almost exact one log-reduction. The biggest change in pH was observed all conditions during the exponential growth phase and can be related to increased lactate secretion. At pH-level below physiological optimum of 7, between 6.6-6.9, the rate of pH decrease slowed down in all conditions, presumably indicating the end of exponential growth phase and begin of second transition phase as shown in VCC and viability drop in Figure 14. To have a better comparison between expansion conditions and to understand the pH limits of NK-92 cells, pH wasn't actively controlled by adding the bicarbonate solution. However, in future fed batch and continuous reactor runs this will be inevitable.

Die approbierte gedruckte Originalversion dieser Diplomarbeit ist an der TU Wien Bibliothek verfügbar
The approved original version of this thesis is available in print at TU Wien Bibliothek.

3.5 Correlation analysis

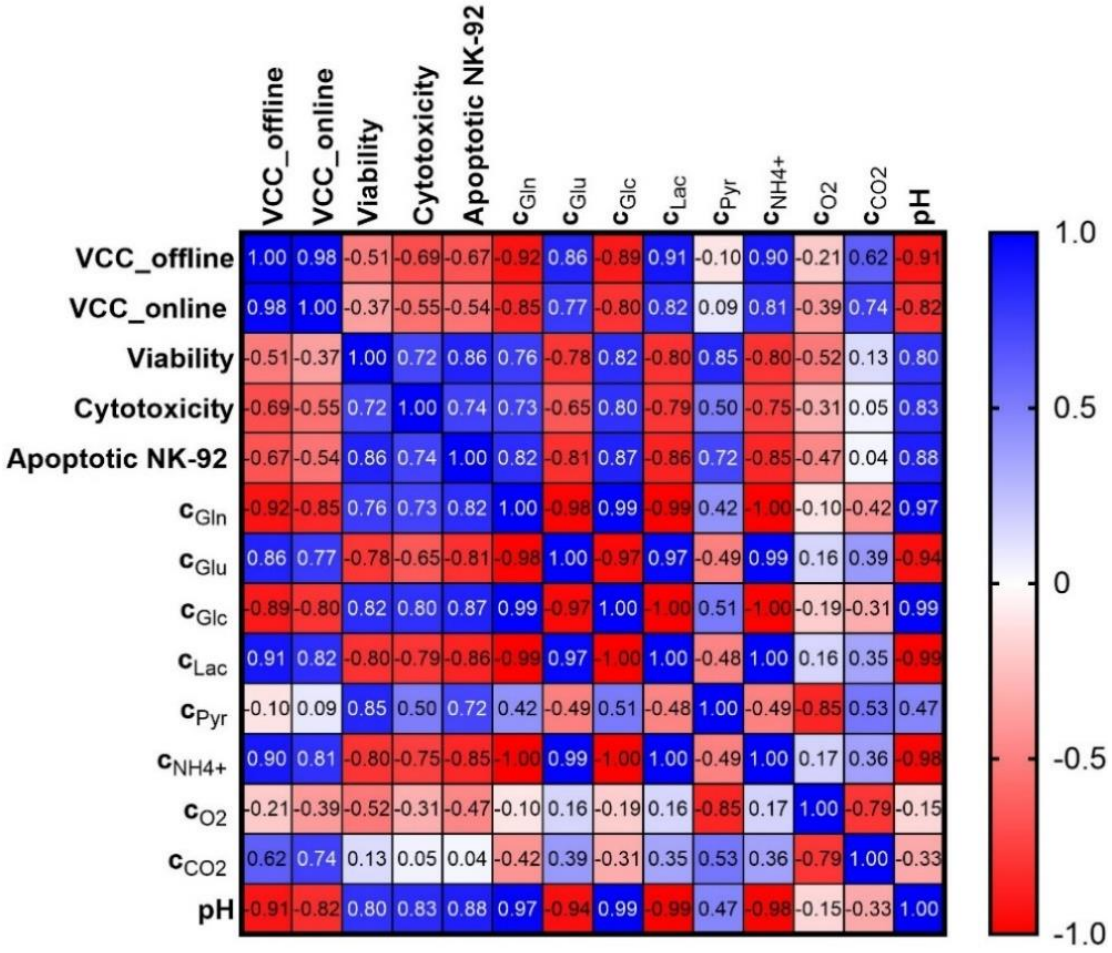

Figure 23: *Pearson correlation matrix with the variables for reactor. Key assumptions for Pearson correlation analysis are: 1) independence 2) linearity 3) homoscedasticity or equal variances. Linearity was inclusively assumed and not tested. Homoscedasticity was tested by the means of one-way ANOVA with failed Brown-Forsythe test ($P < 0.0001$). The probability of mistakenly assuming that there is a relationship between two variables is expressed as p-value and is also summarized in supplementary tables TS 3. Shapiro-Wilk normality test was performed, results are summarized in the supplementary table TS 4. Assuming no influence from the co-variables in the given matrix, it can be concluded that the variables are independent from each other.*

Die approbierte gedruckte Originalversion dieser Diplomarbeit ist an der TU Wien Bibliothek verfügbar
The approved original version of this thesis is available in print at TU Wien Bibliothek.

Correlation analysis is a statistical method used to determine whether a relationship exists between two variables or datasets and to assess the strength of this relationship. However, correlation does not imply causation. In general, numerous strong correlations can be observed in the matrix, which is expected in a complex system such as a mammalian cell line, where various collinearities can occur.

All concentration variables, except for pyruvate in the supernatant and oxygen in the off-gas, exhibited a strong correlation with VCC. Interestingly, oxygen concentration showed only two strong correlations – both negative correlations with pyruvate and carbon dioxide. Secretion of pyruvate out of the cell, accompanied by CO_2 production during the active growth phase in reactor and modest decrease in oxygen concentration (from 20.6 vol.% to 20.3 vol.%) might be the explanation for these negative correlations.

In general, the concentrations of all metabolites and nutrients displayed a high correlation with cytotoxicity, making it difficult to identify a single component in the medium that is essential for supporting cytotoxic activity All accumulated metabolites like Lac, Glu and Ammonium showcase direct correlation to VCC offline/online and indirect correlation to cytotoxicity which may point to cell exhaustion and lose of cytotoxicity as a response to accumulation of toxic lactate and ammonia and inevitability of these two waste products during active cell growth. Correspondently, concentrations of nutrients like glutamine and glucose are in indirect relationship with VCC and in direct correlation to cytotoxicity. It is though the negative correlation of cytotoxicity to VCC in reactor, which may support the observation that cytotoxicity may not be coupled to active cell growth, but rather to presence of specific nutrients in media.

Die approbierte gedruckte Originalversion dieser Diplomarbeit ist an der TU Wien Bibliothek verfügbar
The approved original version of this thesis is available in print at TU Wien Bibliothek.

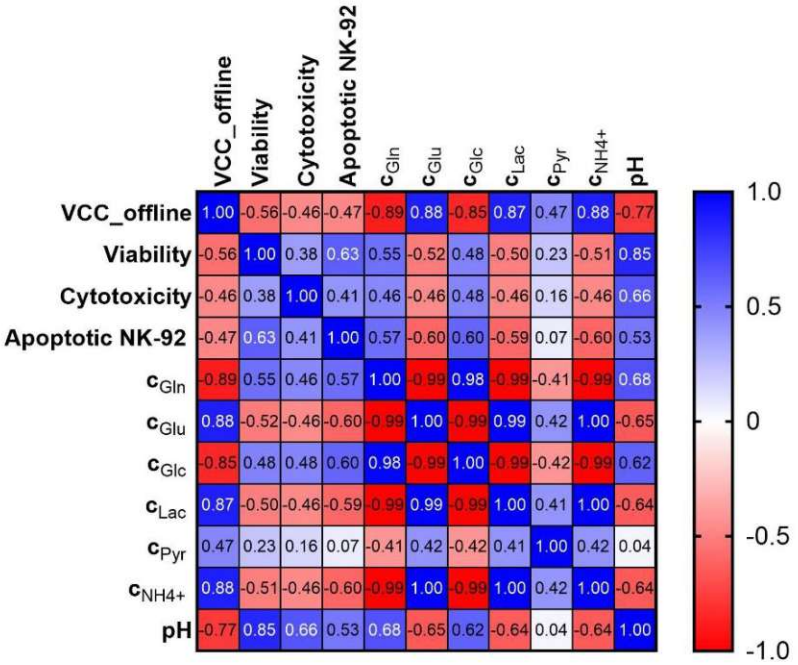

Figure 24: *Spearman correlation matrix with the variables for the shake flasks. Shapiro-Wilk normality test showed almost ¾ of all variables lacking normal distribution (Table TS 6). Therefore, the non-parametrical Spearman correlation coefficient was chosen for analysis*

Like in correlation matrix for reactor, nutrients have an indirect relationship to VCC together with direct correlation of by-products. Compared to reactor, SF cells demonstrated less proclaimed relationship between cytotoxicity and nutrients/by-products, in both direct and indirect way. Pyruvate remained the only metabolite with weakest correlation to all variables, placing it in different niche and hanging the "duality" status, as mentioned in the concentration section in subchapter 3.3. Although these explanations may have some logic behind, statistically seen the p-value gives a red flag, with values higher than 0.05, ergo higher probability to make mistakes by pointing to the existence of correlation between cytotoxicity of the cells and metabolite concentrations (Table *TS 5*). Stronger correlation between VCC and nutrients/by-products than in ST and comparable to R. Altogether, the sign of growth decoupling from cytotoxicity can be carefully highlighted, which was not observed in reactor and T-flasks. Spearman correlation factor allows us to comment on pH correlation, highlighting the strong relationship between the pH/VCC and pH/viability.

Die approbierte gedruckte Originalversion dieser Diplomarbeit ist an der TU Wien Bibliothek verfügbar
The approved original version of this thesis is available in print at TU Wien Bibliothek.

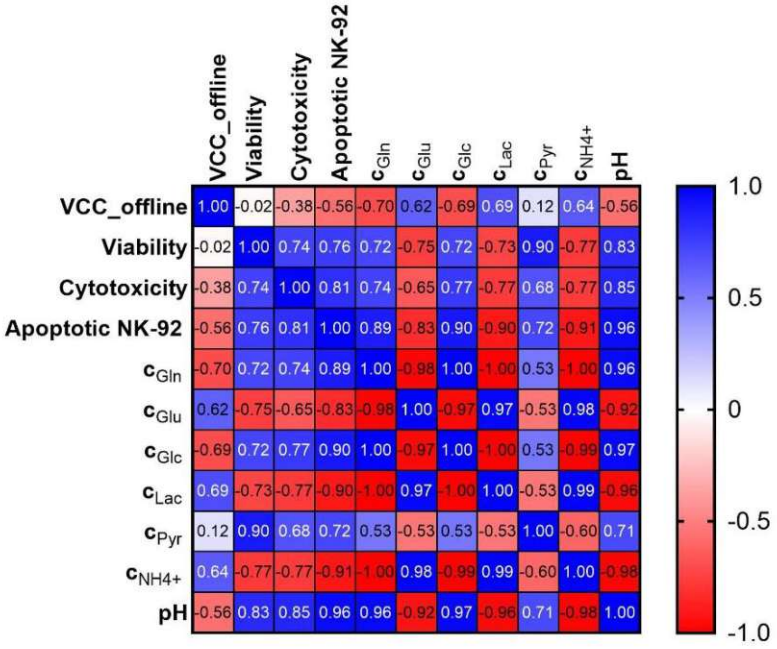

Figure 25: Pearson correlation matrix with the variables for static T-25 flasks. Normal distribution of almost all datasets, except viability allowed the usage of Pearson correlation to analyze the relationships between variables in static condition (Table TS 8).

Pyruvate is related to much stronger direct correlation with cytotoxicity and apoptotic NK-92 cells, compared to SF and R. Perhaps, due to different oxygen availability in static conditions, where less oxygen led to less active TCA-cycle with pyruvate being central metabolite, connecting glycolysis and TCA. In general, the relationship between metabolites/nutrients and cytotoxicity is stronger than in SF and comparable to STR. Interestingly, connection between VCC and metabolites/nutrients, except pyruvate, is less proclaimed than in dynamic conditions SF and R. It might be the case, that the cells in static conditions were more efficient in utilizing the nutrients to support growth and cytotoxicity than in SF and R, which resulted in overall better growth and comparable high cytotoxicity.

Die approbierte gedruckte Originalversion dieser Diplomarbeit ist an der TU Wien Bibliothek verfügbar
The approved original version of this thesis is available in print at TU Wien Bibliothek.

4 CONCLUSION AND OUTLOOK

Since 1970 the changes in the field of advanced cell and gene therapy continue to gain momentum with very high tempo. Scientists from all over the world work hard to understand the nature of immune cells and the possibilities to redirect them for battling with different “invaders “, including cancer as a most prominent one. As a permanent human cell line, NK-92 cells are not only powerful therapy agent for hematologic cancers like leukemia and lymphoma, but also a perfect foothold for research. In this work, we addressed the potential challenges of large-scale cultivation of NK-92 cells by transitioning from well-established expansion techniques to lab-scale 2 L stirred tank bioreactor.

As a result, we successfully cultivated the cells in stirred tank bioreactor and reached the cell number of almost 800 x 10^6 viable cells at the end of growth phase in one batch run (Figure 14). No significant difference in maximum cell growth between the platforms and one complete cell doubling between D3 and D4 are the promising signs of successful future cultivation of NK-92 cells. In terms of maximum cell density and growth speed, the reactor as expansion platform still needs further investigation rounds to improve the cultivation conditions.

To slightly uncover the metabolic scene of NK-92 cells, we made use of the metabolic tracking data. A tumor-like metabolic shift from the citric acid cycle and OXPHOS in the mitochondria toward aerobic glycolysis and preferential production of lactate was observed during the cultivation in all expansion platforms. Additionally to lactate, pyruvate in all expansion platforms was secreted from the cytoplasm during the active cell growth and then transported back and was hypothesized to be utilized only outside of the mitochondria by Lactate Dehydrogenase (LDH) to produce lactate and NAD^+, without entering in TCA. To replenish the TCA cycle, anaplerotic reactions to from Acetyl-Coa, α-ketoglutarate and oxalacetate were suggested to be from great importance to retain homeostasis of cellular metabolism and generate ATP.

High cytolytic activity at ETT-ratio 1:1 resulted in 40% to 60% killed malignant K562 cells in first 4 days of cultivation in all expansion platforms, as depicted in Figure 16. Moreover, with the the progress of cytotoxicity, more NK-92 cells were found to be apoptotic or necrotic, as can be also seen in Figure 16. Another substantial observation was made when compared the cell growth to cytotoxicity in all conditions. Comparing the results from Figure 16 and Figure 16, at the beginning of cultivation in shake flasks, cells from this expansion platform weren’t infringed in the cytolytic capabilities, despite slower growth. This interesting pattern led to suggestion that cell growth may be decoupled from cytotoxicity and is mainly depended on the nutrients in media and preculture conditions.

Die approbierte gedruckte Originalversion dieser Diplomarbeit ist an der TU Wien Bibliothek verfügbar
The approved original version of this thesis is available in print at TU Wien Bibliothek.
TU Bibliothek Your knowledge hub WIEN

As an initial step towards automation and the further development of Process Analytical Technologies (PAT), we demonstrated a strong correlation during the preexponential and exponential growth phase between viable cell concentration (VCC) measured within the bioreactor using a permittivity sensor and VCC measured externally via flow cytometry (R^2 = 0.98, Figure 19). In the bioprocess, which is predominantly influenced by hydromechanical stress arising from stirrer blades, bursting gas bubbles in the bioreactor, and wall contact in shake flasks, appropriate agitation and shaking speed setpoints were critical. Due to the substantial differences in power-introducing elements between shake flasks and bioreactors, scale-up based on the average specific power consumption per unit volume was initially considered unfeasible. However, after an in-depth review of the scientific work by Büchs et al. and Costariol et al., this approach was found to be applicable to our study, enabling the subsequent calculation of agitation speed based on $(P/V)_{Ø}$ in shake flasks.

In summary, this study established a viable approach for cultivating NK-92 cells in a stirred-tank bioreactor. The balancing of reactor was challenging due to the complexity of cell metabolism, low uptake and production rates, and low heat generation. In the absence of active pH and dissolved oxygen (DO) control, the batch process provided valuable insights into the dynamic behavior and limitations of NK-92 cells, laying the foundation for future fed-batch and continuous processing strategies. For future process improvements, it can be recommended to implemet more comprehensive pH and DO control, increasing aeration flow rates, and reducing stirrer speed by approximately 10%. Additionally, in the case of fast-growing cells, initiating a feeding ramp with feed media before D4 is advisable to prevent excessive lactate accumulation and avoid reaching the lower concentration threshold for glutamine.

A potential limitation of the workflow demonstrated in this study is the use of human serum, which is not compliant with FDA regulations for human therapeutic applications due to the risk of viral contamination. Furthermore, the scale-up approach presented here should be considered primarily for mammalian cell cultures with lower oxygen demands. For high oxygen-demanding cultures, direct scale-up from shake flasks to bioreactors is less practical due to significant differences in power-introducing elements.

To gain a deeper understanding of NK-92 cell metabolism, holistic analytical approaches such as transcriptomics, proteomics, and metabolomics could be of great interest. While these methodologies offer valuable insights, their implementation requires substantial financial investment and specialized training.

Die approbierte gedruckte Originalversion dieser Diplomarbeit ist an der TU Wien Bibliothek verfügbar
The approved original version of this thesis is available in print at TU Wien Bibliothek.

5 SUPPLEMENTARY INFORMATION AND FIGURES

5.1 Batch process preparations

S 1: *Inoculation procedure. Cells were pumped from the laminar flow cabinet into the reactor using Watson-Marlow pump (red box).*

S 2 : *NK-92 cells inoculated in T25-flasks and shake flasks placed in incubator at 37°C and 5 %Vol.CO2. Shake flasks were mounted on top of orbital shaker (Edmund Bühler) with 2.5 cm orbital diameter.*

Die approbierte gedruckte Originalversion dieser Diplomarbeit ist an der TU Wien Bibliothek verfügbar
The approved original version of this thesis is available in print at TU Wien Bibliothek.

5.2 $k_L a$ determination

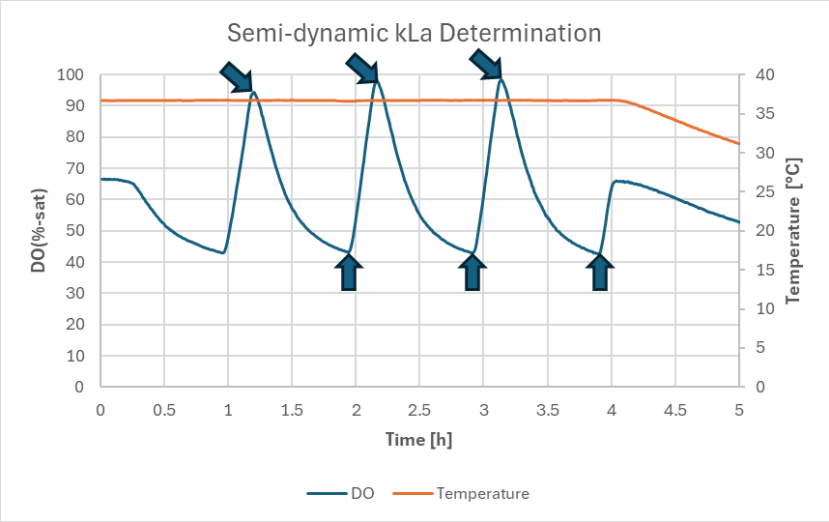

S 3: ***Static gassing out method for $k_L a$ determination***. *Cells were inside but not active. DO decrease was performed with nitrogen flushing. Slopes between the points marked with arrows were analyzed to obtain* $k_L a$. *Set points for temperature, air flow and stirrer speed were held exactly as during the experiment.*

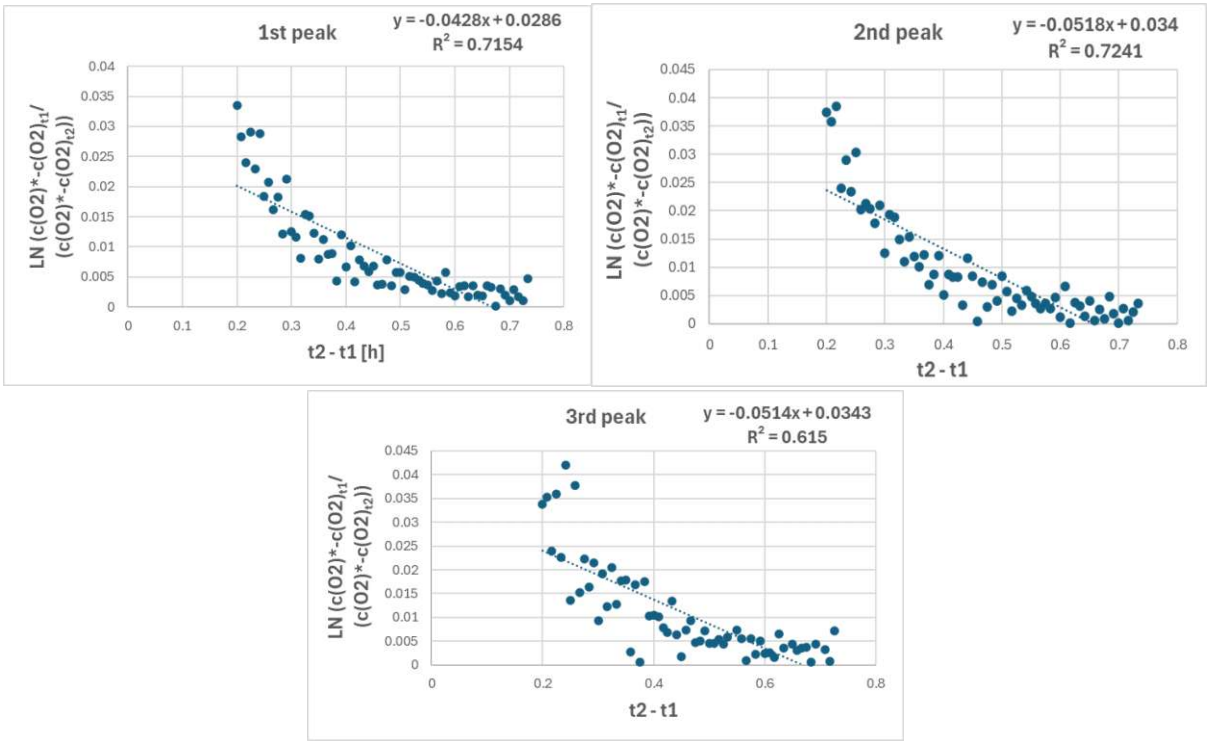

S 4: *Simple linear regression to fit the straight line to the data. The slopes are determined as* $k_L a$.

Die approbierte gedruckte Originalversion dieser Diplomarbeit ist an der TU Wien Bibliothek verfügbar
The approved original version of this thesis is available in print at TU Wien Bibliothek.

Literature sources with similar reactor geometry, sparger, impeller diameter and form are presented in Table TS1 to reflect on $k_L a$ value obtained in this experiment.

$k_L a$ from this experiment	0.05 ± 0.01 [1/h]
Univessel 2L SU, CHO-cells[121]	0.9-1.5 [1/h]
Univessel 2L, SU, CFD simulations[97]	18.7 [1/h]
Cylindrical Pyrex Flask STR, primary NK cells[66]	2.01 [1/h]

TS 1: $k_L a$ *summary table with the values found in literature for similar reactor configuration.*

Typical specific oxygen demands reported for mammalian and insect cells range from about 4-40 nmol/10^6 cells/h. Assuming oxygen solubility in cell culture media at 37°C and 8.5 ppt Salinity of 6.4 mg/L and DO at 30 % saturation, the required $k_L a$ values for a cell density of $1 \cdot 10^6$ cells/mL are between 0.03 and 0.3 h^{-1}, depending on the cell line. Thus, to reflect on our experimental conditions, $k_L a$ value calculated from this small theoretical exercise aligns with the value determined experimentally – 0.05 ± 0.01 [1/h].

Die approbierte gedruckte Originalversion dieser Diplomarbeit ist an der TU Wien Bibliothek verfügbar
The approved original version of this thesis is available in print at TU Wien Bibliothek.

5.3 Consumables and Reagents

Name	Source	Art.No.
Cedex BioHT		
Glucose Cedex Bio HT	Roche Diagnostics (Basel, Switzerland)	6608418001
Glutamate V2 Bio HT	Roche Diagnostics (Basel, Switzerland)	7395566001
Glutamine V2 Bio HT	Roche Diagnostics (Basel, Switzerland)	7395612001
Lactate Bio HT	Roche Diagnostics (Basel, Switzerland)	6608485001
LDH Cedex Bio HT	Roche Diagnostics (Basel, Switzerland)	6608493001
NH3 Bio HT	Roche Diagnostics (Basel, Switzerland)	6608515001
Pyruvate Bio HT	Roche Diagnostics (Basel, Switzerland)	7299818001
Flow Cytometry		
Counting Beads	ThermoFisher	F13838
7-AAD	Miltenyi Biotec (Bergisch Gladbach, Germany)	170-100-042
Annexin V binding buffer (ABB)	ThermoFisher	V13246
FACS-Buffer (1x PBS, 1% BSA, 0.1% NaN_3)	PBS (10x) – Gibco BSA – Sigma Aldrich NaN_3 – Carl Roth	PBS – 70011044 BSA– A9418 NaN_3 - K305
Annexin	Biolegend	640906
PBS buffer	Gibco	70011044

Die approbierte gedruckte Originalversion dieser Diplomarbeit ist an der TU Wien Bibliothek verfügbar
The approved original version of this thesis is available in print at TU Wien Bibliothek.

Cell Culture		
NK-92 Cells	DSMZ	ACC 488
K562-GFP Cells	ATCC (Manassas, VA, USA)	CCL-243-GFP
Fetal bovine serum HI (FBS)	ATCC	ATCC-30-2025
Horse Serum (HS)	PAN Biotech	P30-0702
Human Serum AB off the clot	PAN Biotech	P40-2701
RPMI 1640	Gibco	31800089
a-MEM w/o nucleosides	Gibco	12000063
Human interleukin-2 (IL-2) IS Premium grade	Miltenyi Biotec (Bergisch Gladbach, Germany)	130-097-748
Dimethyl sulfoxide (DMSO)	Carl Roth (Karlsruhe, Germany)	A994.2
Insulin-Transferrin-Selenium (ITS)	ThermoFisher	41400045
Sodium hydrogen carbonate	Roth	6885.1
D-Glucose	Roth	X997.2
L-Glutamine	Roth	HN 08.3
L-Arginine	Merck	A5006
L-Serine	ThermoFisher	J62187.22
L-Asparagine	Roth	HN 23.1
Inositol	Sigma-Aldrich	I7508-50G
β-Mercaptoethanol	Sigma-Aldrich	M3148

TS 2: *List of all reagents used during cultivation of NK-92 cells and K562-GFP cells.*

Die approbierte gedruckte Originalversion dieser Diplomarbeit ist an der TU Wien Bibliothek verfügbar
The approved original version of this thesis is available in print at TU Wien Bibliothek.

5.4 Auxiliary tables for correlation analysis

	VCC_offline	VCC_online	Viability	Cytotoxicity	Apoptotic NK-92	cGln	cGlu	cGlc	cLac	cPyr	cNH4+	cO2	cCO2	pH
VCC_offline		0.0000	0.1296	0.0270	0.0351	0.0001	0.0016	0.0005	0.0003	0.7734	0.0004	0.5672	0.0547	0.0003
VCC_online	0.0000		0.2943	0.0978	0.1061	0.0019	0.0090	0.0057	0.0035	0.8143	0.0047	0.2666	0.0141	0.0038
Viability	0.1296	0.2943		0.0183	0.0013	0.0111	0.0072	0.0035	0.0051	0.0018	0.0057	0.1208	0.7132	0.0058
Cytotoxicity	0.0270	0.0978	0.0183		0.0153	0.0159	0.0418	0.0053	0.0071	0.1403	0.0126	0.3861	0.8999	0.0031
Apoptotic NK-92	0.0351	0.1061	0.0013	0.0153		0.0035	0.0045	0.0012	0.0014	0.0190	0.0019	0.1742	0.9232	0.0009
cGln	0.0001	0.0019	0.0111	0.0159	0.0035		0.0000	0.0000	0.0000	0.2275	0.0000	0.7898	0.2321	0.0000
cGlu	0.0016	0.0090	0.0072	0.0418	0.0045	0.0000		0.0000	0.0000	0.1487	0.0000	0.6590	0.2600	0.0001
cGlc	0.0005	0.0057	0.0035	0.0053	0.0012	0.0000	0.0000		0.0000	0.1311	0.0000	0.5942	0.3755	0.0000
cLac	0.0003	0.0035	0.0051	0.0071	0.0014	0.0000	0.0000	0.0000		0.1630	0.0000	0.6671	0.3282	0.0000
cPyr	0.7734	0.8143	0.0018	0.1403	0.0190	0.2275	0.1487	0.1311	0.1630		0.1513	0.0016	0.1176	0.1702
cNH4+	0.0004	0.0047	0.0057	0.0126	0.0019	0.0000	0.0000	0.0000	0.0000	0.1513		0.6422	0.3067	0.0000
cO2	0.5672	0.2666	0.1208	0.3861	0.1742	0.7898	0.6590	0.5942	0.6671	0.0016	0.6422		0.0070	0.6767
cCO2	0.0547	0.0141	0.7132	0.8999	0.9232	0.2321	0.2600	0.3755	0.3282	0.1176	0.3067	0.0070		0.3472
pH	0.0003	0.0038	0.0058	0.0031	0.0009	0.0000	0.0001	0.0000	0.0000	0.1702	0.0000	0.6767	0.3472	

TS 3: *p-values for reactor correlation matrix. If p < 0.05 (white spaces) then the null hypothesis can be rejected, which means there is indeed correlation between variables.*

	VCC_offline	VCC_online	Viability	Cytotoxicity	Apoptotic NK-92	cGln	cGlu	cGlc	cLac	cPyr	cNH4+	cO2	cCO2	pH
W	0,8691	0,9519	0,8237	0,8454	0,9159	0,8610	0,9363	0,8690	0,8631	0,8788	0,8897	0,9469	0,9752	0,8173
P value	0,0976	0,6906	0,0281	0,0513	0,3241	0,0783	0,5125	0,0973	0,0830	0,1264	0,1681	0,6317	0,9346	0,0235
Passed normality test (alpha=0.05)?	Yes	Yes	No	Yes	Yes	Yes	Yes	Yes	Yes	Yes	Yes	Yes	Yes	No
P value summary	ns	ns	*	ns	ns	ns	ns	ns	ns	ns	ns	ns	ns	*
Number of values	10	10	10	10	10	10	10	10	10	10	10	10	10	10

TS 4: *Shapiro-Wilk normality test to check the assumption of normality distribution of the data from reactor. Viability and pH and not normal distributed, therefore the information about potential correlation between these two variables and the correlation to other variables must be treated carefully.*

	VCC_offline	Viability	Cytotoxicity	Apoptotic NK-92	cGln	cGlu	cGlc	cLac	cPyr	cNH4+	pH
VCC_offline		0.0499	0.1150	0.1057	0.0001	0.0002	0.0005	0.0002	0.1057	0.0002	0.0028
Viability	0.0499		0.2025	0.0251	0.0525	0.0741	0.0971	0.0850	0.4477	0.0782	0.0005
Cytotoxicity	0.1150	0.2025		0.1635	0.1150	0.1198	0.1014	0.1150	0.6040	0.1158	0.0158
Apoptotic NK-92	0.1057	0.0251	0.1635		0.0473	0.0340	0.0340	0.0360	0.8207	0.0343	0.0642
cGln	0.0001	0.0525	0.1150	0.0473		0.0000	0.0000	0.0000	0.1635	0.0000	0.0137
cGlu	0.0002	0.0741	0.1198	0.0340	0.0000		0.0000	0.0000	0.1574	0.0000	0.0194
cGlc	0.0005	0.0971	0.1014	0.0340	0.0000	0.0000		0.0000	0.1574	0.0000	0.0284
cLac	0.0002	0.0850	0.1150	0.0360	0.0000	0.0000	0.0000		0.1635	0.0000	0.0221
cPyr	0.1057	0.4477	0.6040	0.8207	0.1635	0.1574	0.1574	0.1635		0.1585	0.9063
cNH4+	0.0002	0.0782	0.1158	0.0343	0.0000	0.0000	0.0000	0.0000	0.1585		0.0202
pH	0.0028	0.0005	0.0158	0.0642	0.0137	0.0194	0.0284	0.0221	0.9063	0.0202	

TS 5: *p-values for shake flasks correlation matrix. If p < 0.05 (white spaces) then the null hypothesis can be rejected, which means there is indeed correlation between variables.*

	VCC_offline	Viability	Cytotoxicity	Apoptotic NK-92	cGln	cGlu	cGlc	cLac	cPyr	cNH4+	pH
W	0,7870	0,7635	0,8324	0,8979	0,8596	0,9350	0,8026	0,8025	0,8974	0,8495	0,7504
P value	0,0048	0,0026	0,0170	0,1253	0,0380	0,3952	0,0073	0,0073	0,1230	0,0281	0,0019
Passed normality test (alpha=0.05)?	No	No	No	Yes	No	Yes	No	No	Yes	No	No
P value summary	**	**	*	ns	*	ns	**	**	ns	*	**
Number of values	13	13	13	13	13	13	13	13	13	13	13

TS 6: *Shapiro-Wilk normality test to check the assumption of normality distribution. Most of the variables are not normal distribution. In this regard, the Spearman correlation coefficient could be a better option for correlation analysis than Pearson correlation coefficient.*

Die approbierte gedruckte Originalversion dieser Diplomarbeit ist an der TU Wien Bibliothek verfügbar
The approved original version of this thesis is available in print at TU Wien Bibliothek.

	VCC_offline	Viability	Cytotoxicity	Apoptotic NK-92	cGln	cGlu	cGlc	cLac	cPyr	cNH4+	pH
VCC_offline		0.9456	0.2854	0.0943	0.0236	0.0574	0.0257	0.0267	0.7466	0.0442	0.0909
Viability	0.9456		0.0147	0.0104	0.0192	0.0120	0.0178	0.0171	0.0004	0.0089	0.0028
Cytotoxicity	0.2854	0.0147		0.0043	0.0148	0.0409	0.0086	0.0090	0.0313	0.0094	0.0019
Apoptotic NK-92	0.0943	0.0104	0.0043		0.0006	0.0032	0.0003	0.0004	0.0188	0.0003	0.0000
cGln	0.0236	0.0192	0.0148	0.0006		0.0000	0.0000	0.0000	0.1167	0.0000	0.0000
cGlu	0.0574	0.0120	0.0409	0.0032	0.0000		0.0000	0.0000	0.1123	0.0000	0.0001
cGlc	0.0257	0.0178	0.0086	0.0003	0.0000	0.0000		0.0000	0.1127	0.0000	0.0000
cLac	0.0267	0.0171	0.0090	0.0004	0.0000	0.0000	0.0000		0.1113	0.0000	0.0000
cPyr	0.7466	0.0004	0.0313	0.0188	0.1167	0.1123	0.1127	0.1113		0.0650	0.0219
cNH4+	0.0442	0.0089	0.0094	0.0003	0.0000	0.0000	0.0000	0.0000	0.0650		0.0000
pH	0.0909	0.0028	0.0019	0.0000	0.0000	0.0001	0.0000	0.0000	0.0219	0.0000	

TS 7: *p-values for static T25 flasks correlation matrix. If $p < 0.05$ (white spaces) then the null hypothesis can be rejected, which means there is indeed correlation between variables.*

	VCC_offline	Viability	Cytotoxicity	Apoptotic NK-92	cGln	cGlu	cGlc	cLac	cPyr	cNH4+	pH
W	0,9267	0,7792	0,8884	0,8852	0,8662	0,9456	0,8456	0,8568	0,9009	0,8924	0,8595
P value	0,4162	0,0081	0,1627	0,1497	0,0903	0,6167	0,0515	0,0700	0,2240	0,1807	0,0753
Passed normality test (alpha=0.05)?	Yes	No	Yes	Yes	Yes	Yes	Yes	Yes	Yes	Yes	Yes
P value summary	ns	**	ns	ns	ns	ns	ns	ns	ns	ns	ns
Number of values	10	10	10	10	10	10	10	10	10	10	10

TS 8: *Shapiro-Wilk normality test to check the assumption of normality distribution. Viability dataset is not normal distributed.*

Die approbierte gedruckte Originalversion dieser Diplomarbeit ist an der TU Wien Bibliothek verfügbar
The approved original version of this thesis is available in print at TU Wien Bibliothek.
TU Bibliothek Your knowledge hub WIEN

6 REFERENCES

(1) Vivier, E.; Tomasello, E.; Baratin, M.; Walzer, T.; Ugolini, S. Functions of natural killer cells. *Nature Immunology* **2008**, *9* (5), 503-510. DOI: 10.1038/ni1582.

(2) Kiessling, R.; Klein, E.; Pross, H.; Wigzell, H. „Natural" killer cells in the mouse. II. Cytotoxic cells with specificity for mouse Moloney leukemia cells. Characteristics of the killer cell. *European Journal of Immunology* **1975**, *5* (2), 117-121. DOI: https://doi.org/10.1002/eji.1830050209.

(3) Herberman, R. B.; Nunn, M. E.; Holden, H. T.; Lavrin, D. H. Natural cytotoxic reactivity of mouse lymphoid cells against syngeneic and allogeneic tumors. II. Characterization of effector cells. *International Journal of Cancer* **1975**, *16* (2), 230-239. DOI: https://doi.org/10.1002/ijc.2910160205.

(4) Caligiuri, M. A. Human natural killer cells. *Blood* **2008**, *112* (3), 461-469. DOI: 10.1182/blood-2007-09-077438 (acccessed 9/10/2024).

(5) Demaria, O.; Cornen, S.; Daëron, M.; Morel, Y.; Medzhitov, R.; Vivier, E. Harnessing innate immunity in cancer therapy. *Nature* **2019**, *574* (7776), 45-56. DOI: 10.1038/s41586-019-1593-5.

(6) Vivier, E.; Raulet, D. H.; Moretta, A.; Caligiuri, M. A.; Zitvogel, L.; Lanier, L. L.; Yokoyama, W. M.; Ugolini, S. Innate or adaptive immunity? The example of natural killer cells. *Science* **2011**, *331* (6013), 44-49. DOI: 10.1126/science.1198687 From NLM.

(7) Scoville, S. D.; Freud, A. G.; Caligiuri, M. A. Modeling Human Natural Killer Cell Development in the Era of Innate Lymphoid Cells. *Frontiers in Immunology* **2017**, *8*, Perspective. DOI: 10.3389/fimmu.2017.00360.

(8) Grevsen, A. K.; Hviid, C. V. B.; Hansen, A. K.; Hvas, A. M. Platelet count and function in umbilical cord blood versus peripheral blood in term neonates. *Platelets* **2021**, *32* (5), 626-632. DOI: 10.1080/09537104.2020.1786040 From NLM.

(9) Verneris, M. R.; Miller, J. S. The phenotypic and functional characteristics of umbilical cord blood and peripheral blood natural killer cells. *Br J Haematol* **2009**, *147* (2), 185-191. DOI: 10.1111/j.1365-2141.2009.07768.x From NLM.

(10) Brodin, P.; Kärre, K.; Höglund, P. NK cell education: not an on-off switch but a tunable rheostat. *Trends in Immunology* **2009**, *30* (4), 143-149. DOI: 10.1016/j.it.2009.01.006 (acccessed 2024/10/14).

(11) Long, E. O. Ready for prime time: NK cell priming by dendritic cells. *Immunity* **2007**, *26* (4), 385-387. DOI: 10.1016/j.immuni.2007.04.001 From NLM.

(12) Anfossi, N.; André, P.; Guia, S.; Falk, C. S.; Roetynck, S.; Stewart, C. A.; Breso, V.; Frassati, C.; Reviron, D.; Middleton, D.; et al. Human NK Cell Education by Inhibitory Receptors for MHC Class I. *Immunity* **2006**, *25* (2), 331-342. DOI: 10.1016/j.immuni.2006.06.013 (acccessed 2024/10/12).

(13) Lucas, M.; Schachterle, W.; Oberle, K.; Aichele, P.; Diefenbach, A. Dendritic cells prime natural killer cells by trans-presenting interleukin 15. *Immunity* **2007**, *26* (4), 503-517. DOI: 10.1016/j.immuni.2007.03.006 From NLM.

(14) Zwirner, N. W.; Ziblat, A. Regulation of NK Cell Activation and Effector Functions by the IL-12 Family of Cytokines: The Case of IL-27. *Frontiers in Immunology* **2017**, *8*, Mini Review. DOI: 10.3389/fimmu.2017.00025.

(15) Morvan, M. G.; Lanier, L. L. NK cells and cancer: you can teach innate cells new tricks. *Nature Reviews Cancer* **2016**, *16* (1), 7-19. DOI: 10.1038/nrc.2015.5.

(16) Abel, A. M.; Yang, C.; Thakar, M. S.; Malarkannan, S. Natural Killer Cells: Development, Maturation, and Clinical Utilization. *Front Immunol* **2018**, *9*, 1869. DOI: 10.3389/fimmu.2018.01869.

Die approbierte gedruckte Originalversion dieser Diplomarbeit ist an der TU Wien Bibliothek verfügbar
The approved original version of this thesis is available in print at TU Wien Bibliothek.

(17) Granzin, M.; Wagner, J.; Kohl, U.; Cerwenka, A.; Huppert, V.; Ullrich, E. Shaping of Natural Killer Cell Antitumor Activity by Ex Vivo Cultivation. *Front Immunol* **2017**, *8*, 458. DOI: 10.3389/fimmu.2017.00458.

(18) Yokoyama, W. M.; Plougastel, B. F. Immune functions encoded by the natural killer gene complex. *Nat Rev Immunol* **2003**, *3* (4), 304-316. DOI: 10.1038/nri1055 From NLM.

(19) Parham, P. MHC class I molecules and KIRs in human history, health and survival. *Nat Rev Immunol* **2005**, *5* (3), 201-214. DOI: 10.1038/nri1570 From NLM.

(20) Lo Nigro, C.; Macagno, M.; Sangiolo, D.; Bertolaccini, L.; Aglietta, M.; Merlano, M. C. NK-mediated antibody-dependent cell-mediated cytotoxicity in solid tumors: biological evidence and clinical perspectives. *Ann Transl Med* **2019**, *7* (5), 105. DOI: 10.21037/atm.2019.01.42 From NLM.

(21) Pende, D.; Falco, M.; Vitale, M.; Cantoni, C.; Vitale, C.; Munari, E.; Bertaina, A.; Moretta, F.; Del Zotto, G.; Pietra, G.; et al. Killer Ig-Like Receptors (KIRs): Their Role in NK Cell Modulation and Developments Leading to Their Clinical Exploitation. *Frontiers in Immunology* **2019**, *10*, Review. DOI: 10.3389/fimmu.2019.01179.

(22) Joncker, N. T.; Fernandez, N. C.; Treiner, E.; Vivier, E.; Raulet, D. H. NK cell responsiveness is tuned commensurate with the number of inhibitory receptors for self-MHC class I: the rheostat model. *J Immunol* **2009**, *182* (8), 4572-4580. DOI: 10.4049/jimmunol.0803900 From NLM.

(23) Moretta, A.; Marcenaro, E.; Sivori, S.; Della Chiesa, M.; Vitale, M.; Moretta, L. Early liaisons between cells of the innate immune system in inflamed peripheral tissues. *Trends Immunol* **2005**, *26* (12), 668-675. DOI: 10.1016/j.it.2005.09.008 From NLM.

(24) Martín-Fontecha, A.; Thomsen, L. L.; Brett, S.; Gerard, C.; Lipp, M.; Lanzavecchia, A.; Sallusto, F. Induced recruitment of NK cells to lymph nodes provides IFN-gamma for T(H)1 priming. *Nat Immunol* **2004**, *5* (12), 1260-1265. DOI: 10.1038/ni1138 From NLM.

(25) Robbins, S. H.; Bessou, G.; Cornillon, A.; Zucchini, N.; Rupp, B.; Ruzsics, Z.; Sacher, T.; Tomasello, E.; Vivier, E.; Koszinowski, U. H.; et al. Natural killer cells promote early CD8 T cell responses against cytomegalovirus. *PLoS Pathog* **2007**, *3* (8), e123. DOI: 10.1371/journal.ppat.0030123 From NLM.

(26) Aquino-López, A.; Senyukov, V. V.; Vlasic, Z.; Kleinerman, E. S.; Lee, D. A. Interferon gamma induces changes in Natural Killer (NK) cell ligand expression and alters NK cell-mediated lysis of pediatric cancer cell lines. *Frontiers in Immunology* **2017**, *8* (APR), Article. DOI: 10.3389/fimmu.2017.00391 Scopus.

(27) Müller, E.; Christopoulos, P. F.; Halder, S.; Lunde, A.; Beraki, K.; Speth, M.; Øynebråten, I.; Corthay, A. Toll-Like Receptor Ligands and Interferon-γ Synergize for Induction of Antitumor M1 Macrophages. *Frontiers in Immunology* **2017**, *8*, Original Research. DOI: 10.3389/fimmu.2017.01383.

(28) Nedvetzki, S.; Sowinski, S.; Eagle, R. A.; Harris, J.; Vély, F. d. r.; Pende, D.; Trowsdale, J.; Vivier, E.; Gordon, S.; Davis, D. M. Reciprocal regulation of human natural killer cells and macrophages associated with distinct immune synapses. *Blood* **2007**, *109* (9), 3776-3785. DOI: 10.1182/blood-2006-10-052977 (acccessed 10/17/2024).

(29) Prager, I.; Watzl, C. Mechanisms of natural killer cell-mediated cellular cytotoxicity. *Journal of Leukocyte Biology* **2019**, *105* (6), 1319-1329. DOI: 10.1002/jlb.Mr0718-269r (acccessed 10/17/2024).

(30) Chowdhury, D.; Lieberman, J. Death by a Thousand Cuts: Granzyme Pathways of Programmed Cell Death. *Annual Review of Immunology* **2008**, *26* (Volume 26, 2008), 389-420. DOI: https://doi.org/10.1146/annurev.immunol.26.021607.090404.

(31) Sutton, V. R.; Davis, J. E.; Cancilla, M.; Johnstone, R. W.; Ruefli, A. A.; Sedelies, K.; Browne, K. A.; Trapani, J. A. Initiation of Apoptosis by Granzyme B Requires Direct Cleavage of Bid, but Not Direct Granzyme B–Mediated Caspase Activation. *Journal of Experimental Medicine* **2000**, *192* (10), 1403-1414. DOI: 10.1084/jem.192.10.1403 (acccessed 10/17/2024).

Die approbierte gedruckte Originalversion dieser Diplomarbeit ist an der TU Wien Bibliothek verfügbar
The approved original version of this thesis is available in print at TU Wien Bibliothek.
TU Bibliothek Your knowledge hub WIEN

(32) Lopez, J. A.; Susanto, O.; Jenkins, M. R.; Lukoyanova, N.; Sutton, V. R.; Law, R. H. P.; Johnston, A.; Bird, C. H.; Bird, P. I.; Whisstock, J. C.; et al. Perforin forms transient pores on the target cell plasma membrane to facilitate rapid access of granzymes during killer cell attack. *Blood* **2013**, *121* (14), 2659-2668. DOI: 10.1182/blood-2012-07-446146 (acccessed 10/17/2024).

(33) Lopez, J. A.; Jenkins, M. R.; Rudd-Schmidt, J. A.; Brennan, A. J.; Danne, J. C.; Mannering, S. I.; Trapani, J. A.; Voskoboinik, I. Rapid and Unidirectional Perforin Pore Delivery at the Cytotoxic Immune Synapse. *The Journal of Immunology* **2013**, *191* (5), 2328-2334. DOI: 10.4049/jimmunol.1301205 (acccessed 10/17/2024).

(34) Bodmer, J.-L.; Schneider, P.; Tschopp, J. The molecular architecture of the TNF superfamily. *Trends in Biochemical Sciences* **2002**, *27* (1), 19-26. DOI: 10.1016/S0968-0004(01)01995-8 (acccessed 2024/10/18).

(35) Suda, T.; Okazaki, T.; Naito, Y.; Yokota, T.; Arai, N.; Ozaki, S.; Nakao, K.; Nagata, S. Expression of the Fas ligand in cells of T cell lineage. *The Journal of Immunology* **1995**, *154* (8), 3806-3813. DOI: 10.4049/jimmunol.154.8.3806 (acccessed 10/18/2024).

(36) Mariani, S. M.; Matiba, B.; Bäumler, C.; Krammer, P. H. Regulation of cell surface APO-1/Fas (CD95) ligand expression by metalloproteases. *European Journal of Immunology* **1995**, *25* (8), 2303-2307. DOI: https://doi.org/10.1002/eji.1830250828.

(37) Peter, M. E.; Krammer, P. H. The CD95(APO-1/Fas) DISC and beyond. *Cell Death & Differentiation* **2003**, *10* (1), 26-35. DOI: 10.1038/sj.cdd.4401186.

(38) Takeda, K.; Hayakawa, Y.; Smyth, M. J.; Kayagaki, N.; Yamaguchi, N.; Kakuta, S.; Iwakura, Y.; Yagita, H.; Okumura, K. Involvement of tumor necrosis factor-related apoptosis-inducing ligand in surveillance of tumor metastasis by liver natural killer cells. *Nature Medicine* **2001**, *7* (1), 94-100. DOI: 10.1038/83416.

(39) Sato, K.; Hida, S.; Takayanagi, H.; Yokochi, T.; Kayagaki, N.; Takeda, K.; Yagita, H.; Okumura, K.; Tanaka, N.; Taniguchi, T.; et al. Antiviral response by natural killer cells through TRAIL gene induction by IFN–α/β *European Journal of Immunology* **2001**, *31* (11), 3138-3146. DOI: https://doi.org/10.1002/1521-4141(200111)31:11<3138::AID-IMMU3138>3.0.CO;2-B.

(40) Kayagaki, N.; Yamaguchi, N.; Nakayama, M.; Takeda, K.; Akiba, H.; Tsutsui, H.; Okamura, H.; Nakanishi, K.; Okumura, K.; Yagita, H. Expression and Function of TNF-Related Apoptosis-Inducing Ligand on Murine Activated NK Cells1. *The Journal of Immunology* **1999**, *163* (4), 1906-1913. DOI: 10.4049/jimmunol.163.4.1906 (acccessed 10/18/2024).

(41) Prager, I.; Watzl, C. Mechanisms of natural killer cell-mediated cellular cytotoxicity. *J Leukoc Biol* **2019**, *105* (6), 1319-1329. DOI: 10.1002/jlb.Mr0718-269r From NLM.

(42) Hegde, P. S.; Chen, D. S. Top 10 Challenges in Cancer Immunotherapy. *Immunity* **2020**, *52* (1), 17-35. DOI: https://doi.org/10.1016/j.immuni.2019.12.011.

(43) Li, Y.; Hermanson, D. L.; Moriarity, B. S.; Kaufman, D. S. Human iPSC-Derived Natural Killer Cells Engineered with Chimeric Antigen Receptors Enhance Anti-tumor Activity. *Cell Stem Cell* **2018**, *23* (2), 181-192.e185. DOI: https://doi.org/10.1016/j.stem.2018.06.002.

(44) Klichinsky, M.; Ruella, M.; Shestova, O.; Lu, X. M.; Best, A.; Zeeman, M.; Schmierer, M.; Gabrusiewicz, K.; Anderson, N. R.; Petty, N. E.; et al. Human chimeric antigen receptor macrophages for cancer immunotherapy. *Nature Biotechnology* **2020**, *38* (8), 947-953. DOI: 10.1038/s41587-020-0462-y.

(45) Rosenberg, S. A.; Restifo, N. P. Adoptive cell transfer as personalized immunotherapy for human cancer. *Science* **2015**, *348* (6230), 62-68. DOI: doi:10.1126/science.aaa4967.

(46) Beilhack, A.; Schulz, S.; Baker, J.; Beilhack, G. F.; Wieland, C. B.; Herman, E. I.; Baker, E. M.; Cao, Y.-A.; Contag, C. H.; Negrin, R. S. In vivo analyses of early events in acute graft-versus-host disease

Die approbierte gedruckte Originalversion dieser Diplomarbeit ist an der TU Wien Bibliothek verfügbar
The approved original version of this thesis is available in print at TU Wien Bibliothek.

reveal sequential infiltration of T-cell subsets. *Blood* **2005**, *106* (3), 1113-1122. DOI: 10.1182/blood-2005-02-0509 (acccessed 10/19/2024).

(47) Lizana-Vasquez, G. D.; Torres-Lugo, M.; Dixon, R. B.; Powderly, J. D.; Warin, R. F. The application of autologous cancer immunotherapies in the age of memory-NK cells. *Frontiers in Immunology* **2023**, *14*, Review. DOI: 10.3389/fimmu.2023.1167666.

(48) at https://www.clinicaltrials.gov/ (accessed.

(49) Uherek, C.; Tonn, T.; Uherek, B.; Becker, S.; Schnierle, B.; Klingemann, H. G.; Wels, W. Retargeting of natural killer-cell cytolytic activity to ErbB2-expressing cancer cells results in efficient and selective tumor cell destruction. *Blood* **2002**, *100* (4), 1265-1273. From NLM.

(50) Tam, Y. K.; Miyagawa, B.; Ho, V. C.; Klingemann, H. G. Immunotherapy of malignant melanoma in a SCID mouse model using the highly cytotoxic natural killer cell line NK-92. *J Hematother* **1999**, *8* (3), 281-290. DOI: 10.1089/106161299320316.

(51) Gong, J. H.; Maki, G.; Klingemann, H. G. Characterization of a human cell line (NK-92) with phenotypical and functional characteristics of activated natural killer cells. *Leukemia* **1994**, *8* (4), 652-658. From NLM.

(52) Burshtyn, D. N.; Scharenberg, A. M.; Wagtmann, N.; Rajagopalan, S.; Berrada, K.; Yi, T.; Kinet, J. P.; Long, E. O. Recruitment of tyrosine phosphatase HCP by the killer cell inhibitor receptor. *Immunity* **1996**, *4* (1), 77-85. DOI: 10.1016/s1074-7613(00)80300-3 From NLM.

(53) Maki, G.; Klingemann, H.-G.; Martinson, J. A.; Tam, Y. K. Factors Regulating the Cytotoxic Activity of the Human Natural Killer Cell Line, NK-92. *Journal of Hematotherapy & Stem Cell Research* **2001**, *10* (3), 369-383. DOI: 10.1089/152581601750288975 (acccessed 2024/10/20).

(54) Schönfeld, K.; Sahm, C.; Zhang, C.; Naundorf, S.; Brendel, C.; Odendahl, M.; Nowakowska, P.; Bönig, H.; Köhl, U.; Kloess, S.; et al. Selective Inhibition of Tumor Growth by Clonal NK Cells Expressing an ErbB2/HER2-Specific Chimeric Antigen Receptor. *Molecular Therapy* **2015**, *23* (2), 330-338. DOI: https://doi.org/10.1038/mt.2014.219.

(55) Navarrete-Galvan, L.; Guglielmo, M.; Cruz Amaya, J.; Smith-Gagen, J.; Lombardi, V. C.; Merica, R.; Hudig, D. Optimizing NK-92 serial killers: gamma irradiation, CD95/Fas-ligation, and NK or LAK attack limit cytotoxic efficacy. *Journal of Translational Medicine* **2022**, *20* (1), 151. DOI: 10.1186/s12967-022-03350-6.

(56) Arai, S.; Meagher, R.; Swearingen, M.; Myint, H.; Rich, E.; Martinson, J.; Klingemann, H. Infusion of the allogeneic cell line NK-92 in patients with advanced renal cell cancer or melanoma: a phase I trial. *Cytotherapy* **2008**, *10* (6), 625-632. DOI: 10.1080/14653240802301872 (acccessed 2024/10/21).

(57) Boyiadzis, M.; Agha, M.; Redner, R. L.; Sehgal, A.; Im, A.; Hou, J.-Z.; Farah, R.; Dorritie, K. A.; Raptis, A.; Lim, S. H.; et al. Phase 1 clinical trial of adoptive immunotherapy using “off-the-shelf” activated natural killer cells in patients with refractory and relapsed acute myeloid leukemia. *Cytotherapy* **2017**, *19* (10), 1225-1232. DOI: 10.1016/j.jcyt.2017.07.008 (acccessed 2024/10/21).

(58) Zhang, J.; Zheng, H.; Diao, Y. Natural Killer Cells and Current Applications of Chimeric Antigen Receptor-Modified NK-92 Cells in Tumor Immunotherapy. *Int J Mol Sci* **2019**, *20* (2). DOI: 10.3390/ijms20020317 From NLM.

(59) Williams, B. A.; Law, A. D.; Routy, B.; denHollander, N.; Gupta, V.; Wang, X.-H.; Chaboureau, A.; Viswanathan, S.; Keating, A. A phase I trial of NK-92 cells for refractory hematological malignancies relapsing after autologous hematopoietic cell transplantation shows safety and evidence of efficacy. *Oncotarget* **2017**, *8* (51).

(60) Tonn, T.; Schwabe, D.; Klingemann, H. G.; Becker, S.; Esser, R.; Koehl, U.; Suttorp, M.; Seifried, E.; Ottmann, O. G.; Bug, G. Treatment of patients with advanced cancer with the natural killer cell line

Die approbierte gedruckte Originalversion dieser Diplomarbeit ist an der TU Wien Bibliothek verfügbar
The approved original version of this thesis is available in print at TU Wien Bibliothek.
TU Bibliothek Your knowledge hub WIEN

NK-92. *Cytotherapy* **2013**, *15* (12), 1563-1570. DOI: 10.1016/j.jcyt.2013.06.017 (acccessed 2024/10/21).

(61) Jochems, C.; Hodge, J. W.; Fantini, M.; Fujii, R.; Morillon II, Y. M.; Greiner, J. W.; Padget, M. R.; Tritsch, S. R.; Yok Tsang, K.; Campbell, K. S.; et al. An NK cell line (haNK) expressing high levels of granzyme and engineered to express the high affinity CD16 allele. *Oncotarget* **2016**, *7* (52).

(62) Klingemann, H. The NK-92 cell line—30 years later: its impact on natural killer cell research and treatment of cancer. *Cytotherapy* **2023**, *25* (5), 451-457. DOI: 10.1016/j.jcyt.2022.12.003 (acccessed 2024/10/21).

(63) Tonn, T.; Schwabe, D.; Klingemann, H. G.; Becker, S.; Esser, R. L.; Koehl, U.; Suttorp, M.; Seifried, E.; Ottmann, O. G.; Bug, G. Treatment of patients with advanced cancer with the natural killer cell line NK-92. *Cytotherapy* **2013**, *15 12*, 1563-1570.

(64) Stern, M.; Passweg, J. R.; Meyer-Monard, S.; Esser, R.; Tonn, T.; Soerensen, J.; Paulussen, M.; Gratwohl, A.; Klingebiel, T.; Bader, P.; et al. Pre-emptive immunotherapy with purified natural killer cells after haploidentical SCT: a prospective phase II study in two centers. *Bone Marrow Transplantation* **2013**, *48*, 433-438.

(65) Geller, M. A.; Cooley, S.; Judson, P. L.; Ghebre, R. G.; Carson, L. F.; Argenta, P. A.; Jonson, A. L.; Panoskaltsis-Mortari, A.; Curtsinger, J. M.; McKenna, D. H.; et al. A phase II study of allogeneic natural killer cell therapy to treat patients with recurrent ovarian and breast cancer. *Cytotherapy* **2011**, *13 1*, 98-107.

(66) Pierson, B. A.; Europa, A. F.; Hu, W. S.; Miller, J. S. Production of human natural killer cells for adoptive immunotherapy using a computer-controlled stirred-tank bioreactor. *J Hematother* **1996**, *5* (5), 475-483. DOI: 10.1089/scd.1.1996.5.475.

(67) Carlens, S.; Gilljam, M.; Chambers, B. J.; Aschan, J.; Guven, H.; Ljunggren, H.-G.; Christensson, B.; Dilber, M. S. A new method for in vitro expansion of cytotoxic human CD3−CD56+ natural killer cells. *Human Immunology* **2001**, *62* (10), 1092-1098. DOI: 10.1016/s0198-8859(01)00313-5.

(68) Luhm. Large-Scale Generation of Natural Killer Lymphocytes for Clinical Application. **2002**.

(69) Sutlu, T.; Stellan, B.; Gilljam, M.; Quezada, H. C.; Nahi, H.; Gahrton, G.; Alici, E. Clinical-grade, large-scale, feeder-free expansion of highly active human natural killer cells for adoptive immunotherapy using an automated bioreactor. *Cytotherapy* **2010**, *12* (8), 1044-1055. DOI: https://doi.org/10.3109/14653249.2010.504770.

(70) Spanholtz, J.; Preijers, F.; Tordoir, M.; Trilsbeek, C.; Paardekooper, J.; de Witte, T.; Schaap, N.; Dolstra, H. Clinical-grade generation of active NK cells from cord blood hematopoietic progenitor cells for immunotherapy using a closed-system culture process. *PLoS One* **2011**, *6* (6), e20740. DOI: 10.1371/journal.pone.0020740.

(71) Lapteva, N.; Durett, A. G.; Sun, J.; Rollins, L. A.; Huye, L. L.; Fang, J.; Dandekar, V.; Mei, Z.; Jackson, K.; Vera, J.; et al. Large-scale ex vivo expansion and characterization of natural killer cells for clinical applications. *Cytotherapy* **2012**, *14* (9), 1131-1143. DOI: https://doi.org/10.3109/14653249.2012.700767.

(72) Shah, N.; Martin-Antonio, B.; Yang, H.; Ku, S.; Lee, D. A.; Cooper, L. J.; Decker, W. K.; Li, S.; Robinson, S. N.; Sekine, T.; et al. Antigen presenting cell-mediated expansion of human umbilical cord blood yields log-scale expansion of natural killer cells with anti-myeloma activity. *PLoS One* **2013**, *8* (10), e76781. DOI: 10.1371/journal.pone.0076781 From NLM Medline.

(73) Granzin, M.; Soltenborn, S.; Muller, S.; Kollet, J.; Berg, M.; Cerwenka, A.; Childs, R. W.; Huppert, V. Fully automated expansion and activation of clinical-grade natural killer cells for adoptive immunotherapy. *Cytotherapy* **2015**, *17* (5), 621-632. DOI: 10.1016/j.jcyt.2015.03.611.

(74) Kloss, S.; Oberschmidt, O.; Morgan, M.; Dahlke, J.; Arseniev, L.; Huppert, V.; Granzin, M.; Gardlowski, T.; Matthies, N.; Soltenborn, S.; et al. Optimization of Human NK Cell Manufacturing:

Die approbierte gedruckte Originalversion dieser Diplomarbeit ist an der TU Wien Bibliothek verfügbar
The approved original version of this thesis is available in print at TU Wien Bibliothek.
TU Bibliothek Your knowledge hub WIEN

Fully Automated Separation, Improved Ex Vivo Expansion Using IL-21 with Autologous Feeder Cells, and Generation of Anti-CD123-CAR-Expressing Effector Cells. *Hum Gene Ther* **2017**, *28* (10), 897-913. DOI: 10.1089/hum.2017.157 From NLM Medline.

(75) Oberschmidt, O.; Morgan, M.; Huppert, V.; Kessler, J.; Gardlowski, T.; Matthies, N.; Aleksandrova, K.; Arseniev, L.; Schambach, A.; Koehl, U.; et al. Development of Automated Separation, Expansion, and Quality Control Protocols for Clinical-Scale Manufacturing of Primary Human NK Cells and Alpharetroviral Chimeric Antigen Receptor Engineering. *Hum Gene Ther Methods* **2019**, *30* (3), 102-120. DOI: 10.1089/hgtb.2019.039.

(76) Garcia-Aponte, O. F.; Herwig, C.; Kozma, B. Lymphocyte expansion in bioreactors: upgrading adoptive cell therapy. *J Biol Eng* **2021**, *15* (1), 13. DOI: 10.1186/s13036-021-00264-7.

(77) Highfill, S. L.; Stroncek, D. F. Overcoming Challenges in Process Development of Cellular Therapies. *Curr Hematol Malig Rep* **2019**, *14* (4), 269-277. DOI: 10.1007/s11899-019-00529-5 From NLM.

(78) Foster, A. E.; Forrester, K.; Gottlieb, D. J.; Barton, G. W.; Romagnoli, J. A.; Bradstock, K. F. Large-scale expansion of cytomegalovirus-specific cytotoxic T cells in suspension culture. *Biotechnol Bioeng* **2004**, *85* (2), 138-146. DOI: 10.1002/bit.10801 From NLM.

(79) Hilbert, U.; Jelinek, N.; Schmidt, S.; Biselli, M. Bioprocess Development for the Cultivation of Human T-lymphocytes. *Engineering in Life Sciences* **2001**, *1* (1), 20-23. DOI: https://doi.org/10.1002/1618-2863(200107)1:1<20::AID-ELSC20>3.0.CO;2-T.

(80) Costariol, E.; Rotondi, M.; Amini, A.; Hewitt, C. J.; Nienow, A. W.; Heathman, T. R. J.; Micheletti, M.; Rafiq, Q. A. Establishing the scalable manufacture of primary human T-cells in an automated stirred-tank bioreactor. *Biotechnol Bioeng* **2019**, *116* (10), 2488-2502. DOI: 10.1002/bit.27088 From NLM Medline.

(81) Costariol, E.; Rotondi, M. C.; Amini, A.; Hewitt, C. J.; Nienow, A. W.; Heathman, T. R. J.; Rafiq, Q. A. Demonstrating the Manufacture of Human CAR-T Cells in an Automated Stirred-Tank Bioreactor. *Biotechnology Journal* **2020**, *15* (9), 2000177. DOI: https://doi.org/10.1002/biot.202000177.

(82) Tonn, T.; Becker, S.; Esser, R.; Schwabe, D.; Seifried, E. Cellular immunotherapy of malignancies using the clonal natural killer cell line NK-92. *J Hematother Stem Cell Res* **2001**, *10* (4), 535-544. DOI: 10.1089/15258160152509145.

(83) Koehl, U.; Kalberer, C.; Spanholtz, J.; Lee, D. A.; Miller, J. S.; Cooley, S.; Lowdell, M.; Uharek, L.; Klingemann, H.; Curti, A.; et al. Advances in clinical NK cell studies: Donor selection, manufacturing and quality control. *Oncoimmunology* **2016**, *5* (4), e1115178. DOI: 10.1080/2162402X.2015.1115178.

(84) Tam, Y. K.; Martinson, J. A.; Doligosa, K.; Klingemann, H. G. Ex vivo expansion of the highly cytotoxic human natural killer-92 cell-line under current good manufacturing practice conditions for clinical adoptive cellular immunotherapy. *Cytotherapy* **2003**, *5* (3), 259-272. DOI: 10.1080/14653240310001523.

(85) Lee, S.; Joo, Y.; Lee, E. J.; Byeon, Y.; Kim, J. H.; Pyo, K. H.; Kim, Y. S.; Lim, S. M.; Kilbride, P.; Iyer, R. K.; et al. Successful expansion and cryopreservation of human natural killer cell line NK-92 for clinical manufacturing. *PLoS One* **2024**, *19* (2), e0294857. DOI: 10.1371/journal.pone.0294857 From NLM Medline.

(86) Irina Ganeeva, E. Z., Aygul Valiullina, Anna Kudriaeva, Regina Miftakhova, Alexey Rybalov and Emil Bulatov. Recent Advances in the Development of Bioreactors for Manufacturing of Adoptive Cell Immunotherapies. *Bioengineering* **2022**, Bioengineering 2022, 2029, 2808. . DOI: https://doi.org/10.3390/bioengineering9120808.

(87) Fang, F.; Xie, S.; Chen, M.; Li, Y.; Yue, J.; Ma, J.; Shu, X.; He, Y.; Xiao, W.; Tian, Z. Advances in NK cell production. *Cell Mol Immunol* **2022**, *19* (4), 460-481. DOI: 10.1038/s41423-021-00808-3.

Die approbierte gedruckte Originalversion dieser Diplomarbeit ist an der TU Wien Bibliothek verfügbar
The approved original version of this thesis is available in print at TU Wien Bibliothek.
TU Bibliothek Your knowledge hub WIEN

(88) Motallebnejad, P.; Kantardjieff, A.; Cichocki, F.; Azarin, S. M.; Hu, W. S. Process engineering of natural killer cell-based immunotherapy. *Trends Biotechnol* **2023**, *41* (10), 1314-1326. DOI: 10.1016/j.tibtech.2023.03.018 From NLM Medline.

(89) Zhang, L.; Liu, M.; Yang, S.; Wang, J.; Feng, X.; Han, Z. Natural killer cells: of-the-shelf cytotherapy for cancer immunosurveillance. *Am J Cancer Res* **2021**, *11* (4), 1770-1791.

(90) *K562-GFP RPMI 1640 media*. https://www.thermofisher.com/at/en/home/technical-resources/media-formulation.119.html (accessed.

(91) https://www.thermofisher.com/at/en/home/technical-resources/media-formulation.98.html)

(92) van Engeland, M.; Nieland, L. J. W.; Ramaekers, F. C. S.; Schutte, B.; Reutelingsperger, C. P. M. Annexin V-Affinity assay: A review on an apoptosis detection system based on phosphatidylserine exposure. *Cytometry* **1998**, *31* (1), 1-9. DOI: https://doi.org/10.1002/(SICI)1097-0320(19980101)31:1<1::AID-CYTO1>3.0.CO;2-R.

(93) Furuta, Y.; Zhou, Z. How do necrotic cells expose phosphatidylserine to attract their predators-What's unique and what's in common with apoptotic cells. *Front Cell Dev Biol* **2023**, *11*, 1170551. DOI: 10.3389/fcell.2023.1170551 From NLM.

(94) Jin, Q.; Jiang, L.; Chen, Q.; Li, X.; Xu, Y.; Sun, X.; Zhao, Z.; Wei, L. Rapid flow cytometry-based assay for the evaluation of γδ T cell-mediated cytotoxicity. *Mol Med Rep* **2018**, *17* (3), 3555-3562. DOI: 10.3892/mmr.2017.8281.

(95) Doran, P. *Bioprocess-engineering-principles*.

(96) <Bioprozesstechnik_Chmiel_2018.pdf>.

(97) Kaiser, S.; Löffelholz, C.; Werner, S.; Eibl, D. CFD for Characterizing Standard and Single-use Stirred Cell Culture Bioreactors. 2011.

(98) Doi, T.; Kajihara, H.; Chuman, Y.; Kuwae, S.; Kaminagayoshi, T.; Omasa, T. Development of a scale-up strategy for Chinese hamster ovary cell culture processes using the k(L) a ratio as a direct indicator of gas stripping conditions. *Biotechnol Prog* **2020**, *36* (5), e3000. DOI: 10.1002/btpr.3000 From NLM.

(99) al., J. K. e. *Scale-up study for ex-vivo expansion of allogeneic natural killer cells in stirred-tank bioreactor*; 2019.

(100) Büchs, J.; Maier, U.; Milbradt, C.; Zoels, B. Power consumption in shaking flasks on rotary shaking machines: I. Power consumption measurement in unbaffled flasks at low liquid viscosity. *Biotechnol Bioeng* **2000**, *68* (6), 589-593. DOI: 10.1002/(sici)1097-0290(20000620)68:6<589::aid-bit1>3.0.co;2-j From NLM.

(101) Büchs, J.; Maier, U.; Milbradt, C.; Zoels, B. Power consumption in shaking flasks on rotary shaking machines: II. Nondimensional description of specific power consumption and flow regimes in unbaffled flasks at elevated liquid viscosity. *Biotechnology and Bioengineering* **2000**, *68* (6), 594-601. DOI: https://doi.org/10.1002/(SICI)1097-0290(20000620)68:6<594::AID-BIT2>3.0.CO;2-U.

(102) Büchs, J.; Zoels, B. Evaluation of Maximum to Specific Power Consumption Ratio in Shaking Bioreactors. *Journal of Chemical Engineering of Japan* **2001**, *34*, 647-653. DOI: 10.1252/jcej.34.647.

(103) Costariol, E. Establishing a scalable manufacturing process for the clinical scale production of CAR-T cell therapies in stirred-tank bioreactors. University College London, 2020.

(104) Ham, H.; Medlyn, M. J.; Billadeau, D. D. Locked and Loaded: Mechanisms Regulating Natural Killer Cell Lytic Granule Biogenesis and Release. *Frontiers in Immunology* **2022**, *13*.

(105) Wang, Z.; Guan, D.; Wang, S.; Chai, L. Y. A.; Xu, S.; Lam, K.-P. Glycolysis and Oxidative Phosphorylation Play Critical Roles in Natural Killer Cell Receptor-Mediated Natural Killer Cell Functions. *Frontiers in Immunology* **2020**, *11*.

Die approbierte gedruckte Originalversion dieser Diplomarbeit ist an der TU Wien Bibliothek verfügbar
The approved original version of this thesis is available in print at TU Wien Bibliothek.

(106) Mao, Y.; van Hoef, V.; Zhang, X.; Wennerberg, E.; Lorent, J.; Witt, K.; Masvidal, L.; Liang, S.; Murray, S.; Larsson, O.; et al. IL-15 activates mTOR and primes stress-activated gene expression leading to prolonged antitumor capacity of NK cells. *Blood* **2016**, *128* (11), 1475-1489. DOI: 10.1182/blood-2016-02-698027 (acccessed 12/18/2024).

(107) Nachef, M.; Ali, A. K.; Almutairi, S. M.; Lee, S.-H. Targeting SLC1A5 and SLC3A2/SLC7A5 as a Potential Strategy to Strengthen Anti-Tumor Immunity in the Tumor Microenvironment. *Frontiers in Immunology* **2021**, *12*, Review. DOI: 10.3389/fimmu.2021.624324.

(108) Patel, C. H.; Powell, J. D. Targeting T cell metabolism to regulate T cell activation, differentiation and function in disease. *Current opinion in immunology* **2017**, *46*, 82-88.

(109) Scott, K. E. N.; Cleveland, J. L. Lactate Wreaks Havoc on Tumor-Infiltrating T and NK Cells. *Cell metabolism* **2016**, *24 5*, 649-650.

(110) Mirabet, M.; Navarro, A. A. S.; López, A. B.; Canela, E. I.; Mallol, J.; Lluis, C.; Franco, R. Ammonium toxicity in different cell lines. *Biotechnology and bioengineering* **1997**, *56 5*, 530-537.

(111) Salzberger, W.; Martrus, G.; Bachmann, K.; Goebels, H.; Heß, L.; Koch, M.; Langeneckert, A.; Lunemann, S.; Oldhafer, K. J.; Pfeifer, C.; et al. Tissue-resident NK cells differ in their expression profile of the nutrient transporters Glut1, CD98 and CD71. *PLOS ONE* **2018**, *13* (7), e0201170. DOI: 10.1371/journal.pone.0201170.

(112) Bose, S.; Zhang, C.; Le, A. Glucose Metabolism in Cancer: The Warburg Effect and Beyond. *Adv Exp Med Biol* **2021**, *1311*, 3-15. DOI: 10.1007/978-3-030-65768-0_1 From NLM.

(113) Fan, J.; Kang, H.-B.; Shan, C.; Elf, S. E.; Lin, R.; Xie, J.; Gu, T.-l.; Aguiar, M.; Lonning, S. M.; Chung, T.-W.; et al. Tyr-301 Phosphorylation Inhibits Pyruvate Dehydrogenase by Blocking Substrate Binding and Promotes the Warburg Effect*. *The Journal of Biological Chemistry* **2014**, *289*, 26533 - 26541.

(114) Li, X.; Yang, Y.; Zhang, B.; Lin, X.; Fu, X.; An, Y.; Zou, Y.; Wang, J.-X.; Wang, Z.; Yu, T. Lactate metabolism in human health and disease. *Signal Transduction and Targeted Therapy* **2022**, *7* (1), 305. DOI: 10.1038/s41392-022-01151-3.

(115) Juretic, A.; Spagnoli, G. C.; Hörig, H.; Babst, R.; von Bremen, K.; Harder, F.; Heberer, M. Glutamine requirements in the generation of lymphokine-activated killer cells. *Clin Nutr* **1994**, *13* (1), 42-49. DOI: 10.1016/0261-5614(94)90009-4 From NLM.

(116) Picard, L. K.; Niemann, J. A.; Littwitz-Salomon, E.; Waldmann, H.; Watzl, C. Restriction of Glycolysis Increases Serial Killing Capacity of Natural Killer Cells. *International Journal of Molecular Sciences* **2024**, *25* (5), 2917.

(117) Han, Y.; Liu, X. M.; Liu, H.; Li, S. C.; Wu, B. C.; Ye, L. L.; Wang, Q. W.; Chen, Z. L. Cultivation of recombinant Chinese hamster ovary cells grown as suspended aggregates in stirred vessels. *J Biosci Bioeng* **2006**, *102* (5), 430-435. DOI: 10.1263/jbb.102.430 From NLM.

(118) García Aponte, O. F.; Kozma, B.; Egger, D.; Kasper, C.; Herwig, C. Kinetics of NK-92 growth and functionality in pseudo-static cultures. *Biochemical Engineering Journal* **2023**, *196*, 108929. DOI: https://doi.org/10.1016/j.bej.2023.108929.

(119) Sheppard, S.; Srpan, K.; Lin, W.; Lee, M.; Delconte, R. B.; Owyong, M.; Carmeliet, P.; Davis, D. M.; Xavier, J. B.; Hsu, K. C.; et al. Fatty acid oxidation fuels natural killer cell responses against infection and cancer. *Proceedings of the National Academy of Sciences* **2024**, *121* (11), e2319254121. DOI: doi:10.1073/pnas.2319254121.

(120) Fendt, S.-M.; Bell, E. L.; Keibler, M. A.; Olenchock, B. A.; Mayers, J. R.; Wasylenko, T. M.; Vokes, N. I.; Guarente, L.; Heiden, M. G. V.; Stephanopoulos, G. Reductive glutamine metabolism is a function of the α-ketoglutarate to citrate ratio in cells. *Nature Communications* **2013**, *4* (1), 2236. DOI: 10.1038/ncomms3236.

(121) Adiba Zanghi, D. L., Tina Balsara, Lucian Young, Barry Wolf and Ping Huang. Increased efficiency and product quality with the UniVessel ® Single Use bioreactor for CHO fed-batch cultures. 2017.

Die approbierte gedruckte Originalversion dieser Diplomarbeit ist an der TU Wien Bibliothek verfügbar
The approved original version of this thesis is available in print at TU Wien Bibliothek.

Die approbierte gedruckte Originalversion dieser Diplomarbeit ist an der TU Wien Bibliothek verfügbar
The approved original version of this thesis is available in print at TU Wien Bibliothek.